Construction of Minimal Surfaces

H. Karcher (Bonn)

In my contribution to this series of lectures, I will explain how the remarkable minimal surfaces which have been discovered in this decade can be constructed. Also included are famous examples from the last century.

The organization of my lectures will be as follows:

1. Weierstrass Representation and Symmetries
2. Spherical Examples
3. Toroidal Examples
4. Conjugate Plateau Construction
5. Higher Genus Weierstrass Representations

I thank David Hoffman and Harold Rosenberg for frequent discussions which helped my understanding of minimal surfaces a lot. I thank Romain Krust for telling me a result (2.4.1) which fits perfectly into the context of these lectures. The pictures which I use were mostly made by Konrad Polthier (SFB 256 at Bonn). Jörg Hahn and Meinhard Wohlgemuth participated in the initial parts of the program development. In the same way as the pictures help my explanations in these lectures, they also helped to improve our intuition. My thanks for these pictures include the group of SFB 256 who made the

computers reasonably easy to use tools.

These lectures were made possible by a generous invitation to Kanazawa University, arranged jointly by Prof. T. Ochiai, Prof. H. Kitahara and Prof. T. Takahashi. I thank them and their many colleagues who were wonderful hosts to us at many places of Japan. A Kanazawa audience listened to my practice talks from which these notes developped. For the typing I thank K. Matsuo from Kanazawa University, and H. Kawakami for his help in editing the pictures.

1. Weierstrass Representation and Symmetries

1.1 Notations, definitions, basic formulas.

We describe pieces of surfaces as immersions F of parameter domains D into R^3 :

$$\begin{matrix}\text{Immersion } F \\ \text{Gauss map } N\end{matrix} : D^2 \longrightarrow R^3 \quad .$$

The basic invariants of the surface, namely Riemannian metric g and shape operator S, are defined in terms of the derivatives ∂F, ∂N of F and N. We denote directional derivatives in direction X by $\partial F \cdot X$ or $\partial_X F$.

Riemannian metric: $g(X,Y) := \langle \partial F \cdot X, \partial F \cdot Y \rangle$ (cf. 1.4.2)

Shape operator: $\partial F \cdot S \cdot X := \partial N \cdot X$

The eigenvalues of S are called principal curvatures.

Second fundamental form: $b(X,Y) := g(SX,Y)$.

The shape operator also allows to split the second derivative $\partial^2 F$ of F in its tangential and normal part:

$$\langle N, \partial F \cdot Y \rangle = 0 \Rightarrow \langle \partial N \cdot X, \partial F \cdot Y \rangle + \langle N, \partial_X(\partial_Y F) \rangle = 0$$

$$g(SX,Y) + \langle N, \partial_X(\partial_Y F) \rangle = 0 \quad .$$

REMARK. The sign convention is the one preferred in analysis. For surfaces which are levels of functions $f : R^3 \longrightarrow R$ one has a preferred normal $N := \text{grad } f \cdot |\text{grad } f|^{-1}$. If $|\text{grad } f| = 1$ then S equals the Hessian $\partial \text{ grad } f$, and this convention makes the principal curvatures of the sphere ($f(p) := |p|$) positive.

The tangential part of $\partial_X(\partial_Y F)$ is used to define the covariant derivative ∇ of the Riemannian metric.

Covariant derivative: $\partial_X(\partial_Y F) =: \partial F \cdot \nabla_X Y - g(SX,Y) \cdot N$.

The differentiation of tensor fields, e.g. endomorphism fields like S , satisfies the product rule

$$\nabla_X(S \cdot Y) =: \nabla_X S \cdot Y + S \cdot \nabla_X Y \quad .$$

We are heading for a close connection between minimal surfaces and complex analysis. Geometrically, multiplication by i is 90°-rotation $D^{90^\circ} : C \longrightarrow C$. The Riemannian metric g makes every tangent space of (D^2,g) into a euclidean plane. Therefore we have 90°-rotation as an endomorphism field. D^{90° maps parallel vector fields X along curves γ (i.e., $\nabla_{\dot\gamma} X = 0$) to parallel vector fields $Y = D^{90^\circ} X$ along γ . The definition of the covariant derivative of a tensor field

therefore gives

$$\nabla D^{90^\circ} = 0 \quad , \quad 90^\circ\text{-rotation is (covariantly) parallel.}$$

One further differentiation of the definitions of S and ∇ gives two famous equations:

$$\text{Codazzi equation:} \quad \nabla_X S \cdot Y = \nabla_Y S \cdot X$$
$$\text{Gauss equation:} \quad \text{curv}(R^3) = \text{curv}(g) - \det S \quad .$$

(We omit the definition of the curvature tensor of the Riemannian metric g, it will not occur explicitly since we use $\det S$.) Finally, we consider the Riemannian metric g and the shape operator S as *given geometric data* on the parameter domain D^2. Then one can interpret the definitions of S and ∇ as a differential system for N, ∂F, the

SURFACE EQUATIONS:

$$\nabla^2_{X,Y} F := \partial_X(\partial_Y F) - \partial F \cdot \nabla_X Y = - g(SX,Y) \cdot N$$

$$\partial N \cdot X = \partial F \cdot S \cdot X \quad .$$

The Codazzi and Gauss equations are the integrability conditions for this system. To understand how the surface is determined by this differential system from its geometric data g, S observe the following:

If γ is a geodesic in (D^2,g) then the space curve $F\cdot\gamma$ has the principal normal $N\cdot\gamma$ and the binormal $\partial F\cdot D^{90^\circ}\cdot\dot\gamma$. Therefore g and S determine the Frenet data (i.e., curvature κ, torsion τ) of the space curve $F\cdot\gamma$:

FRENET DATA of $F\cdot\gamma$:

$$\kappa := \langle \partial_{\dot\gamma}(\partial_{\dot\gamma} F),\ N\cdot\gamma \rangle = -\, g(S\dot\gamma,\dot\gamma)$$

(1.1.1)

$$\tau := \langle \partial_{\dot\gamma} N,\ \partial F\cdot D^{90^\circ}\dot\gamma \rangle = g(S\dot\gamma, D^{90^\circ}\dot\gamma) \quad .$$

(1.1.2) NOTE:

A geodesic curvature line has $S\dot\gamma \sim \dot\gamma$, i.e., has $\tau \equiv 0$, it is therefore a *planar* curve. A geodesic asymptote line has $S\dot\gamma \perp \dot\gamma$, i.e. $\kappa \equiv 0$, it is therefore a *straight line* on the surface.

1.2 Minimal Surfaces.

By definition the shape operator controls the derivative of the normal along a surface. However, it also controls the change of the metric when going to *parallel surfaces* $F + \varepsilon N$:

$$g_\varepsilon(X,Y) := \langle \partial_X F + \varepsilon\cdot\partial_X N,\ \partial_Y F + \varepsilon\cdot\partial_Y N \rangle$$

$$\frac{d}{d\varepsilon}\, g_\varepsilon(X,Y)\Big|_{\varepsilon=0} = \langle \partial_X N,\ \partial_Y F \rangle + \langle \partial_X F,\ \partial_Y N \rangle$$

$$= 2\, g(SX,Y) \quad .$$

In particular, trace $S = 0$ is the condition for the first variation of area to vanish. Because of the surface equations this is the same as trace $\nabla^2 F =: \Delta_g F = 0$, i.e., the immersion is Laplace-Beltrami harmonic. So we have the equivalent

DEFINITION of MINIMAL SURFACES

$$\text{Tr } S = 0 \quad \text{or} \quad \Delta_g F = 0 \quad .$$

1.3 Connection with Complex Analysis.

Since holomorphic functions are conformal maps it is natural that we start by introducing conformal (or isothermal) coordinates on the surface. In general this is a nontrivial P.D.E. problem; minimal surfaces however are born together with very natural conformal coordinates:

$\Delta_g F = 0$ means that the restriction of any linear function on R^3 to the surface gives us a harmonic function f, $\Delta_g f = 0$. Recall that in the complex plane C a harmonic function f can be considered as the real part of a holomorphic function; the imaginary part f^* can be reconstructed (on simply connected regions) by integrating

$$\text{grad } f^* = i \cdot \text{grad } f \quad .$$

To imitate this construction of conformal maps in the case of minimal surfaces we also first construct a vector field V by 90°-rotation of grad f :

$$V := D^{90^\circ} \cdot \operatorname{grad} f \quad .$$

We proved that D^{90° is ∇-parallel, therefore

$$\nabla V = D^{90^\circ} \cdot \nabla \operatorname{grad} f \quad .$$

This and $\Delta_g f = 0$ give $\operatorname{rot} V = 0$. Therefore we have in the same way as in the complex plane: The vector field V is, on simply connected regions, the gradient of another ("conjugate") function f^* .

$$V = \operatorname{grad} f^* \quad \text{on simply connected regions,}$$

$$\operatorname{grad} f^* = D^{90^\circ} \cdot \operatorname{grad} f \quad \text{or} \quad \partial f^* = - \partial f \cdot D^{90^\circ} \quad .$$

Of course, any pair of functions f , f^* with orthogonal gradients of equal lengths defines a conformal map

$$(f, f^*) : (D^2, g) \longrightarrow R^2 \quad \text{or} \quad f + if^* : (D^2, g) \longrightarrow C \quad .$$

Since $\varphi := f + if^*$ satisfies $\partial\varphi \cdot D^{90^\circ} X = i \cdot \partial\varphi \cdot X$ we now see, that the Riemannian 90°-rotation indeed plays the role of multiplication by i . At this point we have constructed a *natural atlas* of conformal coordinates for a given minimal surface; in other words, we have made the minimal surface into a Riemann surface M^2 .

We can apply the construction of a conjugate F^* to the given minimal immersion F. Since $\partial F^* = - \partial F \cdot D^{90^\circ}$ we see that

(1.3.1) F, F^* define the *same* Riemannian metric g, hence $\Delta_g F^* = 0$: the "conjugate" immersion F^* is also minimal !

(1.3.2) F, F^* have at corresponding points parallel tangent planes; that means: F, F^* have the same Gauss map N !

$$\partial N = \partial F \cdot S = - \partial F \cdot D^{90^\circ} \cdot D^{90^\circ} \cdot S$$

$$= \partial F^* \cdot (D^{90^\circ} \cdot S) = \partial N^* \text{ , hence}$$

(1.3.3) $S^* = D^{90^\circ} \cdot S$, i.e., F , F^* have closely related shape operators.

At this point we have constructed from a given minimal immersion F a holomorphic curve (recall that F^* is only defined on some covering of M^2): $\psi := F + iF^* : \tilde{M}^2 \longrightarrow \mathbb{C}^3$. We observe an additional property of the curve ψ in terms of the $\mathbb{C}$-bilinear extension $\langle\langle \ , \ \rangle\rangle$ of the Euclidean metric $\langle \ , \ \rangle$ on $\mathbb{R}^3$:

(1.3.4)
$$\langle\langle \partial\psi \cdot X, \partial\psi \cdot X \rangle\rangle$$
$$= \langle\langle \partial F \cdot X + i \cdot \partial F^* \cdot X, \partial F \cdot X + i \cdot \partial F^* \cdot X \rangle\rangle$$
$$= \langle \partial F \cdot X, \partial F \cdot X \rangle - \langle \partial F^* \cdot X, \partial F^* \cdot X \rangle$$
$$+ 2i \cdot \langle \partial F \cdot X, \partial F^* \cdot X \rangle$$
$$= 0 \quad .$$

Such holomorphic curves are called *null-curves*.

Conversely, a holomorphic curve ψ has with respect to some complex local coordinate a harmonic real part F. Using $\partial F^* = - \partial F \cdot D^{90^\circ}$ we see that the real part F of a holomorphic *null* curve is *conformally* parametrized. But conformal metrics have the same holomorphic functions and therefore the same harmonic functions; this proves $\Delta_g F = 0$.

So we have seen: Minimal surfaces in R^3 *are precisely the real parts of holomorphic null curves in* C^3.

The (locally) isometric family of minimal surfaces

$$(1.3.5) \qquad F_\varphi := \mathrm{Re}(e^{-i\varphi}(F + iF^*))$$

is called the *associated family* of F.

1.4 Weierstrass Representation.

The holomorphic curve ψ of the previous section can be written as

$$\psi = \int \psi' dz = \int (\partial F - i \cdot \partial F \cdot D^{90^\circ}) , \quad << \psi', \psi' >> = 0 ,$$

where $\psi' dz$ is defined on the given minimal surface M^2 (one does not have to go to a covering).

Weierstrass has written the integrand $\psi' dz$ in a geometrically particularly useful way:

Weierstrass Representation

$$(1.4.1) \qquad \psi' dz = \left(\frac{1}{2}\left(\frac{1}{g} - g \right), \frac{i}{2}\left(\frac{1}{g} + g \right), 1 \right) \cdot dh \quad .$$

First, $<< \psi', \psi' >> = 0$ is true for this Weierstrass formula. Conversely, every $d\psi$ can be written this way:

$$g := \frac{- d\psi_1 - i d\psi_2}{d\psi_3} = \left(\frac{d\psi_1 + i d\psi_2}{d\psi_3} \right)^{-1}$$

because of $<< (d\psi_1, d\psi_2, d\psi_3), (d\psi_1, d\psi_2, d\psi_3) >> = 0$.
Next, dh is defined in terms of the (harmonic) vertical height function F_3 on M^2 (while h is only defined on $\tilde{M}^2$):

$$dh = dF_3 - i \, dF_3 \cdot D^{90^\circ} \quad .$$

And, most important, stereographic projection of g (using the same "vertical" direction as for dh) is the Gauss map N of the surface:

Stereographic Projection of g is N :

$$N := \frac{(2 \operatorname{Re} g, \; 2 \operatorname{Im} g, \; |g|^2 - 1)}{|g|^2 + 1} \quad .$$

Proof: Clearly real and imaginary part of

$\left(\frac{1}{2}\left(\frac{1}{g} - g \right), \frac{i}{2}\left(\frac{1}{g} + g \right), 1 \right)$ represent two (orthogonal) tangent vectors to the surface in R^3 . Therefore

$<< \left(\frac{1}{2}\left(\frac{1}{g} - g \right), \frac{i}{2}\left(\frac{1}{g} + g \right), 1 \right), (2 \text{ Re } g, 2 \text{ Im } g, |g|^2 - 1) >>$

$= \frac{g}{g} - g\cdot\bar{g} + |g|^2 - 1 = 0$ proves that N is indeed normal to the surface.

The Weierstrass representation, therefore, writes a minimal surfaces down in terms of its Gauss map and the differential of its height function.

The Riemannian metric, the Gauss curvature and the shape operator are also quickly obtained from these "Weierstrass data". From (1.3.4) we have

$$< \partial F\cdot X, \partial F\cdot X > = \frac{1}{2} |\partial\psi\cdot X|^2$$
$$= \frac{1}{4}\left(|g| + \frac{1}{|g|} \right)^2\cdot |dh(X)|^2 \quad .$$

To avoid confusion with the Gauss map I'll from now on write the Riemannian metric as

$$(1.4.2) \qquad ds = \frac{1}{2}\left(|g| + \frac{1}{|g|} \right)\cdot |dh| \quad .$$

(Locally of course $|dh| = |h'||dz|$; then $|dz|$ denotes the euclidean coordinate metric.)

The Gauss curvature is by definition the volume distortion of the Gauss map. The Gauss map is conformal, the metric is conformal to a holomorphic coordinate metric, therefore volume ratios are squares of length ratios:

$$K = - \frac{|\partial N \cdot X|^2}{|ds \cdot X|^2} \quad .$$

First with respect to a local coordinate (and recalling that stereographic projection has the conformal factor $4(1 + |g|^2)^{-2}$) and then coordinate free this is

$$(1.4.3) \qquad K = - |g'|^2 \cdot \frac{4}{(1 + |g|^2)^2} \cdot \frac{4}{\left(|g| + \frac{1}{|g|}\right)^2 \cdot |h'|^2}$$

$$= - \left(\frac{2}{|g| + \frac{1}{|g|}} \right)^4 \cdot \frac{\left|\frac{dg}{g}\right|^2}{|dh|^2} \quad .$$

Finally, to describe the second fundamental form, let z denote a local holomorphic coordinate for M^2 and $W \in T_z M^2 = \mathbf{C}$ a tangent vector. Then

$$b(W,W) = - < \partial^2_{W,W} F, \; N > \qquad \text{(Definition of } b \text{)}$$

$$= - < \mathrm{Re}(\psi'' \cdot W^2), \; N > \qquad (F = \mathrm{Re}\, \psi) \quad .$$

Now insert Weierstrass formula for ψ'' :

$$b(W,W) = -\,\mathrm{Re}\left(\frac{dg}{g}(W)\cdot dh(W)\cdot << \left(\frac{1}{2}\left(\frac{-1}{g} - g\right),\ \frac{i}{2}\left(\frac{-1}{g} + g\right), 0 \right),\ N >> \right)$$

and use that N is stereographic projection of g :

$$b(W,W) = \mathrm{Re}\left(\frac{dg}{g}(W)\cdot dh(W) \right) \quad . \tag{1.4.4}$$

Note also that the frequently used quadratic differential on the minimal surface is easily expressed by the Weierstrass data.

Since *geodesic* curvature lines and geodesic asymptote lines will be recognized as symmetry lines we also note (cf. 1.1.2)

(1.4.5) W is an asymptote direction $\iff \frac{dg}{g}(W)\cdot dh(W) \in iR$.

The principal curvature directions on a minimal surface are angle bisectors of asymptote direction i.e.,

W is a principal curvature direction $\iff \frac{dg}{g}(W)\cdot dh(W) \in R$.

1.5 Symmetries of Minimal Surfaces.

1.5.1 Reflection Theorem. If a planar geodesic resp. a straight line lies an a complete minimal surface, then

reflection in the plane of the planar geodesic resp. 180°-rotation around the straight line is a congruence of the minimal surface.

Proof: From $S^* = D^{90^\circ} \cdot S$ (1.3.3) and the Frenet data for geodesics (1.1.1) we see that a planar geodesic on a minimal surface F is a straight geodesic on the conjugate surface F^* and vice versa. We assume that the planar geodesic is in the x-y-plane and that the conjugate straight line is the z-axis. We use the vertical linear function to get a harmonic function on the minimal surface which we use as in 1.3 to get natural holomorphic coordinates. These coordinates map the symmetry line into a curve with constant real part, i.e., the imaginary axis (after translation). The Weierstrass holomorphic curve satisfies in these coordinates

$$\psi(iR) \subset R \times R \times iR \subset C^3 \ !$$

The usual reflection principle now gives

$$\psi(-\bar{z}) = (\overline{\psi_1(z)}, \overline{\psi_2(z)}, -\overline{\psi_3(z)}) \quad .$$

For $F = \mathrm{Re}\,\psi$ this is a reflection in the x-y-plane, for $F^* = \mathrm{Im}\,\psi$ this is a 180°-rotation around the vertical axis.

We shall use this as follows:

1.5.2 Application.

If in some holomorphic coordinates of a minimal immersion F there is a line σ such that the Gauss *image* $g \cdot \sigma$ is contained

in a meridian or the equator of S^2 and if also $h' \cdot \sigma$ is contained in a meridian of S^2, then:

Analytic(= euclidean) reflection in σ does *not change* the values of $\left(|g| + \frac{1}{|g|} \right)$ and of $|h'|$ nor does it change the euclidean metric $|dz|$, therefore this reflection is a Riemannian isometry for the metric (1.4.2)

$$ds = \frac{1}{2}\left(|g| + \frac{1}{|g|} \right) \cdot |h'dz| \quad .$$

The fixed point set, the curve σ, is therefore a *geodesic* for this metric.

These geodesics σ are even more special; by assumption we have first

$g \cdot \sigma$ is either a meridian of S^2, i.e., $\frac{dg}{g}(\dot{\sigma}) \in R$

or $g \cdot \sigma$ is the equator of S^2, i.e., $\frac{dg}{g}(\dot{\sigma}) \in iR$,

and secondly

$\dot{\sigma}$ and $h' \cdot \sigma$ have a constant phase along σ .

Therefore (use 1.4.5) there is a member F_φ in the associate family (1.3.5) such that

$$e^{-i\varphi} \cdot \frac{dg}{g}(\dot{\sigma}) \cdot dh(\dot{\sigma}) \in R \quad ,$$

then $F_\varphi \cdot \sigma$ is a geodesic curvature line, i.e. a line of reflectional symmetry (1.1.2, 1.5.1) for F_φ ; of course $F_{\varphi + \frac{\pi}{2}} \cdot \sigma$ is then a straight line. In particularly interesting cases the associate parameter φ is the same for all the symmetry lines σ .

Remarks. (i) It may seem as if the assumptions of this last application are a little special. We will see that they are satisfied for most embedded and many immersed examples. In these cases the recognition of symmetries from the Weierstrass data on the one hand is a great help in finding such a Weierstrass representation and on the other hand it saves a large amount of residue computations when verifying its properties.

(ii) Minimal surfaces in R^3 are, of course never compact. In the first lecture by M. Koiso Osserman's theorem will be presented. His theory of finite total curvature minimal surfaces is of basic importance for all the examples which I will describe. Its effect is that their *meromorphic* Weierstrass data are defined on *compact* Riemann surfaces. The points which are infinitely far away for the metric (1.4.2) give ends of the minimal surface (this has to be made precise with 2.1.7).

2. Minimal Surfaces which are parametrized by Punctured Spheres

First I quote a recent result:

2.1.1 Theorem (Lopez-Ros[LoR]). An embedded minimal punctured *sphere* is a plane or a catenoid. (The proof depends on [LaR].)

We therefore cannot expect too spectacular surfaces. But the spherical examples will teach us some properties of the Weierstrass representation which we need to know before dealing with more complicated examples.
To start the examples we combine the simplest Gauss map $g(z) = z$ with the simplest differential such that the Weierstrass curve ψ is a *polynomial*. We obtain the data of

2.1.2 Enneper's surface [En].

$$g(z) = z \quad , \quad dh = z\, dz$$

$$\psi(z) = \frac{1}{2}\left(z - \frac{1}{3} z^3,\ i\left(z + \frac{1}{3} z^3 \right),\ z^2 \right) \quad .$$

We discuss its properties in terms of g and dh along the lines of (1.5.2):

Reflections in straight lines through 0 are Riemannian isometries for the metric (1.4.2)

$$ds = \left(\frac{1}{|z|} + |z| \right) \cdot |z| |dz| \quad .$$

All these radial lines are therefore geodesics and rotation around the origin is an *intrinsic isometry group*.
To decide which of these meridians $m(r) = r \cdot z$, $\dot{m} = z$, are curvature or asymptote lines, we use (1.4.5):

$$\frac{dg}{g}(\dot{m}) \cdot dh(\dot{m}) = z^2 \begin{cases} \in R & <=> \quad z \in R \ , \ iR \\ \in iR & <=> \quad z \in e^{\pm i \cdot \frac{\pi}{4}} \cdot R \end{cases} \quad .$$

Now (1.5.2) says that R , iR are planar symmetry lines (reflection) and the 45°-meridians are straight lines on Enneper's surface (180°-rotation).
The Riemannian metric is complete on $S^2 \setminus \{\infty\}$, and it is nondegenerate, i.e., the surface is without branch points.
All the surfaces of the associate family (1.3.5) are congruent, since the above intrinsic isometry group rotates the shape operator of F to the shape operator of F_φ .
For the behaviour near the puncture we use the integrated expression: circles $c(\varphi) = R \cdot e^{i\varphi}$, $R^3 > 3$, are mapped to curves $\varphi \longrightarrow \mathrm{Re}(\psi(c(\varphi)))$ which wind around the vertical axis three times, i.e., a neighbourhood of the puncture is *not embedded*.

Clearly, the same arguments allow to discuss the

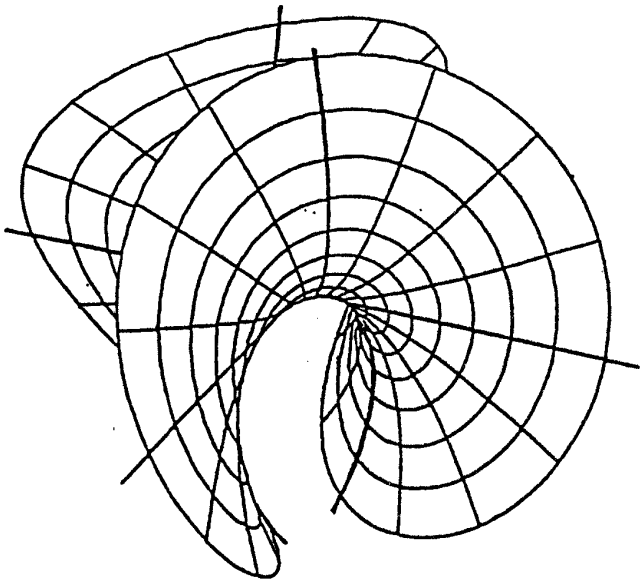

Enneper's surface (2.1.2)

$g(z) = z$

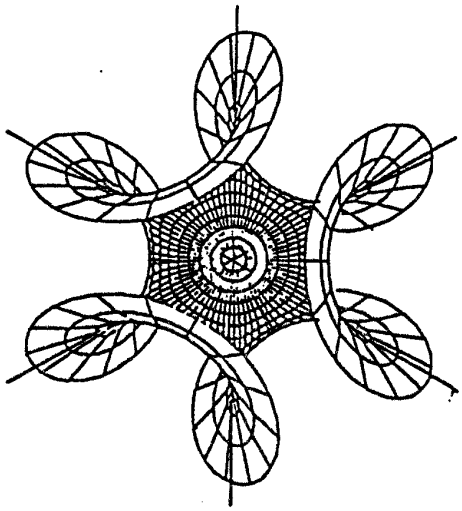

$g(z) = z^2$

and higher order Enneper surfaces (2.1.3).

In all cases $dh = g \cdot dz$.

Parametrization by geodesic polar coordinates.

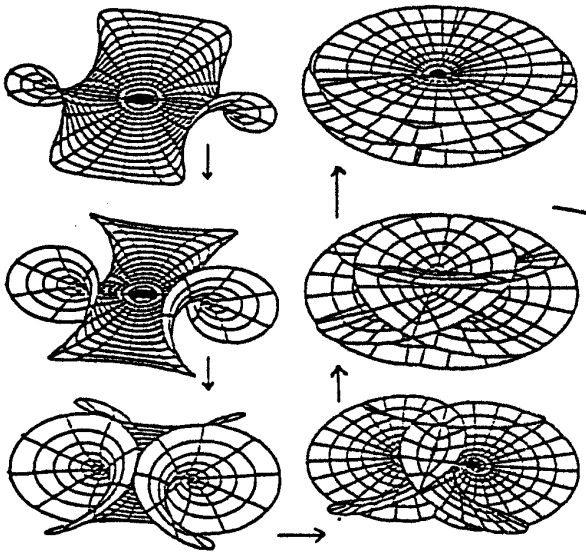

View from increasing distance

$(g(z) = z^2)$

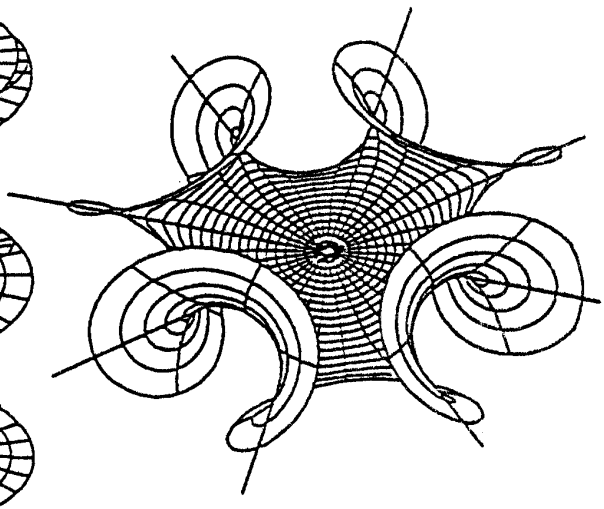

$g(z) = z^3$

2.1.3 Higher order Enneper surfaces.

$$g(z) = z^k \quad , \quad dh = z^k dz \quad .$$

The only difference is that there are more symmetry lines:

$$\frac{dg}{g}(\dot{m}) \cdot dh(\dot{m}) = k \cdot z^{k+1} \begin{cases} \in \mathbb{R} & : \text{planar symmetry line} \\ \in i\mathbb{R} & : \text{straight symmetry line} \end{cases} ,$$

and the end winds $(2k + 1)$ times around the vertical axis.

Note that the Enneper surfaces are very deformable: let $P(z)$ be a polynomial of degree $(k - 1)$ and consider the data

$$(2.1.4) \quad g(z) = z^k + \varepsilon \cdot P(z) \quad , \quad dh = g(z) \cdot dz \quad .$$

The behaviour near ∞ stays (asymptotically) the same, and all these surfaces are without branch points.

Remark. The simplest higher genus minimal immersions are obtained from highly symmetric Riemann surfaces $M^2 \setminus \{1 \text{ point}\}$ with Weierstrass data such that the behaviour near the puncture is the same as for some Enneper surface (3.2.2, 5.5.1/2).

2.1.5 The catenoid.

$$g(z) = z \quad , \quad dh = \frac{dz}{z}$$

$$\mathrm{Re}\left(\psi(r\cdot e^{i\varphi}) \right) = \left((-\,r - \tfrac{1}{r})\cos\varphi,\ (-\,r - \tfrac{1}{r})\sin\varphi,\ \log r \right) .$$

With (1.5.2) we see the symmetries of the explicit formula also from the Weierstrass data:

All meridians and the equator ($= S^1$) allow Riemannian reflections for the metric

$$ds = \left(|z| + \frac{1}{|z|} \right)\cdot \left| \frac{dz}{z} \right| \quad .$$

But now we have for *all* these symmetry lines σ

$$\frac{dg}{g}(\dot\sigma)\cdot dh(\dot\sigma) \in R \quad ,$$

i.e., they are all lines of reflectional symmetry; the surface, therefore, is a surface of revolution with a symmetry plane perpendicular to the rotation axis.
This is an example where Weierstrass data are given on $S^2\setminus\{0,\infty\}$, but dh is *not* the differential of a function on this Riemann surface: integration once around 0 adds $2\pi i$ to ψ_3. The *conjugate* minimal surface is therefore not an immersion of $S^2\setminus\{0,\infty\}$ but of its universal cover. It is called the helicoid. The planar symmetry lines on the catenoid are straight symmetry lines on the helicoid immersion, and the symmetry group is a

skrew motion.

Next I have to explain that the application of (1.5.2) does not always succeed as automatically as the first two examples suggest. In the derivation of the Weierstrass representation a vertical axis was distinguished. As a result, we can detect with (1.5.2) horizontal and vertical symmetry lines without computation — but this is not true for other symmetry lines. As an example consider the

2.1.6 Horizontal catenoid.

$$g(z) = z \quad , \quad dh = \left(z - \frac{1}{z} \right)^{-2} \cdot \frac{dz}{z} \quad .$$

First, the Riemannian metric is complete on $S^2 \setminus \{\pm 1\}$: curves which run into the punctures have infinite length and curves which run "radially" into 0 , ∞ have finite length.
Second, reflection in $\mathbb{R}$, $i\mathbb{R}$, S^1 preserves the metric

$$ds = \left(|z| + \frac{1}{|z|} \right) \cdot \left| \frac{1}{z^2 + z^{-2} - 2} \right| \cdot \left| \frac{dz}{z} \right|$$

and these metric symmetry lines are also curvature lines (since $\frac{dg}{g}(\dot{\sigma}) \cdot dh(\dot{\sigma}) \in \mathbb{R}$), hence planar symmetry lines on the surface. The other symmetries — namely reflection in circles through $+1$, -1 — cannot be seen without computation.

Finally, do the Weierstrass data lead to an immersion of $S^2 \setminus \{\pm 1\}$ or do the punctures cause the same problems as for the helicoid ? We could compute residues to check this, but there is a more effective way.
We introduce the following

2.1.7 Notation. A translational symmetry of a minimal surface, which is obtained by integrating Weierstrass data around a non-trivial closed curve on the Riemann surface, is called a

period of the Weierstrass data.

Integration of Weierstrass data leads to a minimal *immersion* of the Riemann surface iff all periods vanish.

Next we have the following useful

2.1.8 Observation. If a symmetry line runs through a puncture, then a closed curve around the puncture can be assumed symmetric with respect to the symmetry line. The integrated curve on the minimal surface then consists of two congruent pieces which are symmetric

either with respect to the plane of a reflection or with respect to the axis of a 180°-rotation.

The period is the difference vector between the endpoints of the two pieces of the curve, it is therefore

either perpendicular to the plane of the reflection or perpendicular to the axis of the 180°-rotation.

From this we see without computation: the punctures ± 1 above cause no periods, since two nonparallel symmetry planes run through each puncture.

There is another family of explicit examples which are interesting because they are embedded near one puncture, but very differently from the catenoid. They can be found by using only powers of z for the Gauss map and the differential:

2.1.9 Explicit examples with one planar end.

$$g(z) = z^{k+1} \quad , \quad dh = z^{k-1}dz$$

$$\psi(z) = \left(\frac{1}{2}\left(-\frac{1}{z} - \frac{z^{2k+1}}{2k+1} \right), \frac{i}{2}\left(-\frac{1}{z} + \frac{z^{2k+1}}{2k+1} \right), \frac{z^k}{k} \right) .$$

Clearly, the metric

$$ds = \left(|z|^{2k} + |z|^{-2} \right) \cdot |dz|$$

is complete on $S^2 \setminus \{0,\infty\}$. Reflections in all meridians are Riemannian isometries (giving again an intrinsic isometry group). The end at ∞ winds $(2k+1)$ times around the vertical axis, as in the Enneper case. The other end however (around the

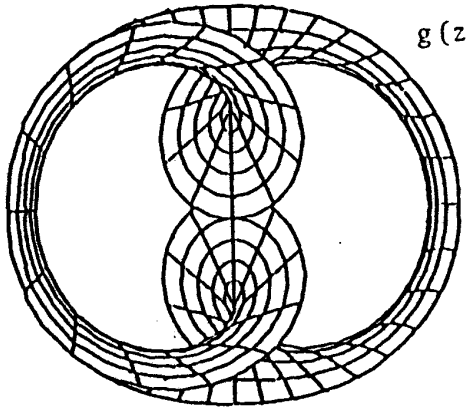

$g(z) = z^2$

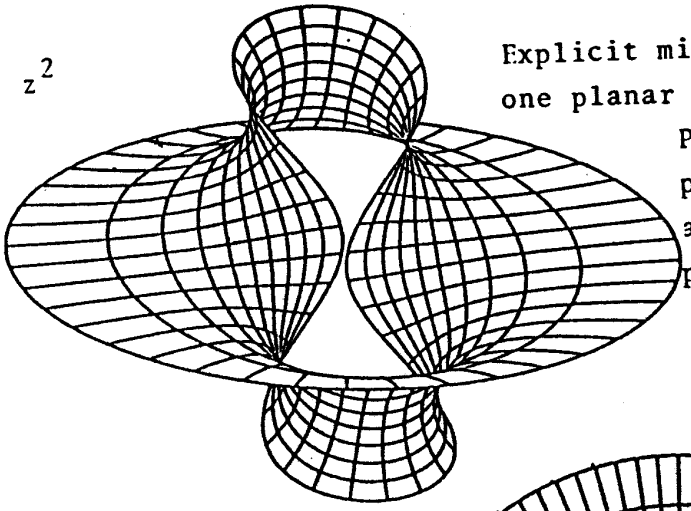

Explicit minimal surfaces with one planar end (2.1.9).

Parametrization by polar coordinates around the antipodal punctures.

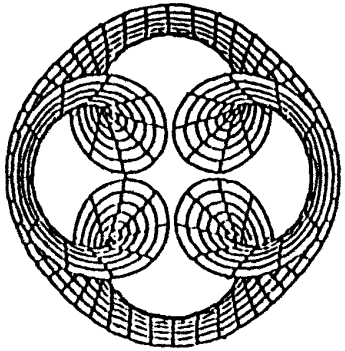

$g(z) = z^3$

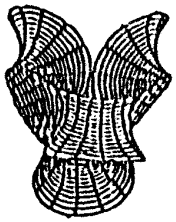

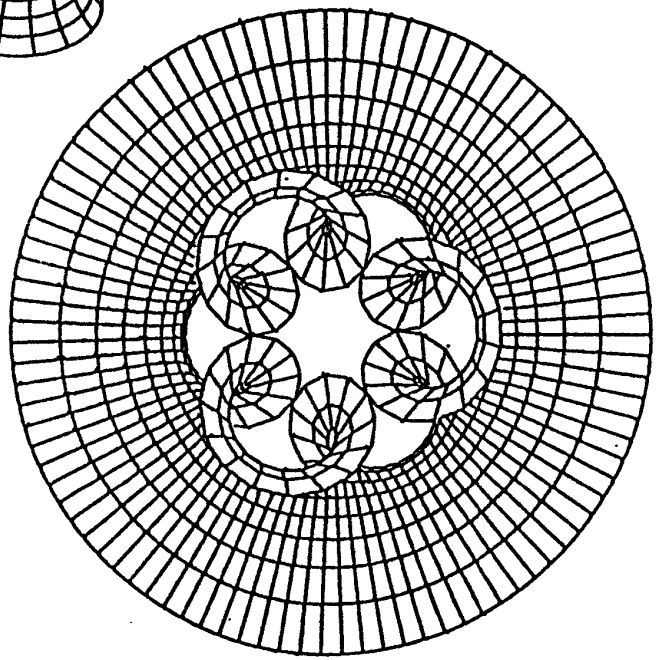

$g(z) = z^4 \rightarrow$

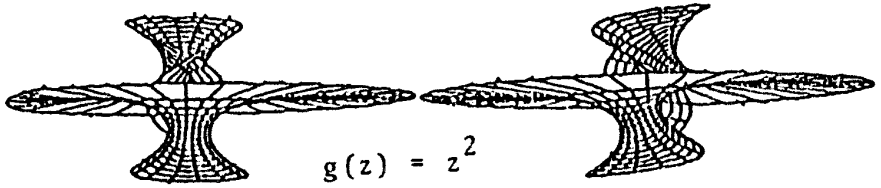

$g(z) = z^2$

puncture 0) is

asymptotic to the x-y-plane !

Fewer of the meridians $m(r) = r \cdot z$ are also extrinsic symmetry lines then in the Enneper case (2.1.3):

$$\frac{dg}{g}(\dot{m}) \cdot dh(\dot{m}) = (k + 1) \cdot z^k \quad .$$

For $k = 1$ we have just one vertical planar symmetry line (R) and one horizontal straight line (iR) run through the punctures. We know from the explicit integration that there are no periods, but the symmetry lines and (2.1.8) give this directly from the Weierstrass data.

2.2. The behaviour of a minimal surface near a puncture depends only on the expansion of g and dh near the puncture. In particular, we can study possible embedded ends (punctured discs) already in spherical examples. We may assume that the puncture is at 0 (local coordinate), and by rotating the minimal surface we may also assume $g(0) = 0$. An embedded end is a graph near the puncture and the only possibility to avoid the multiple winding of an Enneper end is:

(2.2.1) $\frac{1}{g} \cdot dh$ has a double pole at the embedded end.

One then checks quickly, that the catenoid and planar ends, which we already know, exhaust all possibilities. In particular

we note (independent of the rotation to achieve $g(0) = 0$):

(2.2.2) At a catenoid end the Gauss map is simple.

(2.2.3) At a planar end the Gauss map is branched.

(2.2.4) At an embedded end where $g \neq \infty$: $\frac{1}{g} \cdot dh$ has a double pole.

To illustrate that this knowledge is already an important part of the general picture I quote two results (which are proved with the maximum principle):

2.2.5 Theorem (Hoffman-Meeks[HM4]). A complete properly immersed minimal surface contained in a halfspace is the plane.

Here "properly immersed" is important because of the

2.2.6 Example (Rosenberg-Toubiana[RT]). There exist complete minimal annuli which are vertically bounded from above and below and which are transversal to the horizontal planes which they meet.

2.2.7 Theorem (R. Schoen[rSn]). A complete minimal surface of finite total curvature with only two ends and such that the two ends are parallel and embedded is the catenoid.

This implies: A minimal embedding of a punctured Riemann surface of genus > 0 must have one downward catenoid end, one upward catenoid end (to prevent it from being in a halfspace) and at

least one further end. The simplest examples (any genus ≥ 1) have one planar end between two catenoid ends (3.5, 5.5.5).

2.3 Examples with more than two punctures.

More punctures will make the period problem more difficult. On the other hand, periods can also help: We found no interesting embedded punctured spheres, but we will find a rich class of spherical embedded minimal surfaces with one period. The most famous one is

2.3.1 Scherk's saddle tower [Sk].

$$g(z) = z \quad , \quad dh = \frac{1}{z^2 + z^{-2}} \cdot \frac{dz}{z} \quad .$$

The Riemannian metric

$$ds = \left(|z| + |z|^{-1} \right) \cdot \left| z^2 + z^{-2} \right|^{-1} \cdot \left| \frac{dz}{z} \right|$$

is complete on $S^2 \setminus \{\pm 1, \pm i\}$, in particular 0 , ∞ are at finite distance. S^1 , R , iR and the 45°-meridians allow Riemannian reflections and (1.5.2 again !)

$$\frac{dg}{g}(\dot{\sigma}) \cdot dh(\dot{\sigma}) \begin{cases} \in R & \text{for } \sigma = S^1, R, iR, \text{ planar symmetry} \\ \in iR & \text{for } \sigma = e^{\pm i \cdot \pi/4}, \ 180^\circ\text{-symmetry} . \end{cases}$$

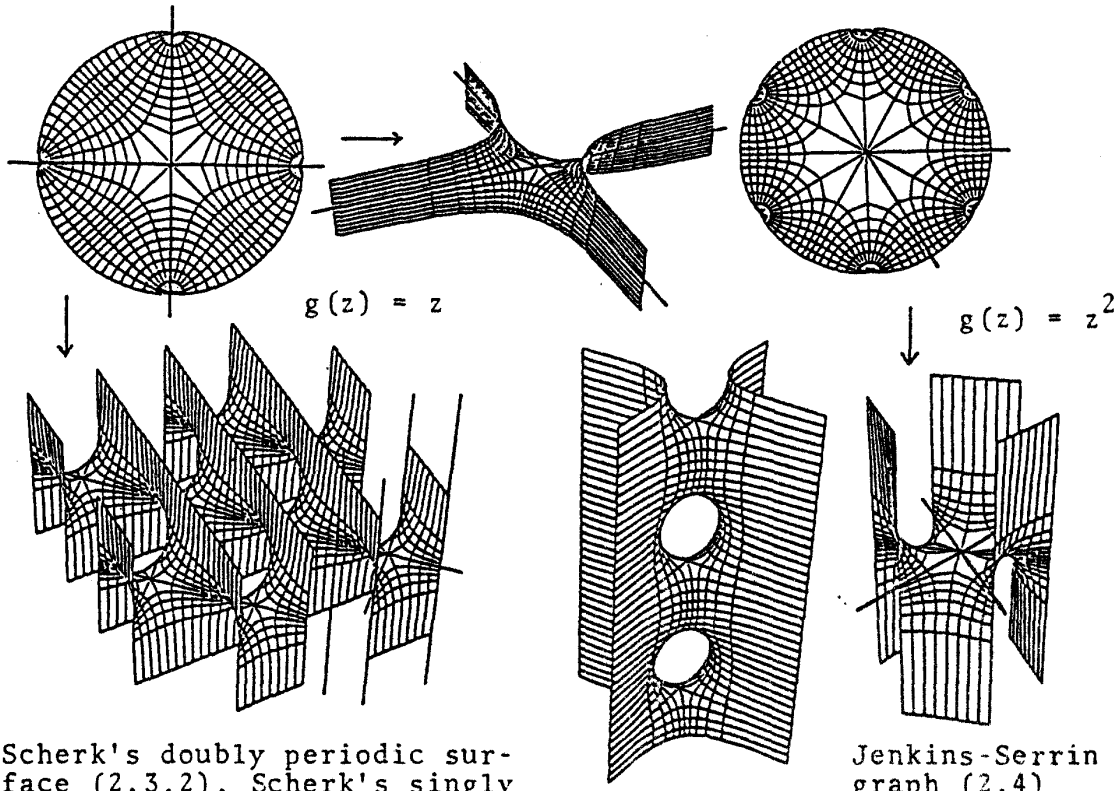

Scherk's doubly periodic surface (2.3.2), Scherk's singly periodic saddle tower (2.3.1) a conjugate pair.

Parametrization by level lines.

Jenkins-Serrin graph (2.4) and conjugate

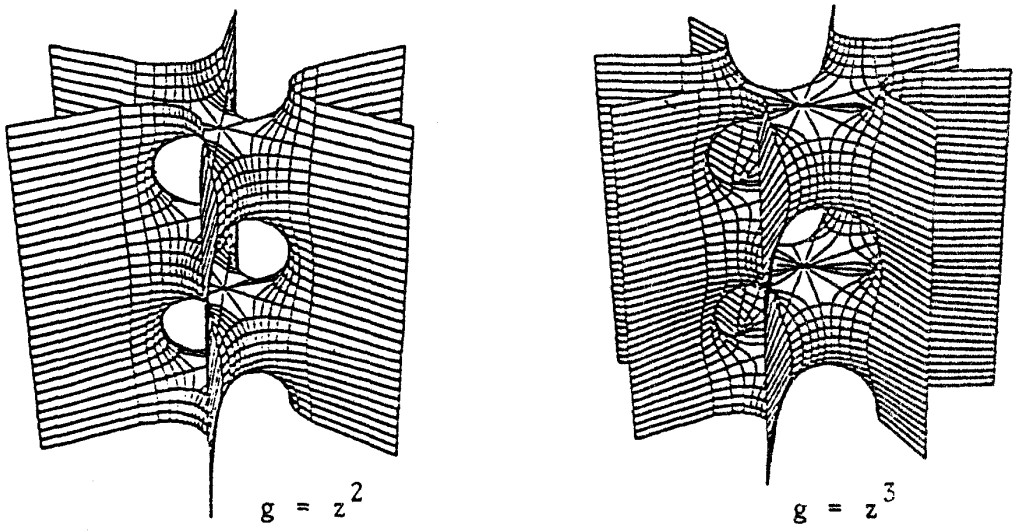

Higher order saddle towers (2.3.3)

In particular we have a horizontal symmetry line (S^1) through each puncture, therefore all periods are vertical — and equal up to sign, since other symmetries permute the punctures.
The Weierstrass image of the unit disc is therefore a minimal surface bounded by four *horizontal* symmetry lines which moreover lie in only *two parallel* planes. Extension by reflection in these planes gives a complete minimal surface with one vertical period (2.1.8). This surface is embedded if the fundamental piece is embedded. We will see later (in 2.4) in a more general situation that it is in fact a graph. Then we will also meet the conjugate surface, in this simplest case also embedded:

2.3.2 Scherk's doubly periodic minimal surface.

$$g(z) = z \quad , \quad dh = i\cdot(z^2 + z^{-2})^{-1}\cdot \frac{dz}{z} \quad .$$

As with Enneper's surface one can easily obtain more complicated ones by increasing the degree of the Gauss map.
The previous discussion applies also to the

2.3.3 Higher order symmetric saddle towers.

$$g(z) = z^{k-1} \quad , \; dh = \left(z^k + z^{-k} \right)^{-1}\cdot \frac{dz}{z} \quad ,$$

$2k$ punctures at roots of 1 .

(Of course the number of symmetry meridians increases with k .)

In addition one can also move the $2k$ punctures. For the following data all the planar symmetry lines (S^1 and $z^k \in R$) remain but no more straight lines exist on the surface:

2.3.4 Less symmetric saddle towers [Ka1].

$$g(z) = z^{k-1} \quad , \quad dh = \left(z^k + z^{-k} - 2 \cos k\varphi \right)^{-1} \cdot \frac{dz}{z} \quad ,$$

$$0 < \varphi \leq \frac{\pi}{2k} \; ; \text{ punctures at } \; e^{\pm i\varphi} \cdot e^{2\pi i \cdot \frac{l}{k}}$$

$$(l = 0 \, , \cdots , \, k-1) \; .$$

(Only the planar symmetry lines were needed to conclude that there are only vertical periods for all the punctures and these agree (up to sign)).

What happens with these examples as $\varphi \longrightarrow 0$? Punctures move together in pairs to become double poles of dh , they moreover lie also on vertical symmetry planes. These k punctures therefore (2.1.8) have no periods and the ends are catenoid ends (2.2.2/4).

(2.3.5) The surfaces (2.3.4) with $\varphi = 0$ are the k-noids of Jorge-Meeks.

The k-noids are not embedded. Indeed, as φ moves away from $\frac{\pi}{2k}$, pairs of neighbouring halfplane wings cross each other and then the saddle towers are no longer embedded.

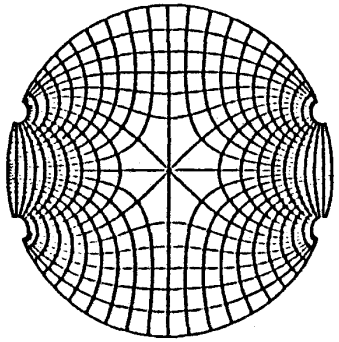

Less symmetric Scherk surfaces (2.3.4), $g(z) = z$, a conjugate pair.

Parametrization by level lines.

↖ This parametrization is also used for the 4-noid (2.3.8).

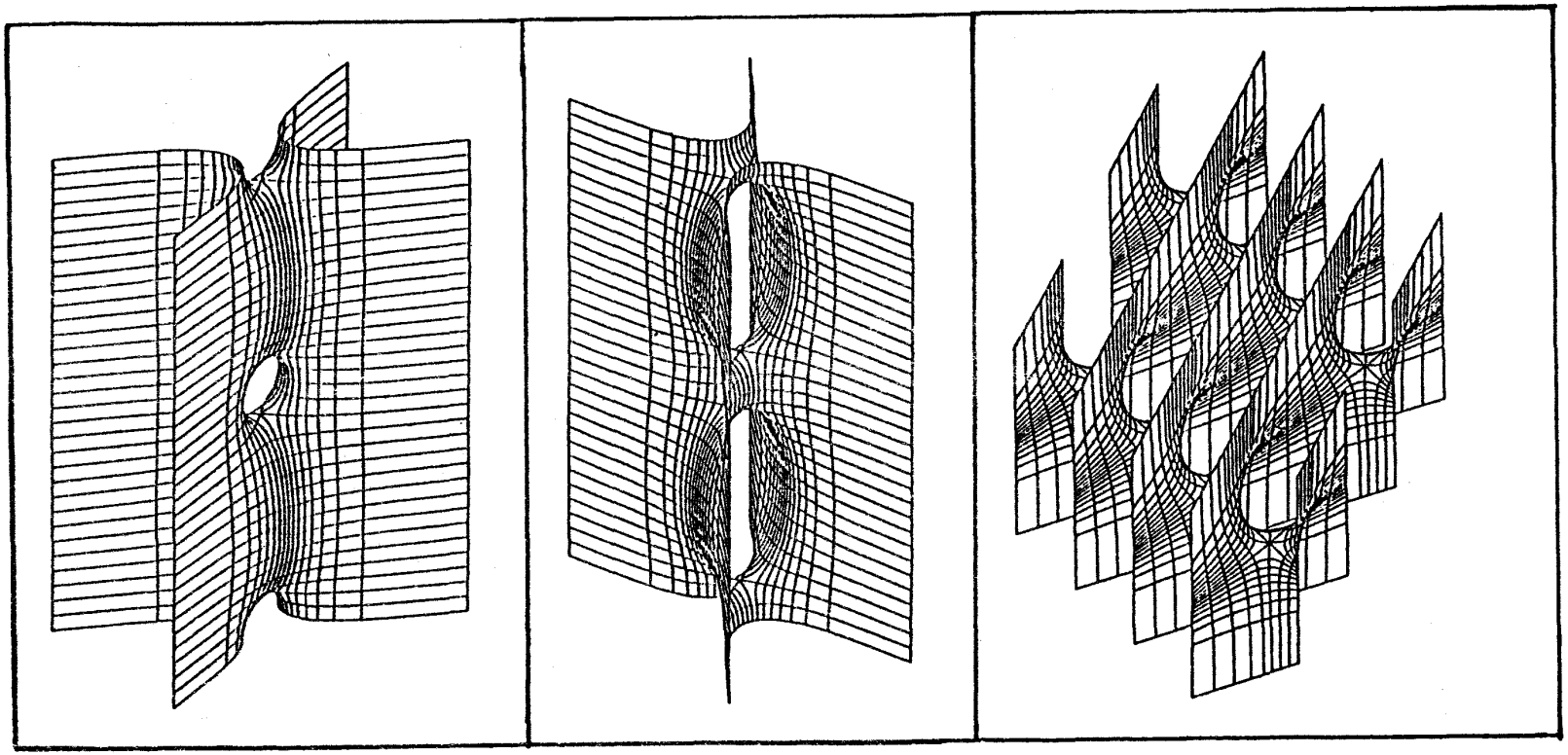

Less symmetric saddle tower (2.3.4), $g(z) = z^2$.

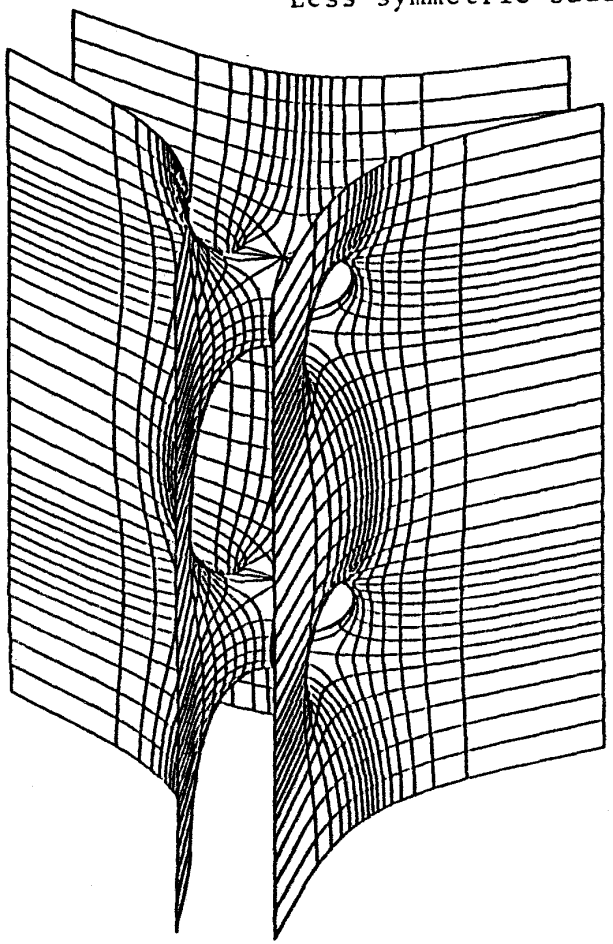

Top view, for somewhat closer pairs of punctures, shows that the wings may intersect, compare (2.4). (By Hoffman/Wohlgemuth, Amherst)

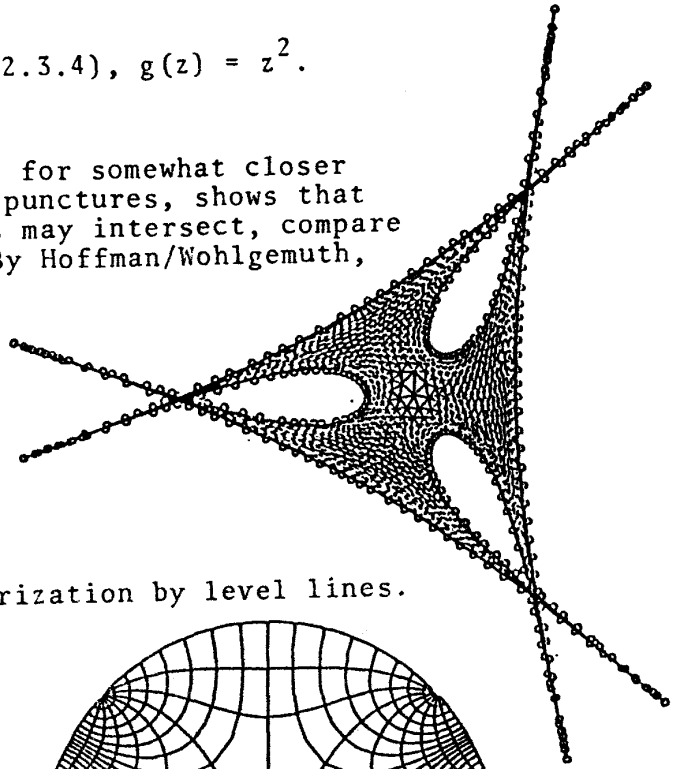

Parametrization by level lines.

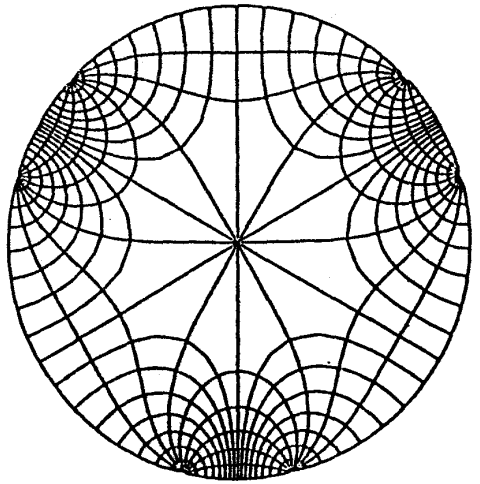

Deformed Scherk surfaces [Ka 1].

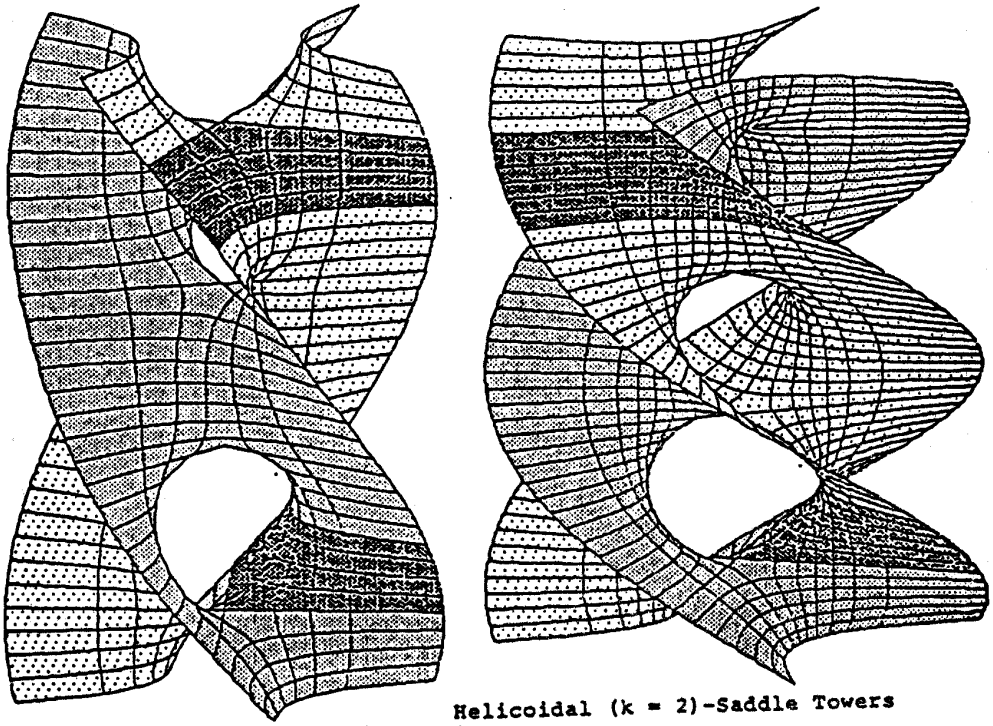

Helicoidal (k = 2)-Saddle Towers

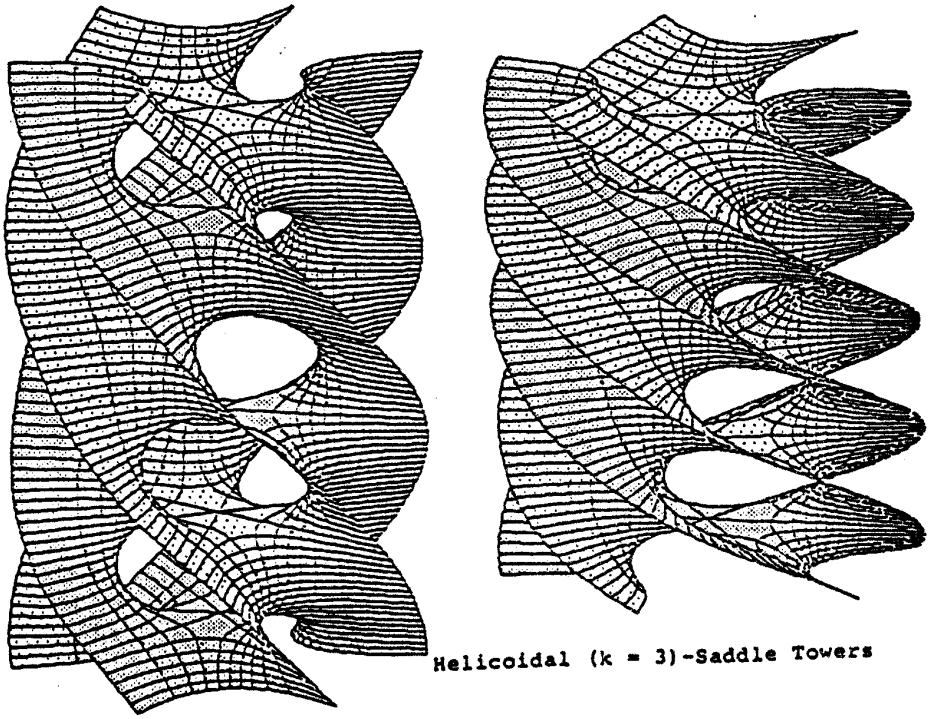

Helicoidal (k = 3)-Saddle Towers

Experience with the Enneper surfaces suggests that these examples with a high order branch point of the Gauss map should have deformations. We postpone this to (2.4), because another method is used. Instead we consider some 4-noids which illustrate more complicated Gauss maps.

First we deform the symmetric 4-noid so that the ± 1 -catenoid ends become *smaller* than the $\pm i$ -catenoid ends. Since the position of the punctures remains fixed, the deformation has to be achieved by splitting the multiple point of the Gauss map (similar to $x^3 \longrightarrow x\cdot(x^2 - a^2)$), but keeping the R , iR , S^1-symmetries. Since we want $g(S^1) \subset S^1$ we write a candidate in terms of Blaschke factors:

$$(2.3.6) \qquad g(z) = z \cdot \frac{z - r}{1 - rz} \cdot \frac{z + r}{1 + rz} \quad .$$

Now we determine (!) the differential dh .

First, dh needs simple zeros at $\pm r$, $\pm \frac{1}{r}$ to prevent that these zeros and poles of g create unwanted ends for the metric $ds = (|g| + |g|^{-1})\cdot|dh|$. Second, dh needs *double* poles at ± 1 , $\pm i$ to make catenoid ends at these punctures possible (2.2.2/4). Finally, powers of z have to be adjusted so that 0 , ∞ are at finite distance. The result is the differential for the

(2.3.7) 4-noid with two different pairs of orthogonal ends

$$dh = \left(1 - \frac{1}{r^2 + r^{-2}} (z^2 + z^{-2}) \right)\cdot\left(z^2 - z^{-2} \right)^{-2}\cdot \frac{dz}{z} \quad .$$

Clearly, the metric is indeed complete on $S^2 \setminus \{\pm 1, \pm i\}$ and has the expected symmetry lines. Therefore the punctures are $\pm e^{\pm i\varphi}$, so that they are permuted by the vertical symmetries. The differential for the

(2.3.8) 4-noid with non-orthogonal ends

$$dh := \left(1 - \frac{1}{r^2 + r^{-2}}\,(z^2 + z^{-2})\right)\cdot\left(z^2 + z^{-2} - 2\cos 2\varphi\right)^{-2}\cdot\frac{dz}{z}$$

is forced as before. All the expected symmetry lines are there. They allow a vertical period, which is usually $\neq 0$ unless we choose $2\cos 2\varphi = \frac{4r^2}{1 + r^4}$ to make res. $dh\big|_{e^{i\varphi}} \in iR$, which kills the period.
Without discussion I list some more examples for illustration purposes, see figures.

2.3.9 4-noids with two large vertical and two small nonhorizontal ends:

$$g(z) = z \cdot \frac{z^2 - R^2}{1 - r^2 z^2}$$

$$dh = \left(z^2 - R^2\right)\cdot\left(\frac{1}{z^2} - r^2\right)\cdot\left(\frac{z}{\rho} - \frac{\rho}{z}\right)^{-2}\cdot\frac{dz}{z} \quad .$$

The punctures at 0, ∞ are without periods; $\rho = \rho(r,R)$ has to be chosen to kill the horizontal periods of the punctures

Jorge-Meeks 3-noid
(2.3.6) limit of
previous saddle
towers
$g(z) = z^2$

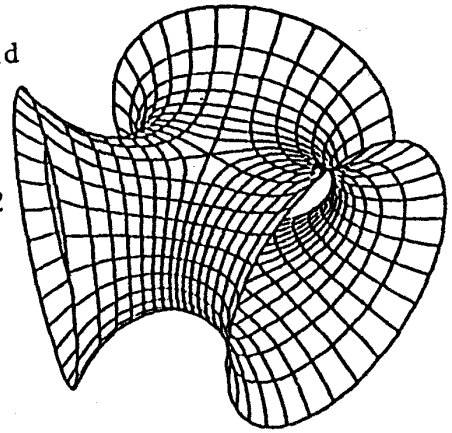

4-noids

(2.3.7)

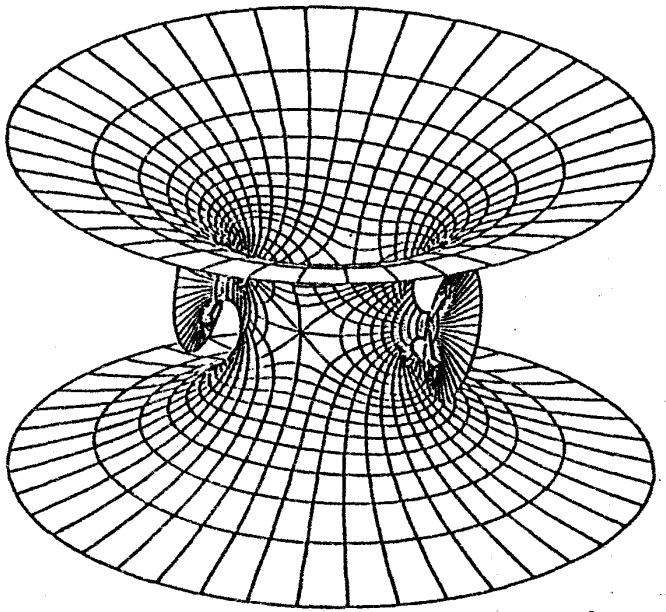

2 orthogonal symmetry planes through each puncture

Polar coordinates near all punctures of (2.3.9)

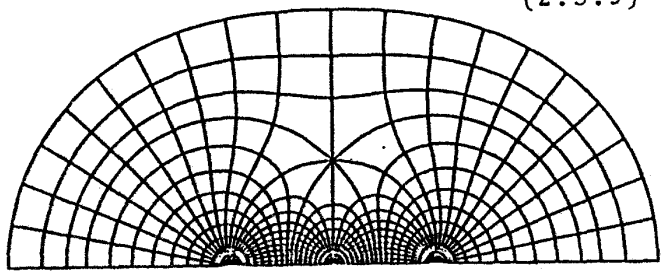

(2.3.9)

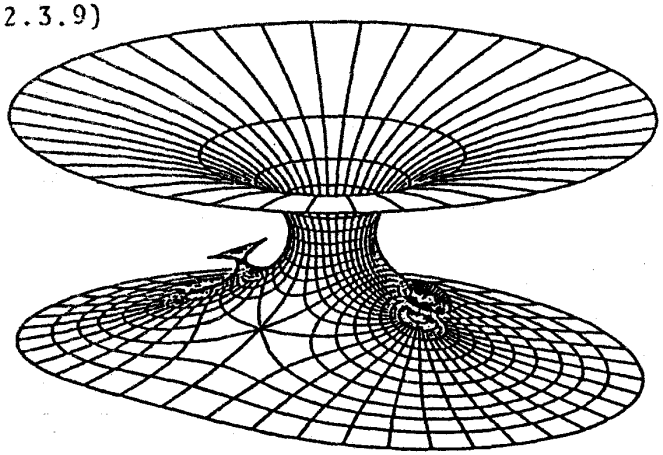

More 4-noids (2.3.8)

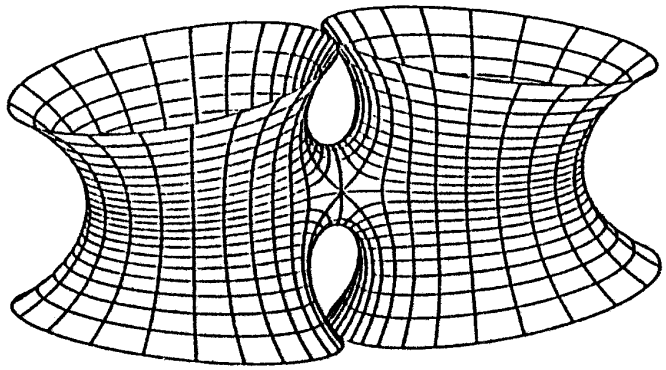

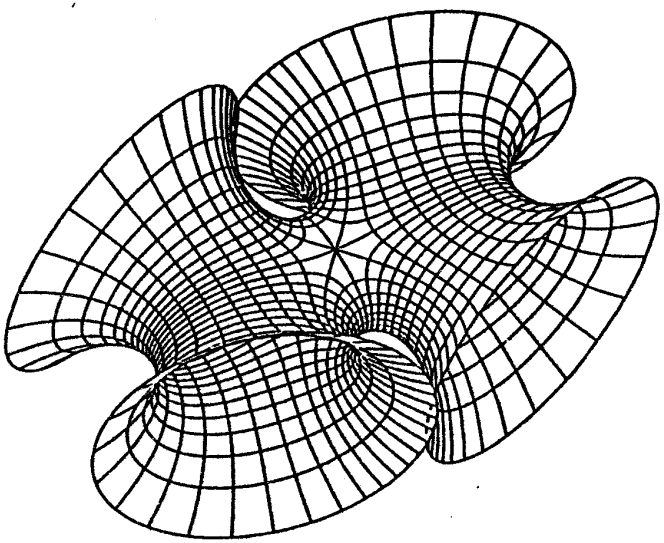

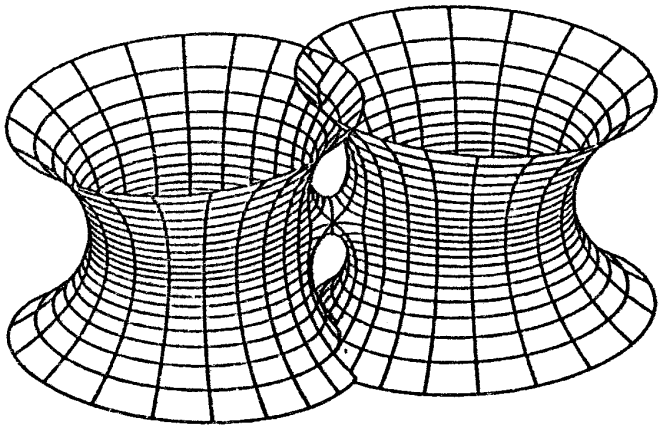

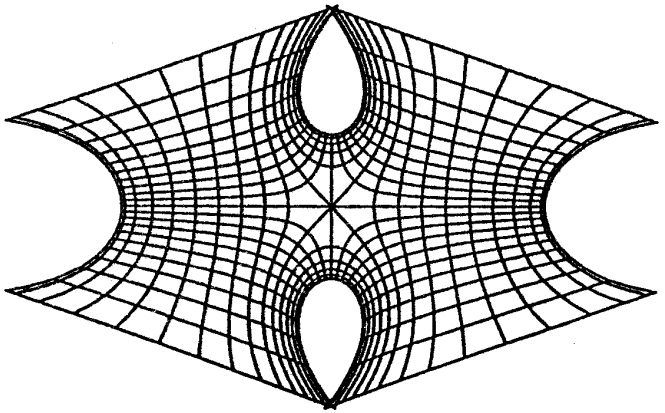

Convergence to two catenoids with common tangent plane

at $\pm \rho$.

2.3.10 Two Enneper surfaces, joined by a catenoidal annulus (or neck):

$$g(z) = z \cdot \frac{z^2 - R^2}{R^2 z^2 - 1}$$

$$dh = \left(1 - \frac{1}{R^2 + R^{-2}} \cdot (z^2 + z^{-2}) \right) \cdot \frac{dz}{z} \quad .$$

2.3.11 The same as before, but with the two Enneper ends rotated so that no symmetry lines remain:

$$g(z) = z \cdot \frac{z \cdot (R \cdot e^{i\alpha})^{-1} - R \cdot e^{i\alpha} \cdot z^{-1}}{R \cdot e^{i\alpha} \cdot z - (R \cdot e^{i\alpha} \cdot z)^{-1}}$$

$$dh = e^{i\varphi} \cdot \left(z^2 + z^{-2} - R^2 \cdot e^{2i\alpha} - (R^2 \cdot e^{2i\alpha})^{-1} \right) \cdot \frac{dz}{z} \quad .$$

To kill the vertical period choose:

$$tg\ \varphi = - tg\ 2\alpha \cdot \left(R^2 - \frac{1}{R^2} \right) \cdot \left(R^2 + \frac{1}{R^2} \right)^{-1} \quad .$$

2.3.12 Replace the catenoid ends of a 3-noid by Enneper ends:

$$g(z) = z^2 \cdot \frac{z^3 - R^3}{1 - R^3 z^3}$$

$$dh = \frac{1 - (R^3 + R^{-3})^{-1} \cdot (z^3 + z^{-3})}{(z^3 + z^{-3} - 2)^2} \cdot \frac{dz}{z} \quad .$$

Doubled Enneper surfaces:

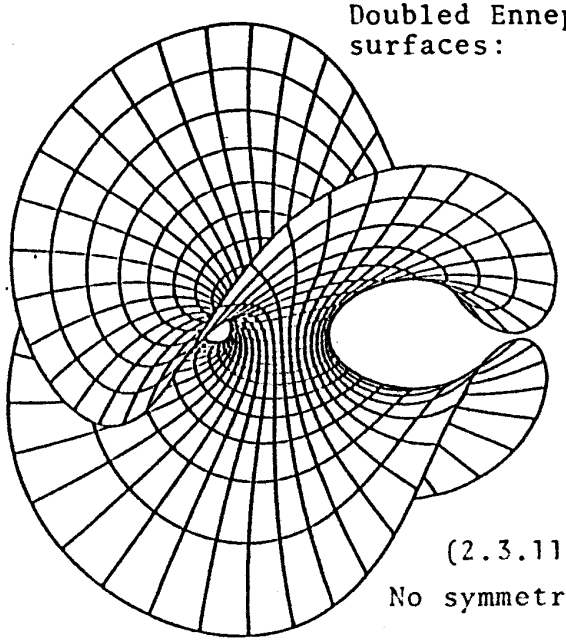

(2.3.11)

No symmetry planes

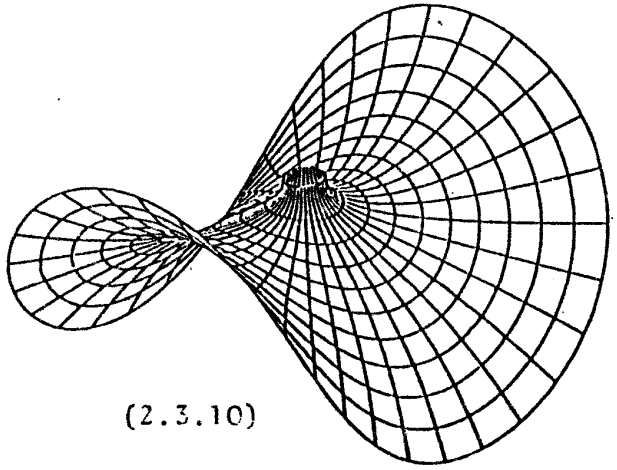

(2.3.10)

The "neck" does not join the "midpoints" of the two Enneper surfaces

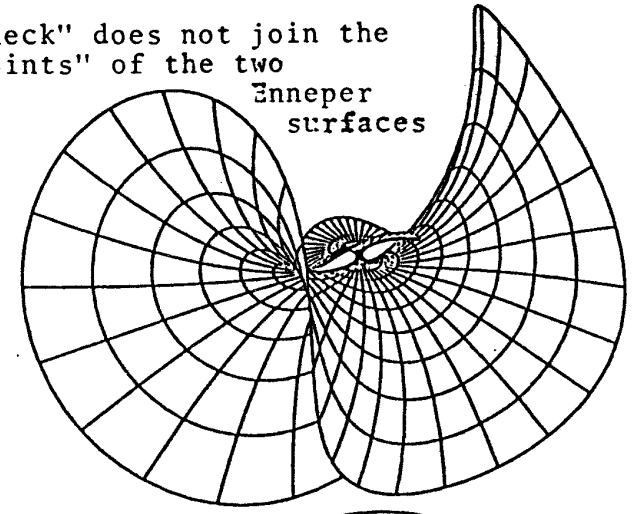

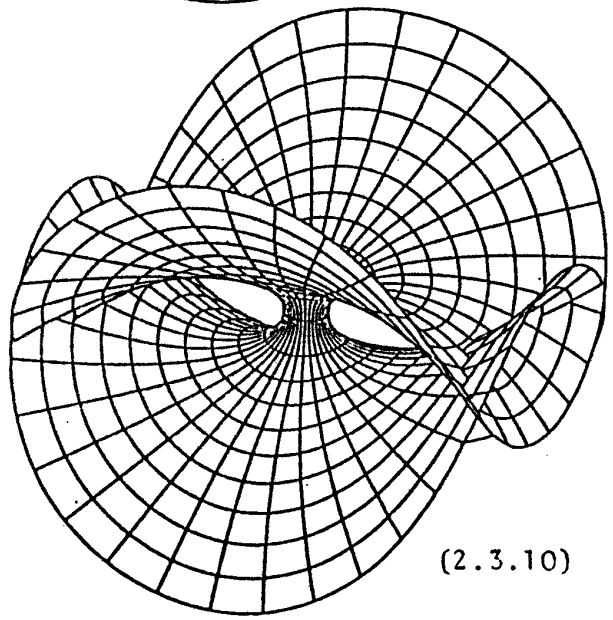

(2.3.10)

2.4. The conjugate construction of embedded saddle towers.

First, I derive a useful fact which I owe to R. Krust (Paris VII), including the proof. Note that it implies the embeddedness statements in [Sm] immediately.

2.4.1 Theorem (R. Krust[Kr]). If a piece of a minimal surface F is a graph over a convex domain D then the conjugate piece F^* is also a graph.

Proof: From the Weierstrass data we define two holomorphic functions:

$$\sigma := -\int g\, dh \quad , \quad \tau := \int \frac{1}{g}\, dh \quad .$$

The projection into the x-y-plane, or conveniently the $(x + iy)$-plane, can be written in terms of σ and τ :

$$\pi := F_1 + iF_2 = \bar{\tau} + \sigma \quad (F_1 = \mathrm{Re}(\tau + \sigma) \quad \text{etc.})$$

$$\pi^* := F_1{}^* + iF_2{}^* = i\bar{\tau} - i\sigma \quad .$$

The graph assumption says $|g| > 1$ and therefore $|g \cdot dh| > \left|\frac{1}{g} \cdot dh\right|$ (on nonzero vectors). Since F is a graph over a convex domain we find for any two points $p_0 \neq p_1 \in D$ a curve γ on the Riemann surface such that $\pi \circ \gamma$ is the line segment from p_0 to p_1 ; we also assume that $\pi \circ \gamma$ is linearly parametrized. This gives

$$d\pi\cdot\gamma'(t) = \left(\overline{\frac{1}{g}\cdot dh} - g\cdot dh \right)\cdot\gamma'(t)$$

$$= p_1 - p_0 \neq 0 \quad .$$

We rotate the conjugate projection by 90° and scalar multiply by $p_1 - p_0$:

$$< p_1 - p_0,\ i\cdot\pi^*\cdot\gamma\Big|_0^1 >$$

$$= < p_1 - p_0,\ -\int_\gamma \left(g\cdot dh + \overline{\frac{1}{g}\cdot dh} \right) >$$

$$= -\,\mathrm{Re}\left((p_1 - p_0)\cdot\int_\gamma \left(\overline{g\cdot dh} + \frac{1}{g}\cdot dh \right) \right)$$

$$(\ < z, w > = \mathrm{Re}(z\cdot\bar{w})\ )$$

$$= \int_0^1 \mathrm{Re}\left(\left(\overline{g\cdot dh} + \frac{1}{g}\cdot dh \right)(\gamma')\cdot\left(g\cdot dh - \overline{\frac{1}{g}\cdot dh} \right)(\gamma') \right) dt$$

$$(\text{insert } p_1 - p_0\ )$$

$$= \int_0^1 \left(|g\cdot dh(\gamma')|^2 - \left|\frac{1}{g}\cdot dh(\gamma')\right|^2 \right) dt > 0$$

$$(\ |g| > 1\ ) \quad .$$

This prove $\pi^*\cdot\gamma(0) \neq \pi^*\cdot\gamma(1)$, i.e., F^* is a graph.

The main analytic ingredient in our conjugate construction is a result by Jenkins - Serrin [JS]. They proved that certain Dirichlet problems with infinite boundary values can be solved for minimal surface graphs. We quote a special case in which their sufficient condition becomes much more explicit than in their more general case.

2.4.2 **Theorem (Jenkins-Serrin).** Let D be a convex $2k$-gon with all edges of the *same* length. Mark the edges alternatingly $+\infty$, $-\infty$. Then there is a unique minimal graph over D which converges to $\pm\infty$ as one approaches the edges of D. As a minimal surface this graph is bounded by the vertical lines over the vertices of D. It has finite total curvature.

Analytic continuation of the Jenkins-Serrin graph by 180°-rotation around all vertical lines gives a complete minimal surface. Any two such rotations define a translational symmetry. The translations identify two adjacent Jenkins-Serrin-pieces to a sphere with $2k$ punctures. The Gauss map is well defined on this sphere, i.e., it is a rational function. The degree is $(k - 1)$ since along each vertical line the normal rotates by $(\pi$-(exterior angle of D)). The translation group generated by the vertical rotations is in some more cases discret, but *only* if $k = 2$, i.e., D an equilateral 4-gon, is the complete surface embedded. These embedded surfaces are the one-parameter family (angle of the 4-gon) of

Scherk's doubly periodic surfaces (2.3.2).

2.4.3. Finally, we consider the conjugate piece F^* of a Jenkins-Serrin-graph F [Ka1]. By R. Krust's result the conjugate is again a graph, hence embedded. The boundary consists of horizontal lines of reflectional symmetry which are conjugate to the vertical lines of F. The intrinsic Riemannian

distance between adjacent vertical lines is of course the same as between the corresponding planar symmetry lines. Since the Gauss map has a limiting normal at the puncture, the intrinsic distance equals in both cases the euclidean distance in R^3 .
In other words: The vertical periods of the conjugate piece F^* are equal to the edgelengths of D — which were all the same by construction. The horizontal symmetry lines of the embedded conjugate piece therefore lie in only *two* horizontal planes. Extension by reflection builds an *embedded saddle tower*. The number of deformation parameters of an equilateral 2k-gon is (2k - 3), more than we found for Enneper surfaces with the same degree of the Gauss map.

2.5 **Examples with planar ends only.** In this case the differentials of the Weierstrass integrand are without residues and therefore integrate to rational functions. These surfaces have been studied in detail by R. Bryant [Br].

3. Minimal Surfaces which are parametrized by Punctured Tori

3.1 Elliptic Functions.

We will have to work with holomorphic maps $f : T^2 \longrightarrow S^2$ ("elliptic functions") in the same way as we used rational functions on S^2 in the previous lecture. In particular we will need to know some simple elliptic functions together with their symmetries. I will use the Riemann mapping theorem to describe such functions because in this way we get the desired symmetries by definition.

The Riemann mapping theorem gives us for every pair of simply connected domains $B , D \subsetneq \mathbb{C}$ a *biholomorphic* map $f : B \longrightarrow D$. Such an f is unique if we prescribe at some $b \in B$ the value $f(b)$ and the phase of $f'(b)$. — If moreover B and D are bounded by piecewise analytic arcs then f extends *continously* to the boundary. This allows us to use a more convenient normalizing condition: we can prescribe for *three* boundary points of B their values in ∂D . Furthermore, f can be analytically continued by *reflection* in corresponding analytic subarcs of ∂B and ∂D .

Finally, f' does *not* vanish at interior points of these analytic subarcs (and of course not in B). With this knownledge it is easy to define elliptic functions on rectangular tori :

Consider a rectangle B :

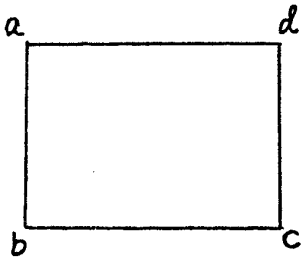

and the quarter circle D :

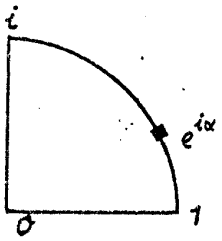

The Riemann mapping theorem and the normalizing condition $\gamma(a) = i$, $\gamma(b) = 0$, $\gamma(c) = 1$ define a unique map $\gamma : B \longrightarrow D$. The value $\gamma(d) = e^{i\alpha}$ depends on the ratio of the rectangle ; we call α the *conformal parameter* of the rectangle in the range of γ .

Analytic continuation by reflection in the straight lines through b and $0 = \gamma(b)$ defines γ from the union of four such rectangles to the unit disc. This shows also that γ' does *not* vanish *except* in d and the reflected points of d . — Two more such reflections define γ on a still larger rectangle and onto the twice covered Riemann sphere; finally, this map can be extended as a doubly periodic map.

Since the vertices a, b, c, d will play no further role, I find it useful to write the *values* of γ at these points into the *domain*. This also emphasizes the symmetries.

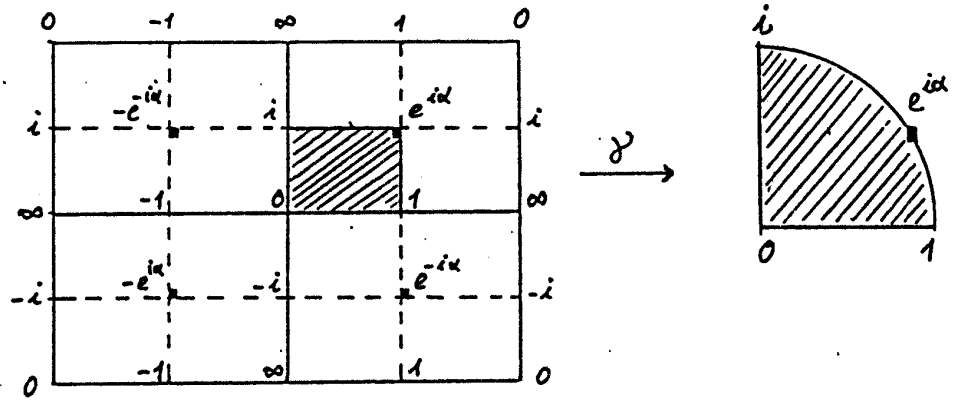

Domain with distinguished *values* of γ .

The first rectangle (before the analytic continuation) is shaded. The branch points of γ are marked. The doubly periodic extension is clear.

To show the effectiveness of this definition, we read the differential equation of γ from this picture. The function $\frac{\gamma'}{\gamma}$ has zeros at the (simple) branch points of γ , and $\frac{\gamma'}{\gamma}$ has poles at the zeros and poles of γ . Therefore

$$(3.1.1) \qquad \left(\frac{\gamma'}{\gamma}\right)^2 = (\text{pos. const.})\cdot(\gamma^2 + \gamma^{-2} - 2\cos 2\alpha)$$

(Proof: The functions on both sides have the same zeros and poles

and therefore are proportional; both functions are positive on the segment between 0 and 1 . — The positive constant depends on the scale of the domain rectangle, it is irrelevant for our purposes.)

Since γ is a degree 2 elliptic function, there should be a simple relation with the Weierstrass p-function. Indeed

$$q := i \cdot \frac{\gamma + e^{i\alpha}}{e^{i\alpha} - \gamma} \qquad \text{(branch value: } q(\gamma)\Big|_{\gamma = e^{-i\alpha}} = \operatorname{ctg}\,\alpha \text{)}$$

has $0, \infty$ as double values, and the rectangle with vertices at the branch points is mapped to the upper halfplane. This *shifted* Weierstrass function will not be useful, we need the Weierstrass function with its zeros and poles at the zeros of γ . We obtain it from the following mapping problem:

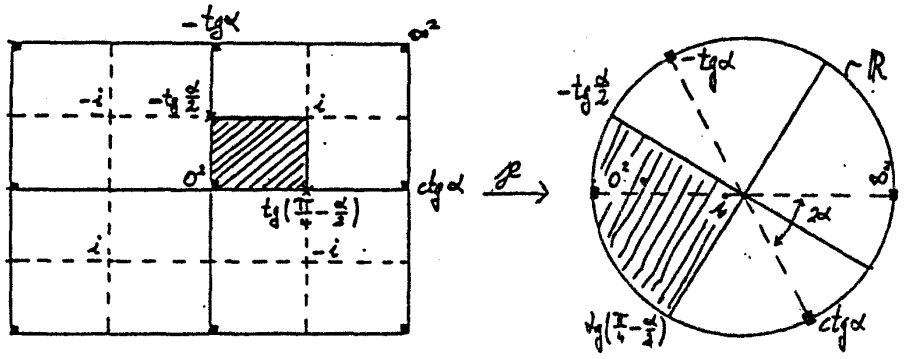

Domain with distinguished values of p-function.

(Note that we use a geometric normalization, not the Mittag Leffler expansion $p(z) = 1 \cdot z^{-2} + \cdots$.) The disc represents the upper halfplane, bounded by R , and with the symmetry lines between 0 , $\operatorname{ctg} \alpha$, ∞ , $-\operatorname{tg} \alpha$. Note that I use the *same* parameter α to describe the branch values of γ and p ; this is implied by the branch values of q above.

Again, the differential equation for p is immediate from this definition: p' has simple zeros at the three finite branch points of p , and p' has a triple pole at the pole of p , therefore:

$$(3.1.2) \qquad p'^2 = (\text{pos. const.}) \cdot p \cdot (\operatorname{tg} \alpha - p) \cdot (p + \operatorname{ctg} \alpha) \ .$$

In the same way we find an equation between γ and p :

$$(3.1.3) \qquad \gamma^2 = \frac{-\operatorname{tg} \alpha - \operatorname{ctg} \alpha}{p - \frac{1}{p} + \operatorname{tg} \alpha - \operatorname{ctg} \alpha} \ .$$

Proof: The functions on both sides have the same (double) zeros and poles; their proportionality factor is determined since $\gamma = i$ at a point where $p = -\operatorname{tg} \frac{\alpha}{2}$ and $-\operatorname{tg} \frac{\alpha}{2} + \operatorname{ctg} \frac{\alpha}{2} = 2 \operatorname{ctg} \alpha$. In the same way we find

$$(3.1.4) \qquad p' \cdot \gamma = (\text{pos. const.}) \cdot p \ .$$

The symmetries of the p-function include reflection (of the values) in circles which are not meridians or the equator S^1. Since this is less convenient we introduce one more elliptic function by the following mapping problem:

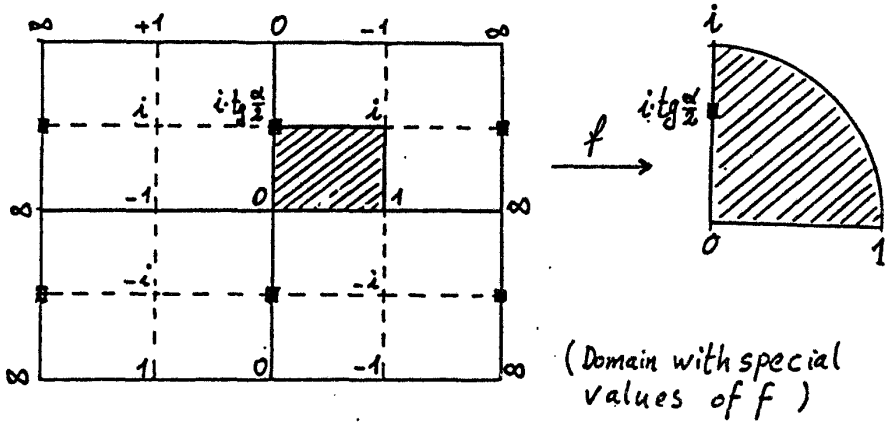

We could define f in terms of γ, p:

$$f\cdot\gamma = \frac{p}{\cos\alpha - p\cdot\sin\alpha} \quad , \tag{3.1.5}$$

but this formula does not show all the symmetries of f as obviously as the mapping definition.

3.2 First Toroidal Minimal Surfaces.

We start with a surface which is particularly simple to imagine, the following "fence of catenoids" (from discussions with D. Hoffman):

(3.2.1)

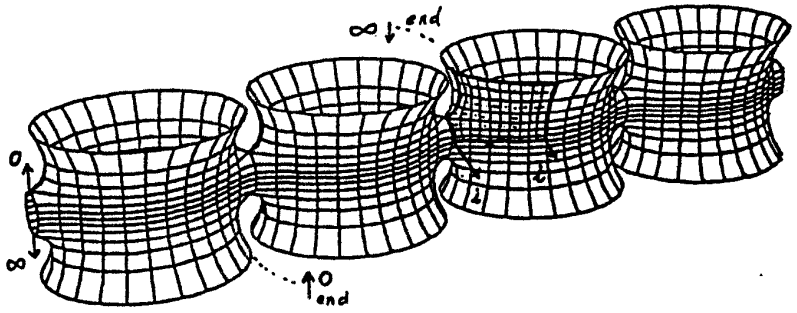

If we divide out the translational symmetry, we see a torus with two embedded catenoid ends. Recall that, by Schoen's Theorem (2.2.7), such Weierstrass data necessarily must have at least one period. The horizontal and vertical symmetry planes cut the minimal surface (or the torus with its Riemannian metric) into eight congruent pieces. The Gauss map is an elliptic function which maps the symmetry lines to S^1, R, iR; we recognize this function immediately if we write the known special *values* into the domain ($= T^2$), at the vertices of the tessalation:

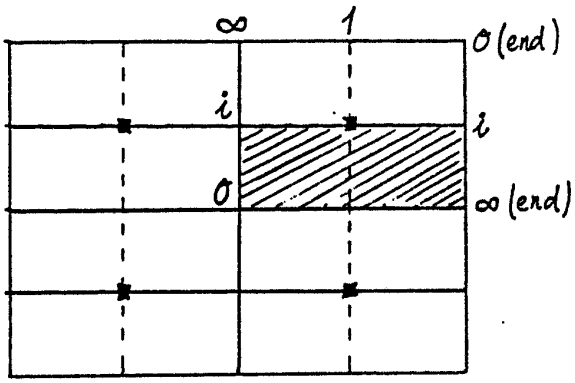

Torus with values of g

We recognize the elliptic function γ. Therefore we found the *Gauss map* of this example:

$$g := \gamma .$$

The differential dh needs simple zeros at those two points with vertical normal which are not ends (to keep these points at finite distance for 1.4.2) — and no other zeros. On a torus we need the same number of zeros and poles, but poles of dh always create ends for the Riemannian metric (1.4.2), therefore we have to put the poles of dh at the punctures — in agreement with (2.2.4). We have determined the following 0-∞-pattern for dh :

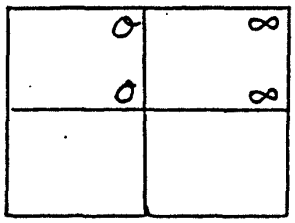

it implies the differential for the fence of catenoids: dh := f dz .

The symmetries of f and γ immediately imply that reflections in the expected symmetry lines σ are Riemannian isometries for the metric $ds = \left(|\gamma| + \frac{1}{|\gamma|} \right) \cdot |f||dz|$.
It is also immediately that all these are curvature lines, since

$$\frac{d\gamma}{\gamma}(\dot{\sigma}) \cdot f \cdot dz(\dot{\sigma}) \in \mathbb{R} \qquad \text{(see 1.5.2).}$$

Finally, two orthogonal symmetry lines run through each puncture — therefore these have no periods and are catenoid ends (2.1.8, 2.2.4). One of the generators of the fundamental group crosses a vertical and a horizontal symmetry plane — and is therefore closed on the minimal surfaces. The other generator crosses two parallel symmetry planes — reflections in these generate the

period translations. Therefore all properties visible in the picture have been deduced from the Weierstrass data.

3.2.2 The Chen-Gackstatter Surface [CG].

This surface is the first immersed minimal torus (i.e., no periods) with one puncture which was discovered. It can be described as an Enneper surface with a handle:

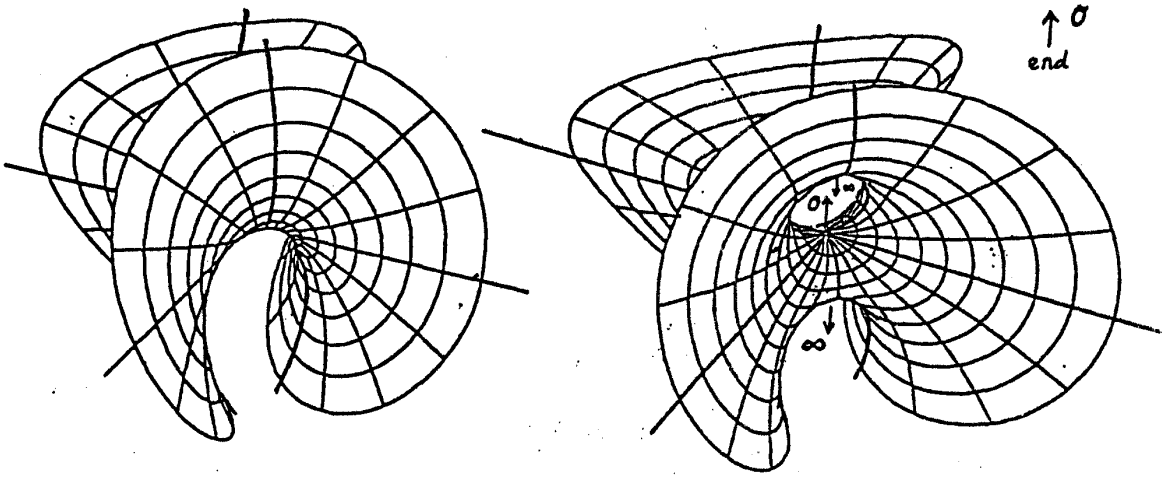

(2.1.2) Chen-Gackstatter surface

The planar symmetry lines of this surface cut it into four congruent pieces. In addition, the asymptote lines through the middle saddle are straight lines on the surface. For the torus this is a *diagonal* symmetry, so the torus is the square torus. Again we write distinguished values of the Gauss map at the vertices of the tessalation of the torus:

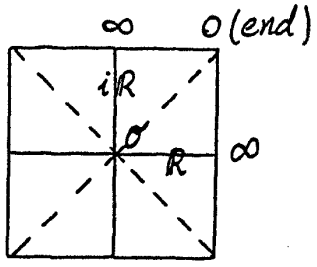

domain torus with distinguished *values* of g . The middle saddle is drawn at center.

We see: The zeros and poles are those of the elliptic function γ, but we know no finite value of the Gauss map. Therefore we can only conclude:

$$g = r \cdot \gamma \,, \qquad r \in \mathbb{R}_+ \,.$$

The differential dh needs simple zeros at the three points with vertical normal which are *not ends*; a pole can only be at the end, therefore a triple pole in this case:

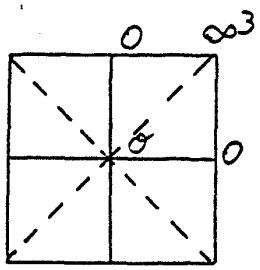

Again the 0-∞-pattern determines the differential

$$dh = p'dz \,.$$

All expected symmetry lines are mapped to meridians by g and p' , reflections are therefore Riemannian isometries for (1.4.2).

$$\frac{dg}{g}(\dot\sigma)\cdot p'dz(\dot\sigma) \in \begin{cases} iR & \text{for the diagonals} \\ R & \text{for the other expected symmetry lines.} \end{cases}$$

This shows that our 1-parameter family of Weierstrass data define complete metrics on $T^2 \setminus \{1 \text{ point}\}$; the data imply the expected symmetries for the minimal surface by (1.5.2), and the behaviour near the puncture is as for Enneper's surface. The puncture has no period because of the symmetries. The two generators have equal periods (in size) because of the diagonal symmetries. The period is horizontal because the generator starts and ends on a vertical symmetry plane. To kill the period we look at the first component of the Weierstrass integral:

$$\operatorname{Re} \Psi_1 = \operatorname{Re} \int_{\text{generator}} \left(\frac{1}{r \cdot \gamma} - r \cdot \gamma \right) \cdot p' \cdot dz \quad .$$

We choose the generator as the real symmetry line which does *not* run into the puncture. Then both integrals

$$\int \frac{1}{\gamma} \cdot p' \cdot dz \quad \text{and} \quad \int \gamma \cdot p' \cdot dz$$

exist because the zeros of p' cancel the poles of $\gamma^{\pm 1}$. Also, both integrals are positive ! Therefore r^2 can be chosen so that $\int \frac{1}{\gamma} \cdot p' \cdot dz - r^2 \int \gamma \cdot p' \cdot dz = 0$. For this choice the Weierstrass data have no period and we obtain the Chen-Gackstatter surface.

3.2.3 Comment for computation. So far the given formulas seem to require that we have to *evaluate elliptic functions* for drawing pictures of these surfaces. However, the differential

$dh = p'dz = dp$ strongly suggests that we should take p as a *coordinate function on the torus* (away from its branch points). Then g and γ are multivalued on S^2 (= range of the coordinate p), defined by

$$\gamma^2 := \frac{-\operatorname{tg}\alpha - \operatorname{ctg}\alpha}{p - \frac{1}{p} - \operatorname{tg}\alpha - \operatorname{ctg}\alpha} \quad , \quad g := r\cdot\gamma \quad .$$

The sign is defined via analytic continuation. Now we can evaluate $g(p)$ as an elementary function and the Weierstrass integral reduces to

$$\Psi = \int \left(\frac{1}{2}\left(\frac{1}{g(p)} - g(p)\right), \frac{i}{2}\left(\frac{1}{g(p)} + g(p)\right), 1 \right) dp \quad .$$

3.3 Doubly periodic embedded examples.

Maybe the pictures of these surfaces can be better looked at if I give the following description: Consider a family of parallel vertical planes and one more vertical plane (orthogonal) to the others; now imagine that one could replace a neighbourhood of each of the vertical intersection lines of these planes by a Scherk saddle tower. This situation will be particularly simple if the horizontal ("saddle") points on neighbouring towers are on the same levels; in this case the symmetries of the expected surfaces are such that all the straight lines which lie on the Scherk saddle towers could also lie on the new surfaces. If we

make this (optimistic) hypothesis then these lines cut the surfaces into pieces which can be *defined* as Jenkins-Serrin graphs (see 2.4), thus proving existence of these most symmetric cases [Ka1]. The assumption that the saddles of neighbouring towers are on the same level can be realized in two different ways:

3.3.1.

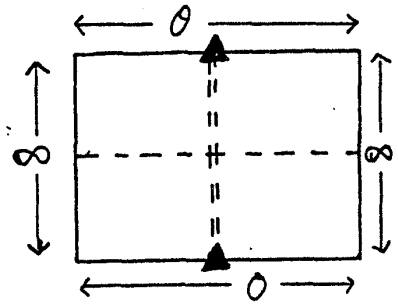

Boundary values for a Jenkins-Serrin graph such that extension by 180°-rotations gives a doubly periodic surface, which has *vertical symmetry planes* between adjacent saddle towers. The symmetry planes of the graph are indicated as --- === , and branch points are marked ▲ .

3.3.2.

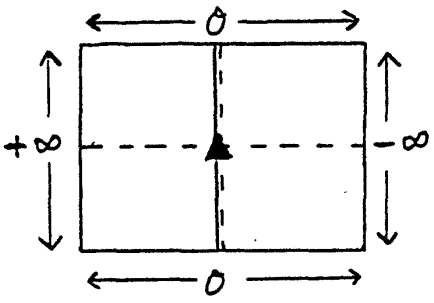

Boundary values for a Jenkins-Serrin graph such that extension by 180°-rotation gives a doubly periodic surface which has *vertical lines* (180°-rotation symmetry) between adjacent saddle towers. The symmetry plane of the graph is indicated as --- , another straight line as === and the branch point as ▲ .

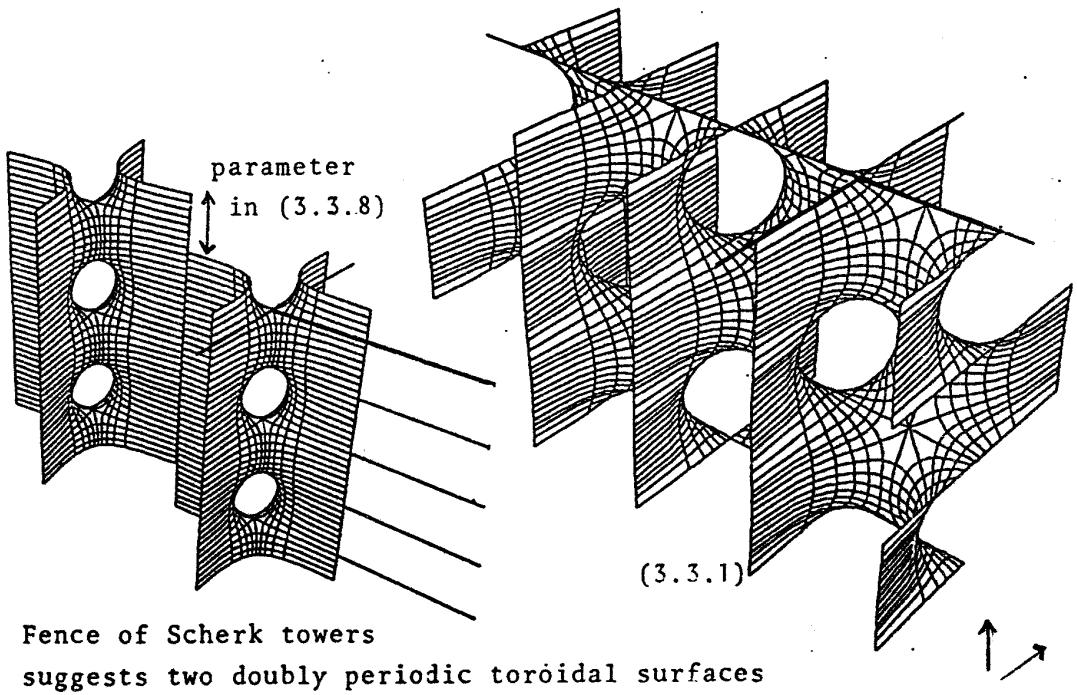

Fence of Scherk towers
suggests two doubly periodic toroidal surfaces

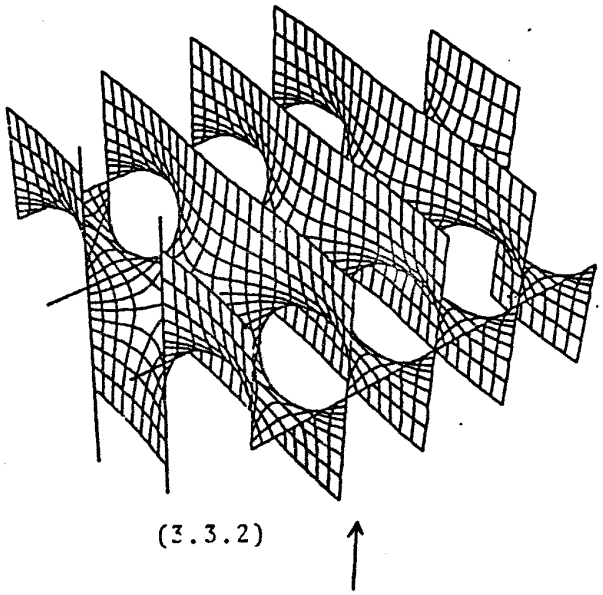

Conjugate pair of embedded
doubly periodic min. surfaces

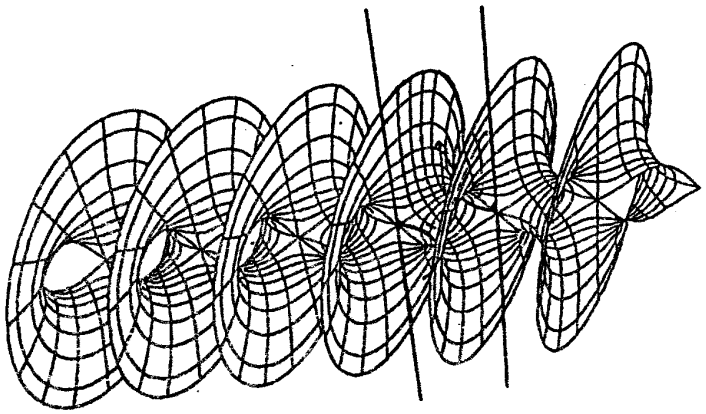

Riemann's minimal surface (3.4)

(3.4) can be viewed as a singly periodic limit under deformation of (3.3.3)

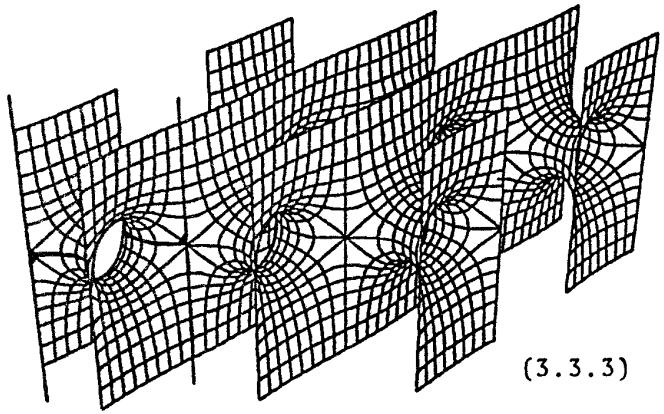

3.3.3. The conjugate surface of (3.3.2) is also doubly periodic and embedded (2.4.1). It can be described as a family of parallel planes which are connected by a checkerboard array of horizontal tunnels.

The Weierstrass representation is easily derived (3.3.5). It gives these surfaces parametrized by rectangular tori. In each case one can — on a fixed rectangular torus — continuously change the Weierstrass data from case (3.3.1) to case (3.3.2); this corresponds to minimal surfaces where the saddles of adjacent towers are not on the same level. These intermediate surfaces have not enough symmetries to construct them as Jenkins-Serrin graphs, but enough to describe them qualitatively. In each of the cases (3.3.1, 3.3.2) there is another 1-parameter deformation of the Weierstrass data (still on a fixed rectangular torus); these surfaces look as if they were made of saddle towers (2.3.4, $k = 2$) whose limit planes are not orthogonal. All together this gives a 3-parameter family of examples. Meeks-Rosenberg [MR] have already generalized (3.3.1 - 3.3.3) to a 3- parameter family of examples; I have not yet checked whether it is the same family, but I expect this.

These toroidal examples and Scherk's doubly periodic surfaces (2.2.2/4) are the only known doubly periodic embedded minimal surfaces. The collection of examples of triply periodic, or of simply periodic or of examples without periods (= finite total curvature) is much richer. The behaviour near the punctures is typical:

3.3.4 Theorem (Meeks-Rosenberg[MR]). If one divides a doubly periodic embedded minimal surface by its orientation preserving translational symmetries and if this quotient has finite total curvature then the ends are flat annuli — as in the known examples.

3.3.5. We derive the Weierstrass representation for the doubly periodic examples. Four Jenkins-Serrin pieces fit together to give a fundamental domain for the translational symmetries. The Gauss map g is therefore of degree 2, in particular g is simple at the punctures. Each Jenkins-Serrin piece is therefore a conformal rectangle — i.e., the Weierstrass data live on a torus. For simplicity we rotate the surface so that the normals at the ends are vertical ($= 0, \infty$); since there are no other vertical normals the differential dh can have no zeros (and hence no poles), necessarily we must have $dh = \text{const.} \cdot dz$. We copy the special values of the Gauss map into a more usual picture of a torus:

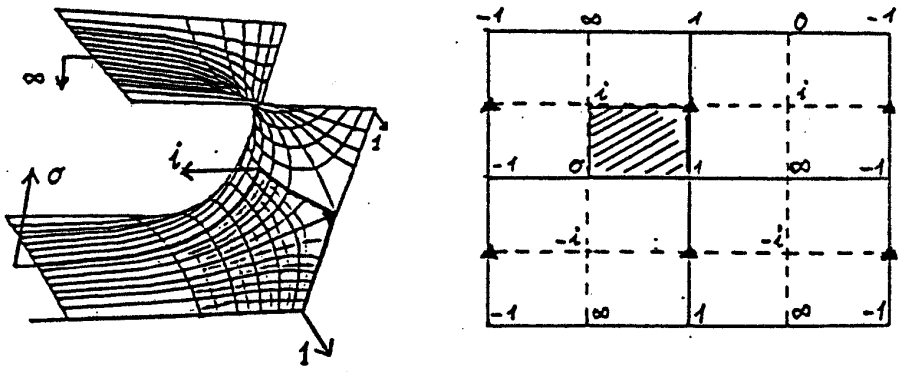

These data are recognized easily:

3.3.6. Weierstrass data for (3.3.1)

$$g = \gamma \quad (3.1), \quad dh = i\,dz = i\cdot\frac{d\gamma}{\gamma} \quad (3.1.1).$$

With (1.5.2) we conclude immediately that these data define a surface with the expected symmetry lines (the lines through "± 1" are straight, the others planar).

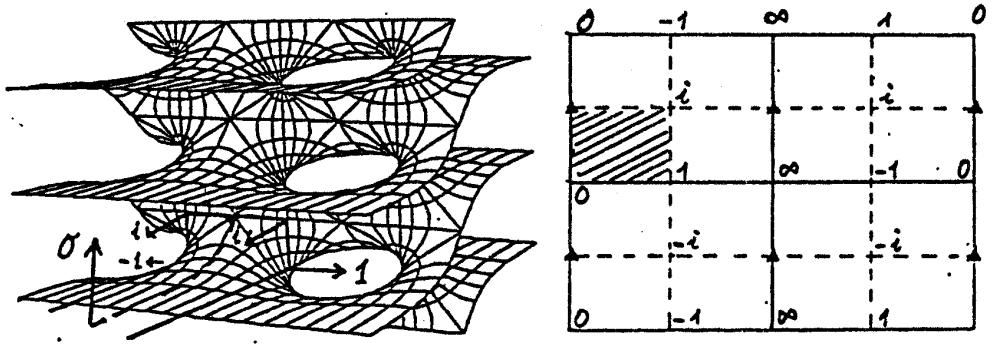

3.3.7. Weierstrass data for (3.3.2)

$$g = \frac{\gamma + 1}{\gamma - 1}, \quad dh = i\,dz = i\cdot\frac{d\gamma}{\gamma}$$

resp. for (3.3.3) $dh = dz$.

Again the expected symmetries follow immediately from (1.5.2). The comment (3.2.3) for computational simplification also applies; for our pictures only elementary functions (though multi-valued) were integrated.

3.3.8. First deformation of the Weierstrass data

$$g = \frac{\gamma + \varepsilon}{\varepsilon\gamma - 1}$$

$$dh = i\,dz$$

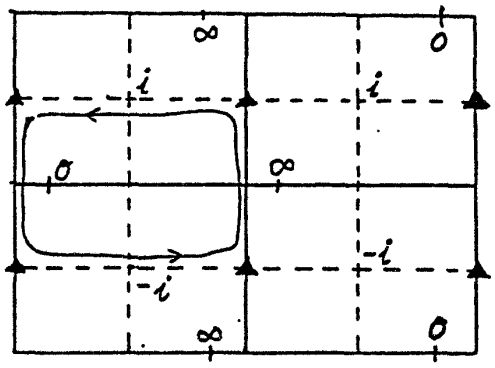

The straight lines into the punctures survive the deformation. 180°-rotation around the normals in direction $\pm i$ are symetries and also $-\mathrm{id}$ with respect to each branch point. The period from one generator is obtained by the two rotations around the $+i$-normals, the period from the other generator by rotations around $+i$ and $-i$ normals. The periods can also be obtained by two suitably chosen $-\mathrm{id}$ symmetries at branch points. This shows that the period obtained from a puncture is contained in the lattice spanned by the periods from the generators ! Therefore the surface is doubly periodic. The period from a puncture is of course perpendicular to the lines through that puncture. This says that these surfaces look like a fence of orthogonal saddle towers; one period translates each tower vertically up, the other period moves the towers but not horizontally.

3.3.9. Second deformation of the Weierstrass data

$$g = \frac{\gamma + e^{i\varphi}}{-\gamma + e^{i\varphi}}$$

$$dh = i\,dz$$

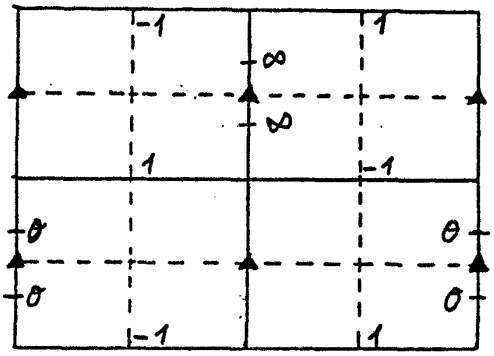

The planar symmetry lines from the punctures to the branch points and the straight lines connecting the branch point (of 3.3.7) survive the deformation. Rotation around the ± 1 normals and $-\mathrm{id}$ with respect to each branch point are further symmetries. Again, the periods from the punctures are contained in the lattice spanned by the periods of the generators. — The normals at the ends are no longer parallel to the period lattice.
If one combines the deformations (3.3.8/9) then only the $-\mathrm{id}$ symmetries remain, as in Meeks-Rosenberg's family.

3.4 Riemann's Minimal Surface [Ri].

We describe a simply periodic embedded example which is a torus with two planar ends and one period.
Modulo orientation preserving translations there are only two planar symmetry lines and two (parallel) straight lines. They

cut the surfaces into four simply connected pieces; these are relatively "large" and therefore not so easy to visualize. Each piece has one more symmetry, a 180°-rotation around the normal which is also the middle line between two straight symmetry lines. This implies: If we can find such data then we have no further period problem, namely, the *two* planar symmetry arcs on the boundary of one of the simply connected pieces are automatically in the *same plane* because of the 180°-rotation symmetry around a normal.

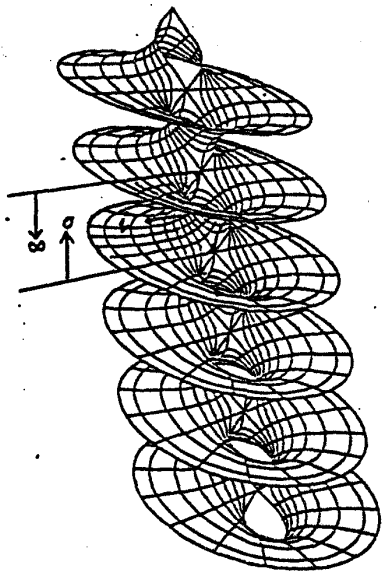

We write special values of the Gauss map into a picture of the rectangular domain torus:

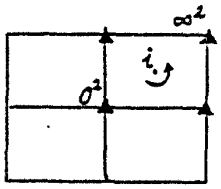

Double vertical normals $(0,\infty)$ at the two planar ends (2.2.3) and two further branch points where the straight and the planar symmetry lines meet.

This picture also shows that dh cannot have zeros or poles. This gives us the Weierstrass data of *Riemann's example*:

3.4.1. $\quad g = p\,, \quad dh = dz = \frac{1}{p}\cdot dp\,.$

This is another case where (1.5.2) succeeds immediately: Reflections in the expected symmetry lines indeed are Riemannian isometries for $ds = \left(|g| + \frac{1}{|g|} \right)|dz|$ (1.4.2) and $\frac{dg}{g}(\dot\sigma)\cdot dh(\dot\sigma) \in R$ resp. $\in iR$ on the expected planar resp. straight symmetry lines. The punctures have no periods because of these symmetries (2.1.8) and g is branched, i.e., we have planar ends (2.2.3). The period of the generator which is transversal to the planar symmetry arcs is zero because of the 180°-symmetry. In other words: The data (3.4.1) indeed define a minimal surface with all the qualitative properties which we read off the picture.

3.5 Costa's Surface [Co].

Finally I describe an embedded minimal torus with one planar and two catenoid ends.

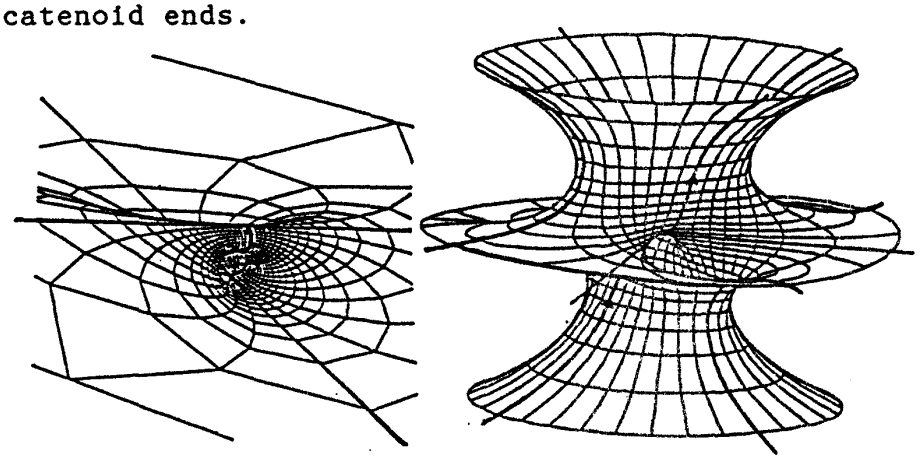

torus with one planar end Costa's surface

Maybe, before Osserman's results it was difficult to look systematically for minimal surfaces with specific properties. Then it took almost another 20 years before the Chen-Gackstatter immersion and Costa's embedding were found. The former surface remained fairly unknown in spite of the fact that it was the first torus with only one puncture; certainly the surface was difficult to imagine from the formulas. Whether Costa's surface was embedded or not remained a mystery for another two years. The symmetries were not known at first. And the surface was so difficult to imagine, that the first computer pictures by Hoffman and Meeks did not help them too much in convicing people that the surface was embedded. I had to recall this since now, with good pictures available, it is not too difficult to reconstruct the Weierstrass data and prove the desired properties.

The picture shows two vertical symmetry planes which cut the minimal surface — and the parametrizing Riemann surface — into four simply connected piece, moreover these are conformal rectangles (= four 90°-angles of each piece). The asymptote lines through the saddle are straight lines on the surface, and these symmetries make the underlying torus (as in the Chen-Gackstatter case) the square torus ($\mathrm{tg}\ \alpha = 1$ in 3.1.3). Of course it is now easy to write special values of the Gauss map onto the square torus which is tessalated by the expected symmetry lines (no such expectations when the surface was first found !). That picture then implies the 0-∞-pattern for the differential:

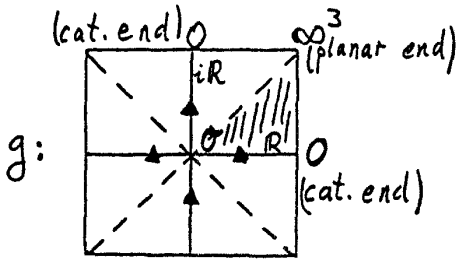

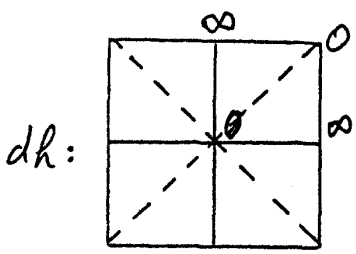

At the planar end the Gauss map has a triple pole, because the saddle and the catenoid ends are simple points for g .

Without difficulty we recognize the

Weierstrass data for Costa's surface

$$g = r \cdot p' = r \cdot \frac{p}{\gamma} \qquad (3.1.4)$$

$$dh = \gamma \cdot dz \begin{cases} = \frac{\gamma}{\gamma'} \cdot d\gamma & (3.2.3) \\ = \frac{2}{1 - p^2} \cdot dp & (3.1.3/4) \end{cases}$$

Clearly the metric (1.4.2) is complete on $T^2 \setminus \{\text{poles of } \gamma,\ p\}$. Since p and γ map the expected symmetry lines into meridians, reflections in these lines are Riemannian isometries — so the lines are geodesics (once more 1.5.2).

$$\frac{dg}{g}(\dot\sigma) \cdot dh(\dot\sigma) \in \begin{cases} iR & \text{on the diagonal} \\ R & \text{on the other expected symmetry lines.} \end{cases}$$

Costa's embedded minimal torus (3.5).
Parametrization by level lines.

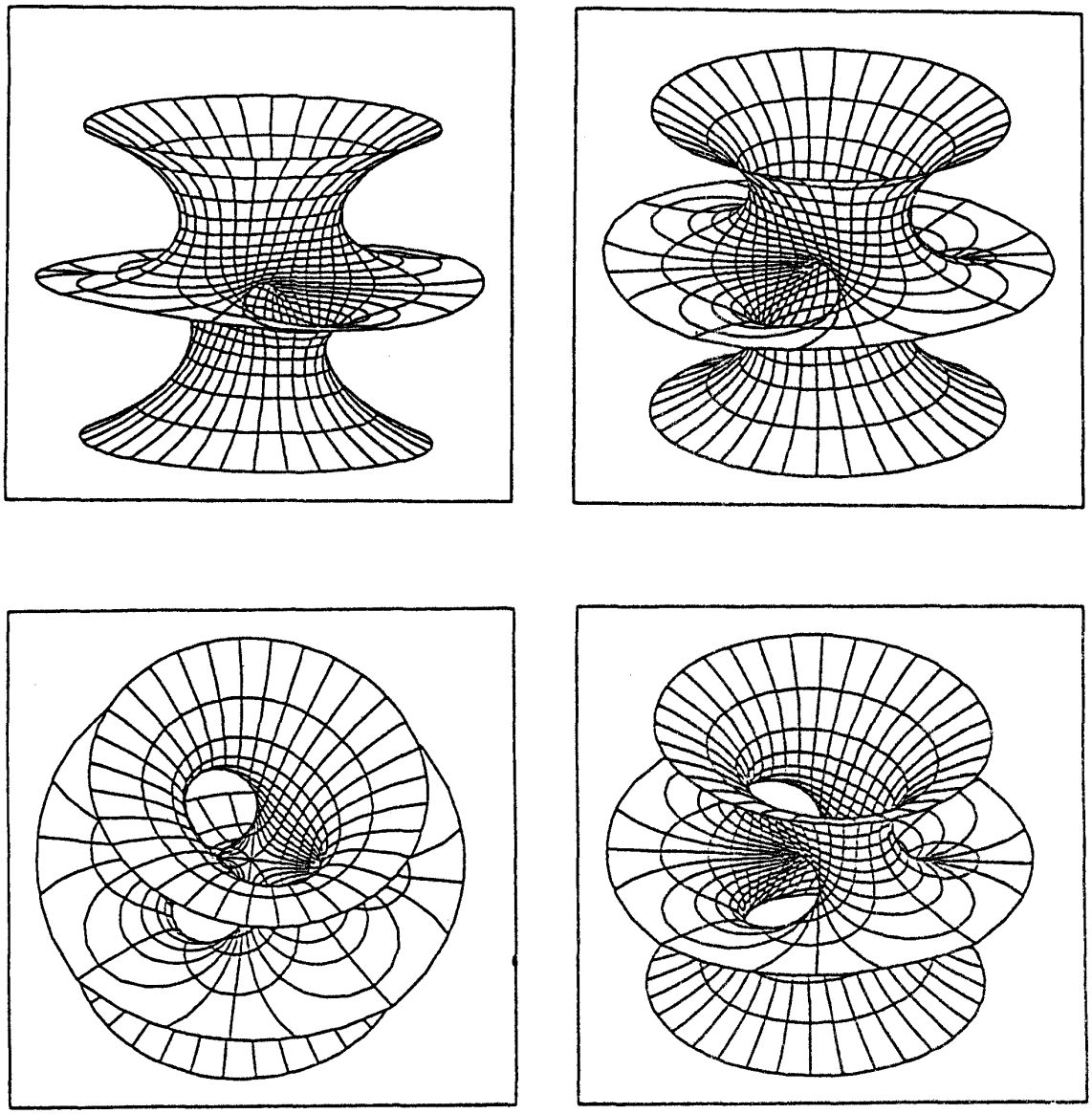

This shows that the above Weierstrass data lead to a minimal surface with the expected symmetry lines and three punctures without periods ! The generators of the fundamental group start and end on vertical symmetry planes — so they have horizontal periods, which are moreover equal in size because of the 45°-symmetries. As in the Chen-Gackstatter case we have to use the parameter r to kill the horizontal periods.

A horizontal period is $\operatorname{Re} \int_{\text{generator}} \frac{1}{2}\left(\frac{1}{g} - g \right) dh$.

It can be made 0 by choice of r if the following two integrals have the *same sign*:

$$\operatorname{Re} \int p \, dz \quad \text{and} \quad \operatorname{Re} \int \frac{\gamma^2}{p} \, dz = 2 \operatorname{Re} \int \frac{dz}{1 - p^2} \qquad (3.1.3).$$

We cannot use the symmetries of p for both integrals on the same path, but on homotopic ones; the first integral exists and is *positive* on this path:

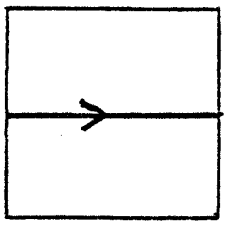

the second exists and is positive on this one:

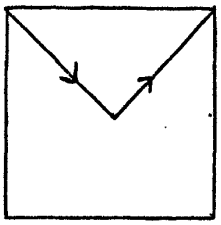

From now on r is choosen so that our Weierstrass data have no period and therefore define an immersed torus with embedded ends. It remains to show that the surface is embedded.
The Gauss map maps one quarter of the torus to the following spherical domain which is bounded by pieces of R and iR :

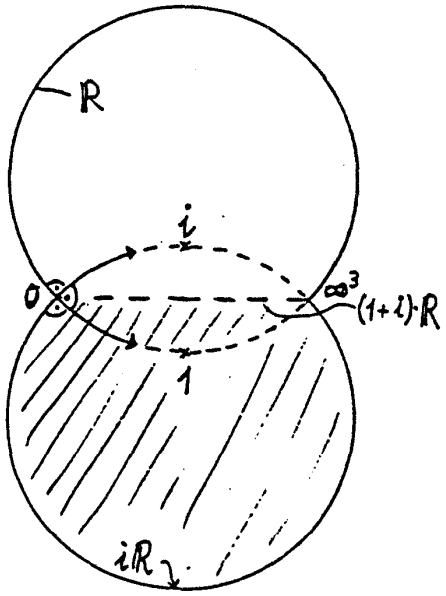

Half of this, the shaded part, is the Gauss image of one of the eight congruent pieces of the minimal surface (or triangles of the torus). One can see that orthogonal projection in the directional + 1 is an immersion.

The boundary of this minimal surface piece consists of three symmetry lines resp. arcs:

(i) A horizontal half line from the saddle to the planar end.

(ii) A vertical symmetry arc with inflection point, going from the saddle to a catenoid end; the tangent of this curve is horizontal only at the saddle.

(iii) A convex vertical symmetry arc which joins the catenoid end to the planar end; convexity follows since $K \neq 0$ along this curve; this curve is strictly falling from the catenoid end to the planar end.

This leaves only two possibilities for the orthogonal projection of these boundary curves:

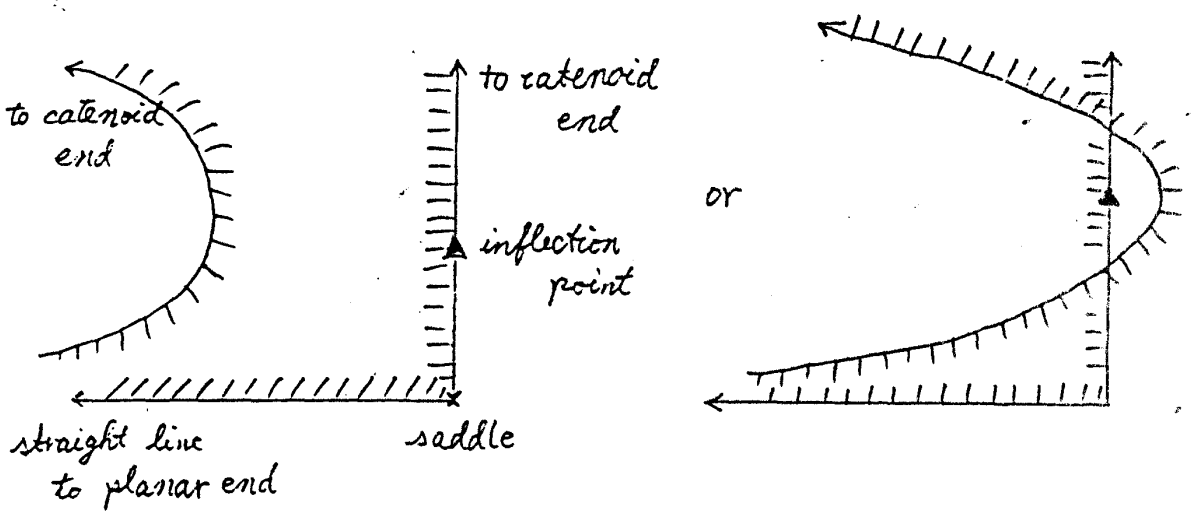

Near the strictly convex curvature line the orthogonal projection must map the minimal surface to the nonconvex side. The second picture is not compatible with the orthogonal projection being an immersion. The projection is therefore an immersion onto a simply connected domain; the surface piece is therefore a graph over this domain, in particular embedded.

The embedded piece lies in one octon of R^3 and the symmetry

group is simply transitive on these octons. The eight embedded pieces therefore fit together to an embedded minimal surface.

3.6 Further remarks about tori.

3.6.1. The Costa-surface can be deformed to give embeddings of rectangular tori (Hoffman-Meeks [HM2]). The middle end is no longer planar, i.e., the triple pole of the Gauss map is split into three simple poles, two of them finite points with vertical normal. This leads to

$$g = r\cdot\frac{1}{\gamma}\cdot\frac{p}{p+M}\,, \qquad dh = \gamma\cdot(\,p+M\,)\cdot dz\,.$$

The 45°-symmetries are no longer there so that *two* horizontal periods have to be killed. For each conformal parameter α (in the equation 3.1.3 between γ and p) one has the two adjustable parameters r, M . Hoffman and Meeks have shown that these suffice to kill the periods.

3.6.2. Other embedded tori are not known. Costa has proved that the 3-ended examples cannot be made with non-rectangular tori, and embedded tori with more than 3-ends so far could not be constructed, compare (2.1.1).

3.6.3. We know other shapes then (3.4.1) of *simply periodic* embedded toroidal minimal surfaces. (i) One can put vertical tunnels be-tween adjacent saddles of the symmetric saddle towers

(2.3.3) for $k > 2$, $k = 2$ (Scherk) is impossible [Ka 1].

(ii) The following picture "shows" two of many complicated toroidal examples (*not* rectangular). Their discovery involves the cristallographers Fischer and Koch (Marburg) [FK], David Hoffman and our group in Bonn.

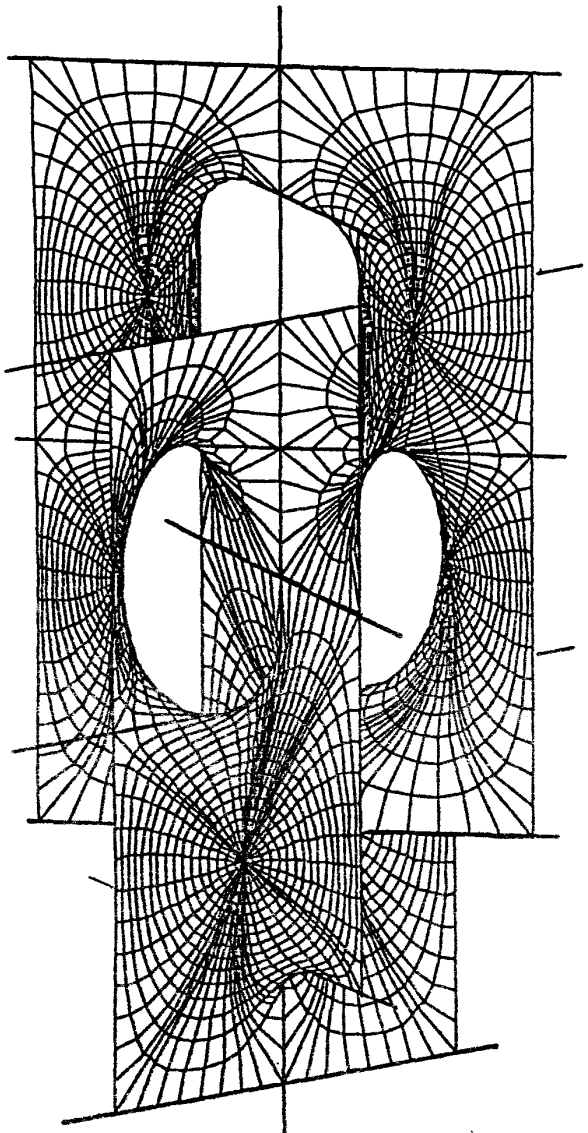

Triply periodic min. surfaces (Fischer-Koch)

Singly periodic toroidal minimal surface.

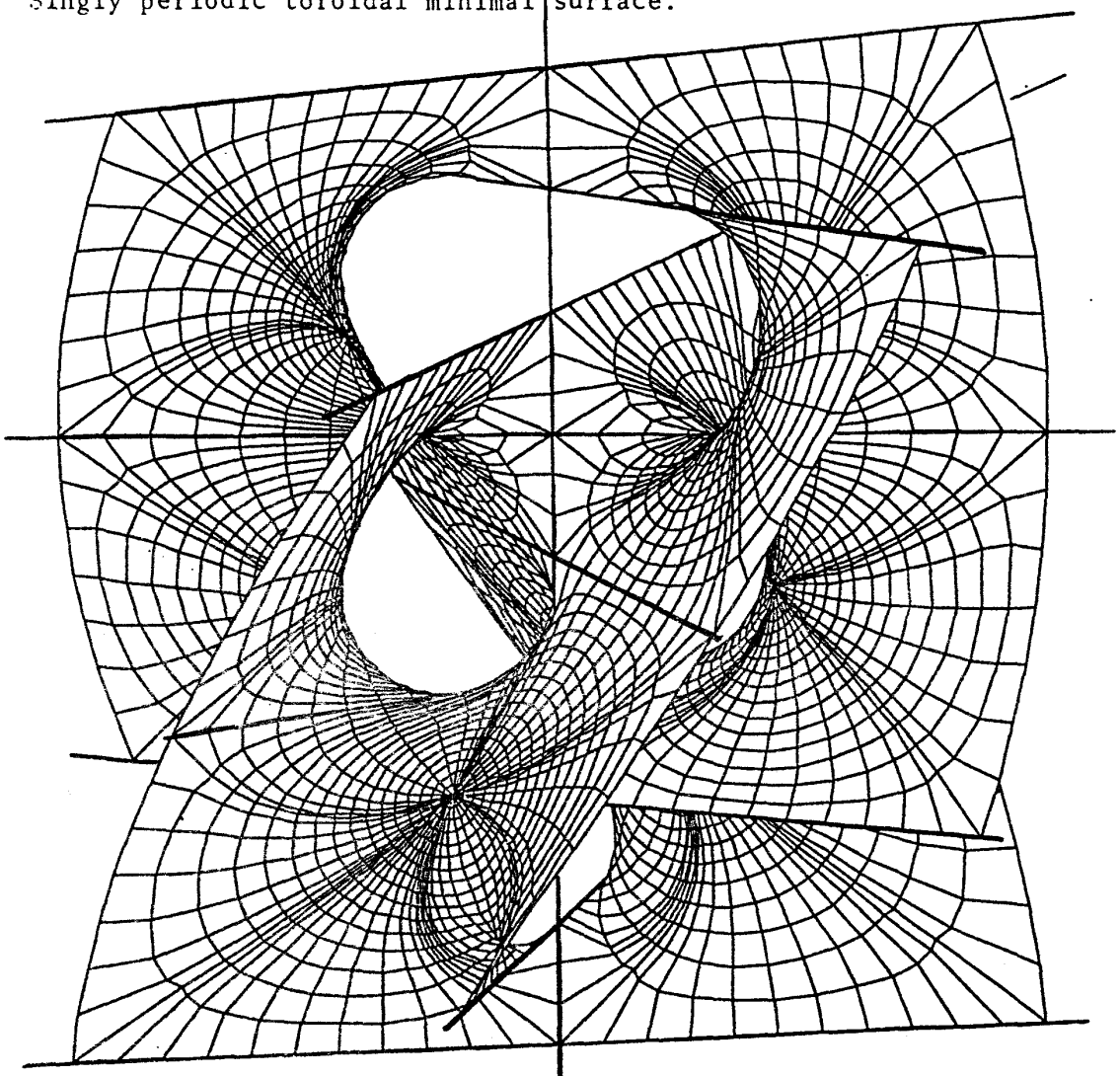

suggested by the Fischer-Koch example

Plateau solver by O. Wohlrab

4. The Conjugate Plateau Construction of Triply Periodic Minimal Surfaces

Five triply periodic embedded minimal surfaces have been known by H.A. Schwarz [Sz] and his students. Alan H. Schoen [aSn] described in a 1970 NASA report 12 more such examples. For the description he used terms not familiar in mathematics and he did not give too many mathematical details either. So his work was unfortunately either ignored or disbelieved.
I'll describe in these notes the conjugate construction and then apply it to only a few examples since I wrote on this material before [Ka 2].

4.1.1 Basic observation. Let F describe a simply connected minimal surface piece which is bounded by *planar symmetry lines*. The conjugate surface F^* (1.3) is then a minimal surface piece bounded by *straight line segments* (1.1.2, 1.4.5). Since the pieces have the same Riemannian metric, *angles* at corresponding vertices also are the *same*. This suggests the following

4.1.2 Strategy: If one wants to construct some specific triply periodic minimal surface, then one may first assume planes of *reflectional symmetry* which cut the surface into simply connected pieces. Of course one knows the angles between the symmetry lines at the vertices of such a piece. One can therefore take any polygon in R^3 with the correct angles at the vertices, solve the Plateau problem (!), *conjugate the Plateau solution*,

obtain a minimal surface piece bounded by planar lines of reflectional symmetry with the correct angles at the vertices — and hope that this piece is part of the desired minimal surface (e.g. 2.4).

This hope in general fails, because the angle between symmetry planes which do not meet at a vertex is of course also important. These angles are controlled by the rotation of the surface normal (= principal normal of the planar curve) along the bounding symmetry arcs. The following formula shows that these are almost (namely: mod 2π) determined by the above polygon contour without further reference to the Plateau solution:

$$\left(\begin{array}{l}\text{rotation of}\\ \text{the normal}\end{array}\right) = \int \kappa \, ds$$

$$= \int -\tau^* \, ds \qquad (1.3.3,\ 1.1.1) \tag{4.1.3}$$

$$= \left(\begin{array}{l}\text{total rotation of the tangent}\\ \text{plane of the Plateau solution}\\ \text{along the edge of the polygon}\end{array}\right).$$

The boundary regularity of the Plateau solution implies that the tangent plane at a polygon vertex exists and is spanned by the edges which meet at that vertex. In general, by looking at one edge of such a polygon one cannot say (even knowing the position of the tangent planes at the endpoints) which way around and how often the tangent plane of a Plateau solution rotates. In our applications the polygons will always be *on the boundary of a convex polyhedron !* Then a Plateau solution stays inside the polyhedron — therefore:

4.1.4. A polygon on the boundary of its convex hull determines the total turn of any Plateau solution along each edge.

If we now apply the outlined strategy to a polygon with the correct angles at the vertices and the correct rotation of tangent planes of Plateau solutions, then the boundary arcs of the conjugate piece give symmetry planes such that *all* pairwise angles are correct. The same method was used in [Sm]. Finally we want some qualitative information like: The whole minimal surface piece stays *on one side* of each of its bounding symmetry planes. For this we have two pieces of information; first, by Krust's theorem (2.4.1):

4.1.5. For all directions, for which the Plateau-polygon has a convex projection, we know from the maximum principle that its (unique) Plateau solution is a graph — and therefore the conjugate piece is also a graph (2.4.1).

Secondly:

4.1.6. If the Gauss curvature is $\neq 0$ along an arc of reflectional symmetry, then its curvature κ does not change sign; therefore its tangent rotates *monotonly* from a known initial direction to a known final direction — i.e., we have a well controlled convex arc.

4.1.7. The points where the Gauss curvature K vanishes are

the branch points of g and the index of a curvature line field equals

$$-\frac{1}{2} \cdot (\text{branching order of } g).$$

This allows us to control the zeros of κ by the Plateau-polygon without further reference to the Plateau solution. The triply periodic minimal surface is identified to a compact Riemann surface by dividing out translational symmetries. This Riemann surface is tessalated by the above simply connected pieces (the ones into which the symmetry planes cut the minimal surface). Now

$$\int_{M^2} K \, dA = 2\pi \cdot \sum (\text{indices of a curvature line field})$$

and each piece has the same contribution to both sides, namely:

$$\int_{\text{piece}} K \, dA = 2\pi - \sum (\text{exterior angles of the piece}).$$

The exterior angles are given with the Plateau contour, therefore the contribution to the index sum is known — and this sharply limits the zeros of K.

4.1.8 Example. For a 90°- hexagon we get

$$\int K \, dA = 2\pi - 6 \cdot \frac{\pi}{2} = -\pi .$$

Such a hexagon therefore has

(i) One interior simple branch point, or

(ii) At interior edge points two simple or one double branch point, or

(iii) More such possibilities with branch points at vertices.

Note: In many examples we know some branch points from symmetries and then 4.1.7 concludes that there are no others.

On the following pictures of triply periodic minimal surfaces (with A. Schoen's names) the simply connected pieces and their conjugate Plateau contours have been indicated. The visible convexity properties of the symmetry lines follow from (4.1.6/7), the embeddedness of fundamental pieces from (4.1.5).

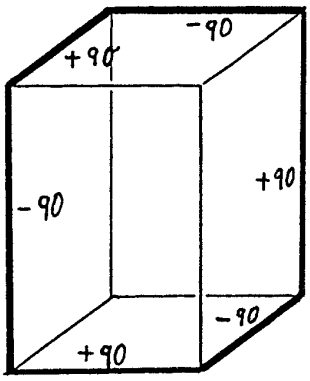

conjugate contour
(also generates a
triply periodic surface)

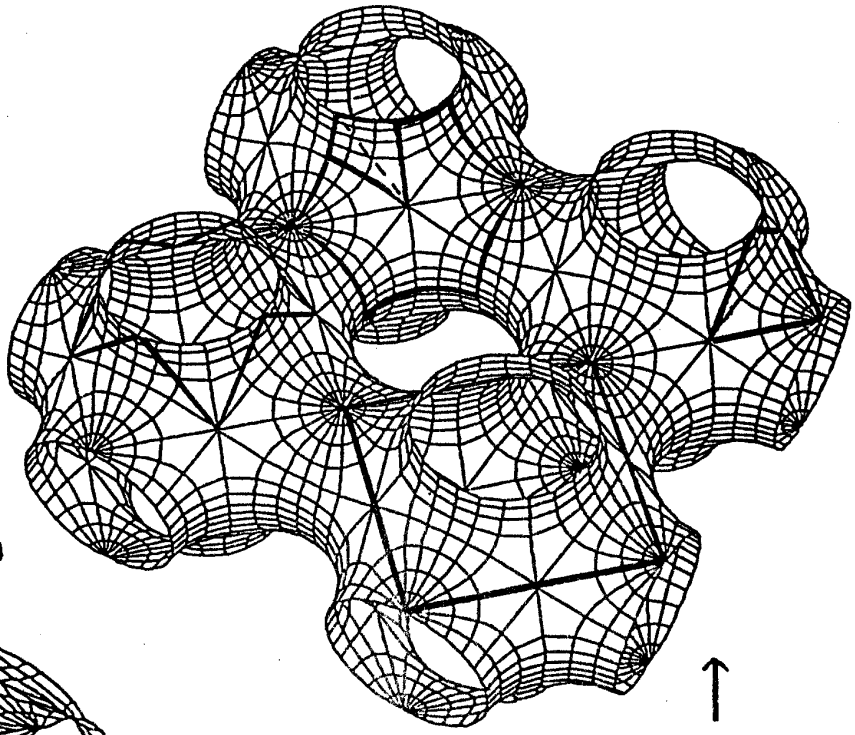

H.A. Schwarz' P.surface
and deformations (4.1, 5.2)

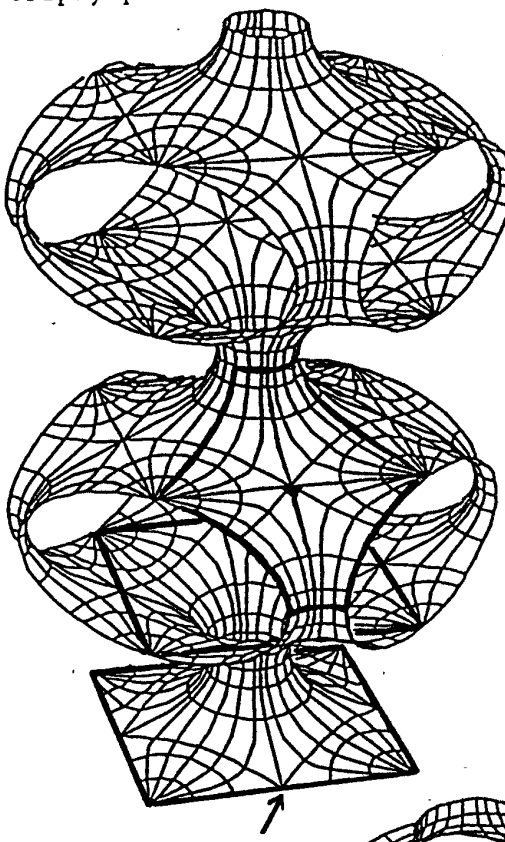

With annulus
bounded by
two squares.

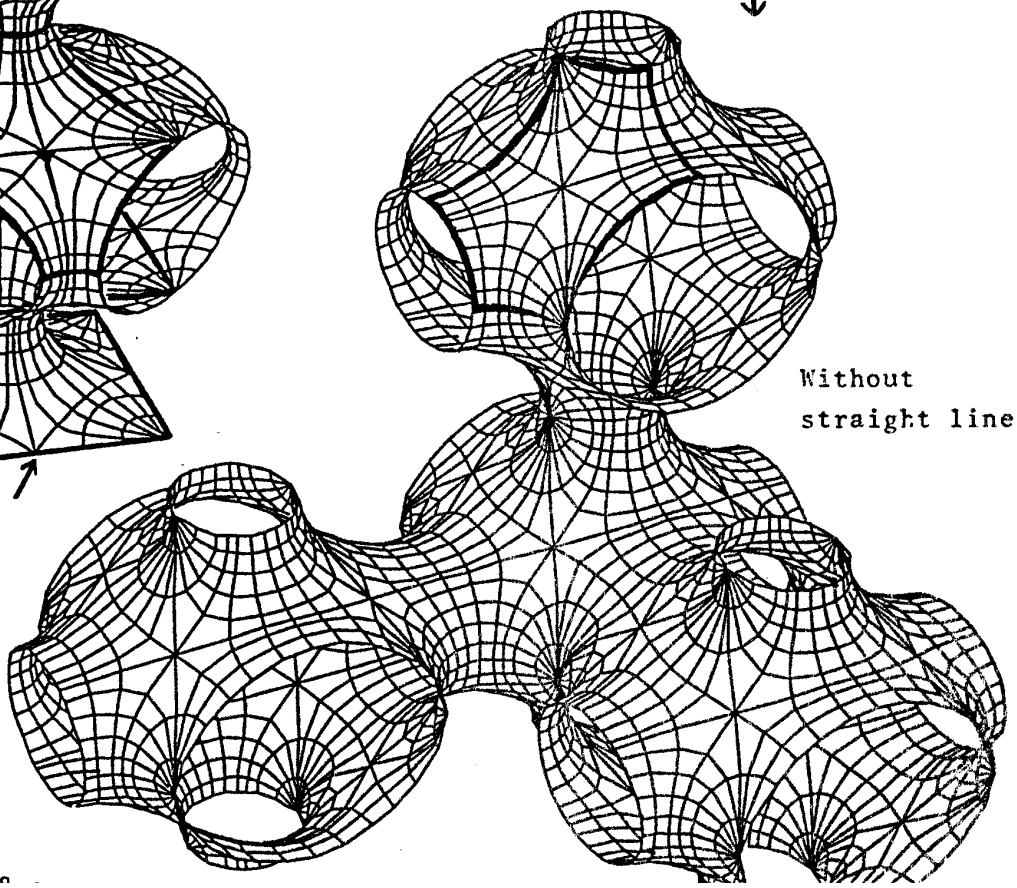

Without
straight lines

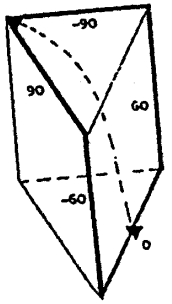

conjugate
contour

H.A. Schwarz' "H"-surface.
It carries annuli bounded by two triangels ⟷

Another annulus bounded by two triangles. For edge-length = 2, height = $1/\sqrt{3}$ this annulus is part of the conjugate of Schwarz' P-surface.

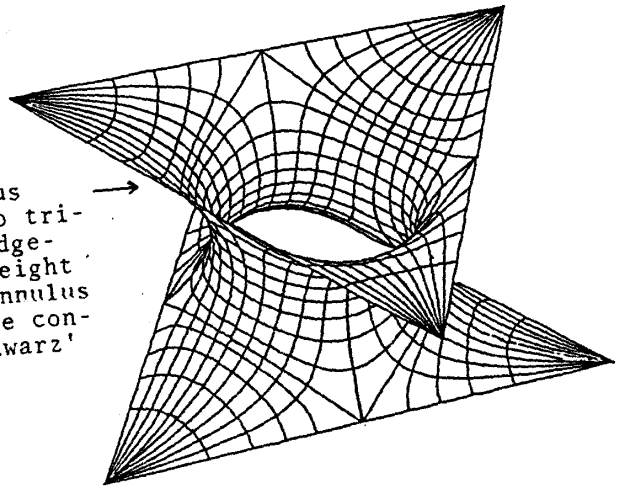

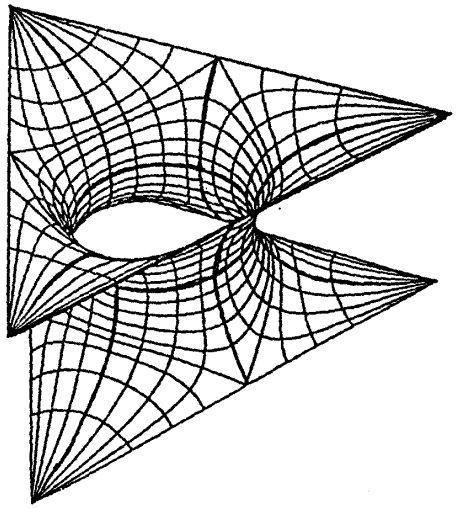

Views of Schwarz' CLP-surface

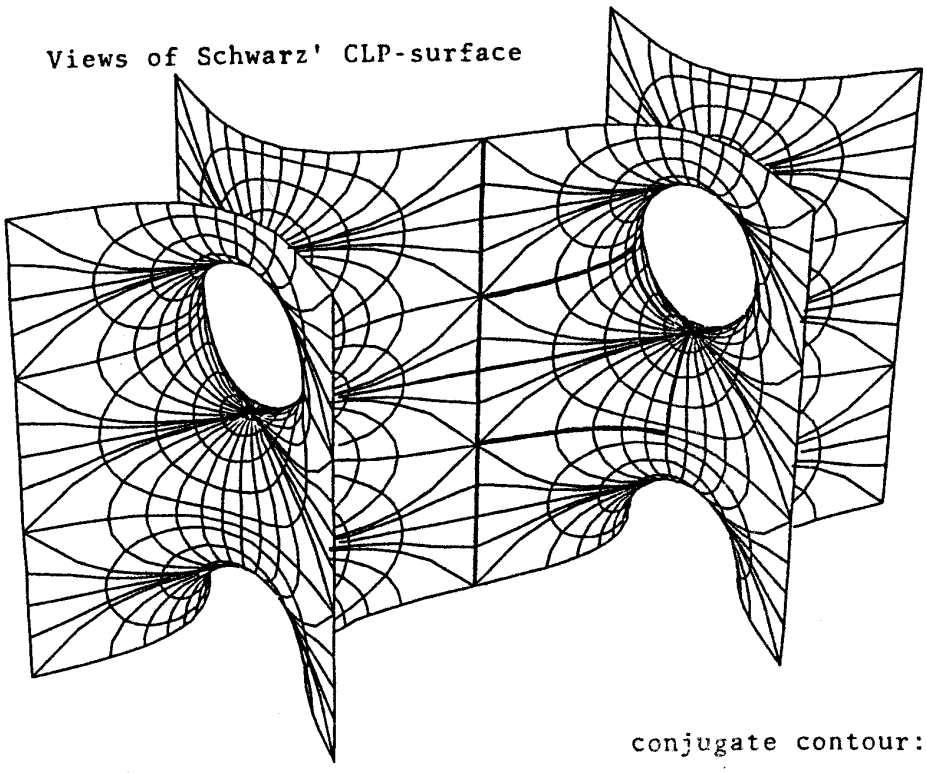

conjugate contour:

If the horizontal edge-pairs do not have the same length then this surface has no horizontal straight lines.

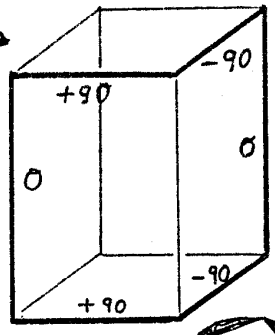

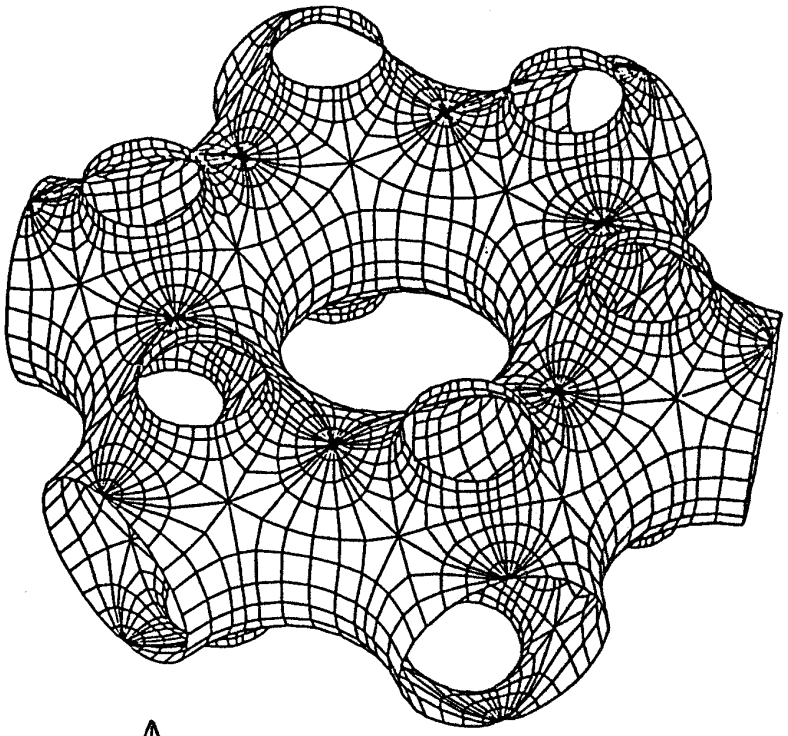

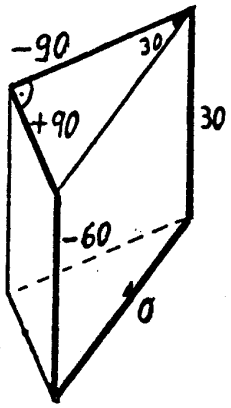

Conjugate contour. Weierstraß representation (5.3)

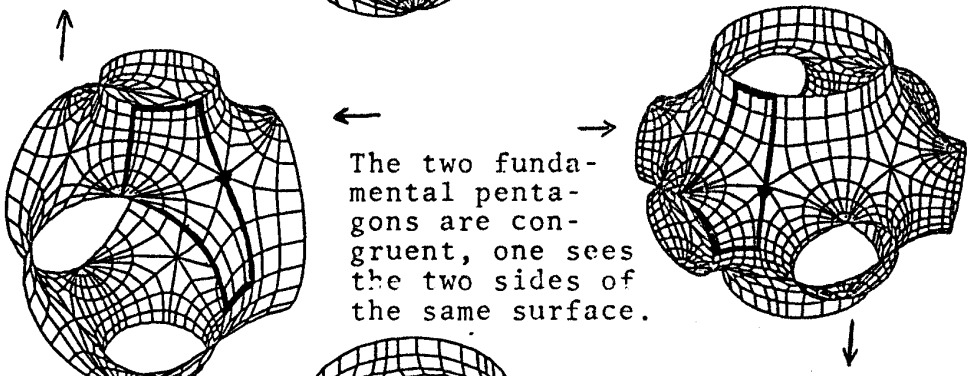

The two fundamental pentagons are congruent, one sees the two sides of the same surface.

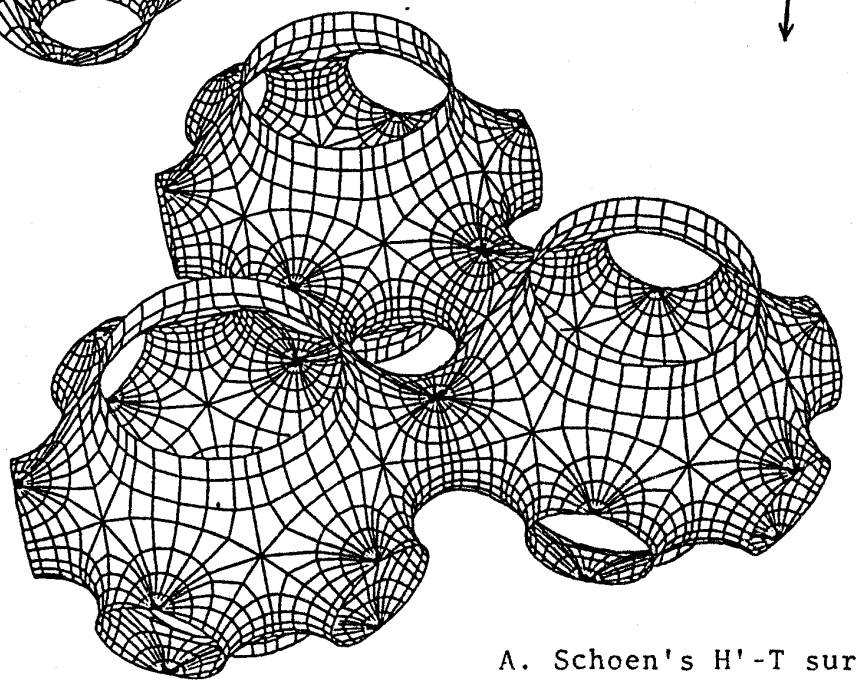

A. Schoen's H'-T surface in a trigonal or the dual hexagonal cell.

Conjugate contour:

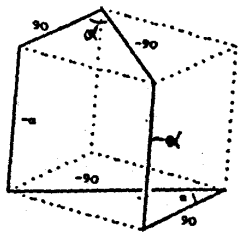

α = 45°

α = 60°

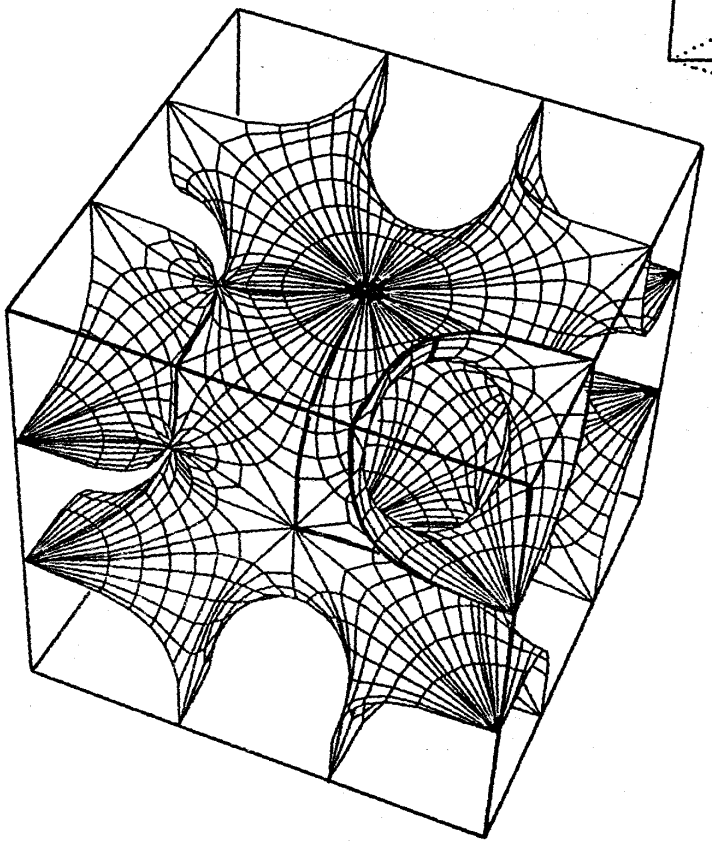

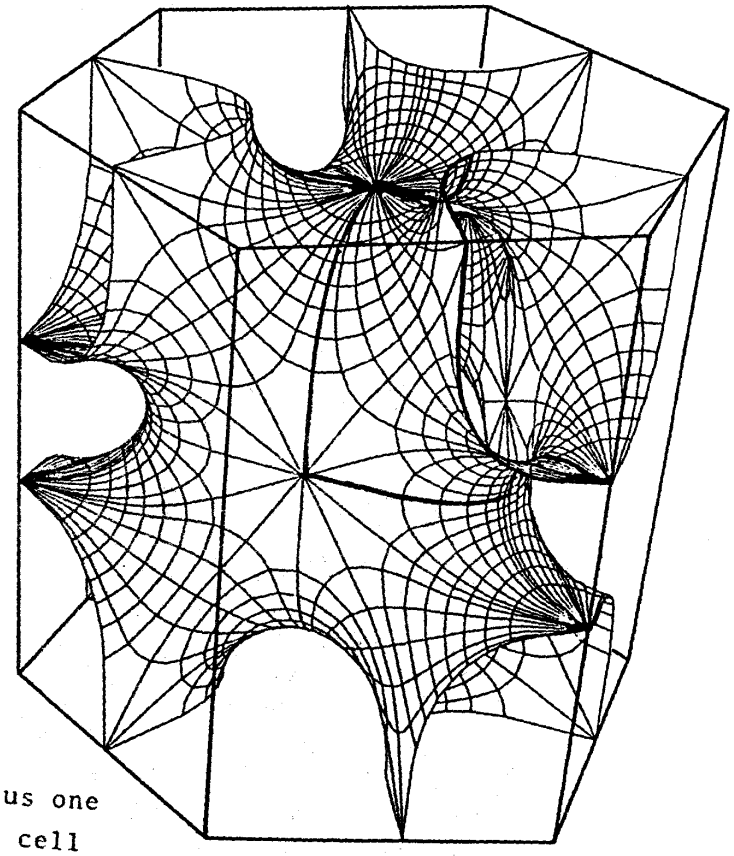

A. Schoen's I-Wp surface and analoguous one in hexagonal cell [Ka 2]

A. Schoen's S'-S" surface

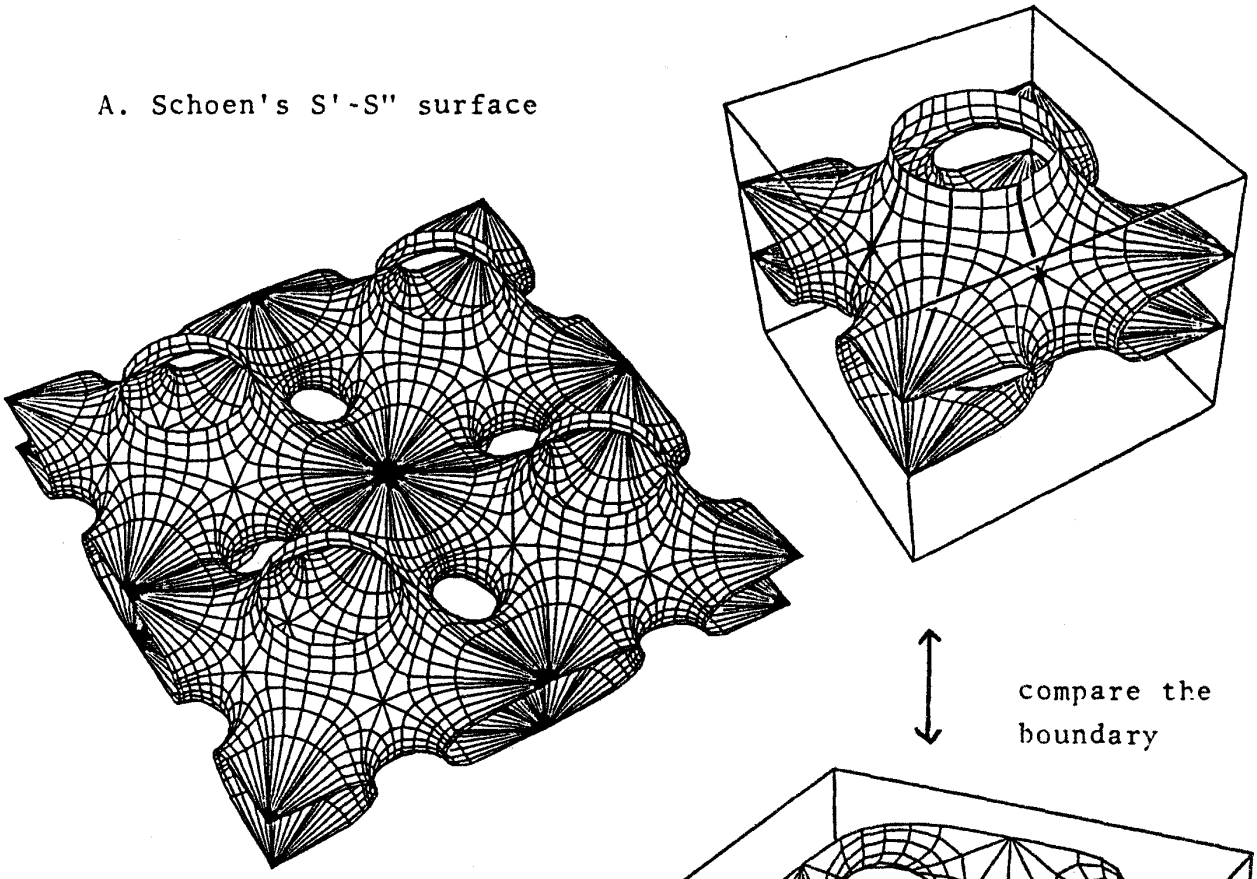

compare the boundary

conjugate contour

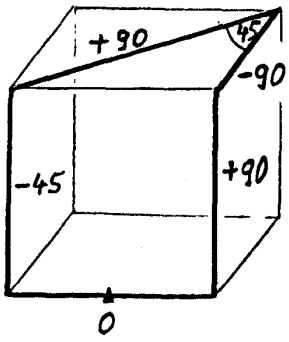

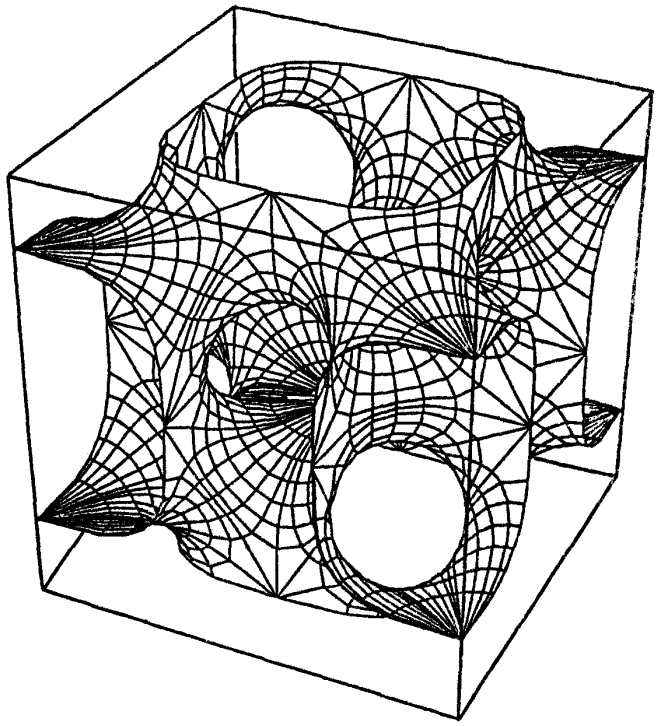

Another view of Schoen's I-Wp surface.
Note that it solves the same free boundary value problem on the faces of the cube - but with more complicated topology (previous picture).

4.2. The previous examples are particularly simple in the following sense: The fundamental piece does *not* have two different symmetry arcs which are supposed to lie in the same plane. If two symmetry lines occur which have to be in the same plane then our arguments will only give: The conjugate piece has the two relevant symmetry lines in *parallel* planes which are not necessarily the same. Such situations arise easily, e.g., most of our surfaces for which the cristallographic cell is a quadratic prisma cannot be made in a rectangular prisma without dealing with that difficulty. Already on Schoen's list were two similar cases: Imagine that in the example "I-W_p" the piece in one cube is joined to all the pieces in neighbouring cubes by tunnels perpendicular to the faces of the cube; the conjugate construction allows to produce such tunnels "easily", more precisely: it gives two halftunnels, because in general two such halfs will not be long enough to meet on the face of the cube. To deal with this we want to apply an intermediate value argument — but Plateau solutions in general do not depend continuously on parameters. However, in a large number of cases the following result of Nitsche applies (quoted for a special case):

4.2.1 Theorem (Nitsche[Ni2]). Given a compact convex domain D and continuous Dirichlet boundary data for a minimal graph over D *except* at finitely many points; at these points left and right limits of the boundary data exist. Then this Dirichlet problem has a unique minimal graph solution. As a minimal surface its boundary contains vertical segments over the jump points which

join the given continuous boundary arcs. For these "Nitsche graphs" a maximum principle holds and this implies that the *solutions change continuously* as we vary the continuous parts of the boundary data.

4.2.2. In particular, for pieces which are conjugates of (polygonal) Nitsche graphs we can vary the lengths of intended tunnels or the height difference of two parallel symmetry planes *continuously*.
For the construction of a specific example all what remains to check (because of the intermediate value theorem) then is that the above height difference can be made positive and negative or the above tunnel can be made too long and too short.

4.2.3. As an example we show how the pairs of points with horizontal tangent plane on the Schwarz-P-surface can be joined by vertical tunnels. For simplicity we keep the vertical 45°-symmetry planes. The conjugate contour for the Schwarz piece is:

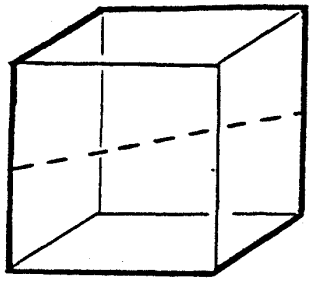

The 45°-degree line lies on the Plateau solution, it gives a 45°-vertical symmetry arc on the conjugate piece.

We plan to "puncture" the Schwarz-P-surface at the horizontal points and pull such vertical tunnels out. The two vertical symmetry lines to a "puncture" remain symmetry lines but their final tangents change by 90° ; they do not meet anymore, but a new horizontal symmetry line joins them. ("Puncture" is in quotes because, conformally, a disc is removed.) This leads to the following conjugate contour:

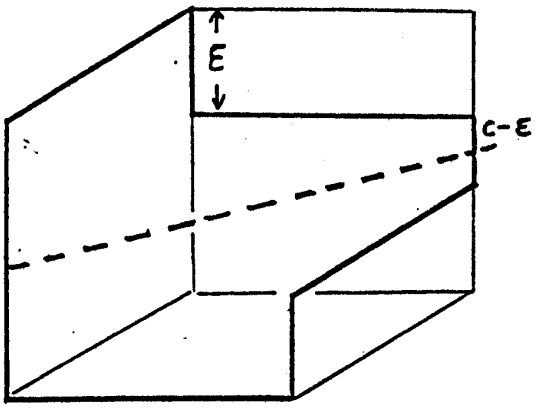

This contour is a Nitsche graph for the vertical direction. The solution depends continuously on ε , including the limits $\varepsilon \longrightarrow 0$, $\varepsilon \longrightarrow c$.

In the limit $\varepsilon \longrightarrow 0$ the "moving edge" has a vertical normal at the left endpoint, a horizontal one on the right; the corresponding convex symmetry arc (4.1.6/8) is *falling* from left to right. In the limit $\varepsilon \longrightarrow c$ the situation is reversed, the moving edge gives a *rising* convex arc on the conjugate piece ! In other words:
If we call the horizontal symmetry lines corresponding to two neighbours of the moving edge the "ε-line" and the "$(c - \varepsilon)$-line" then: for small ε is the "ε-line" above the "$(c - \varepsilon)$-line", for small $(c - \varepsilon)$ it is below. If we choose ε such

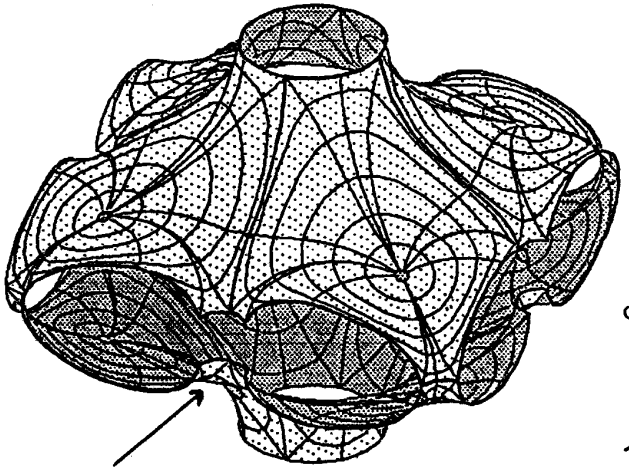

tunnel is too short, ε too small

Vertical tunnels glued into Schwarz' P-surface

(4.2.3, 5.4.2)

Family of conjugate contours

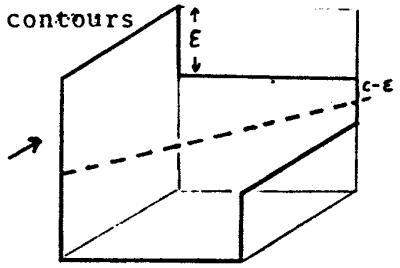

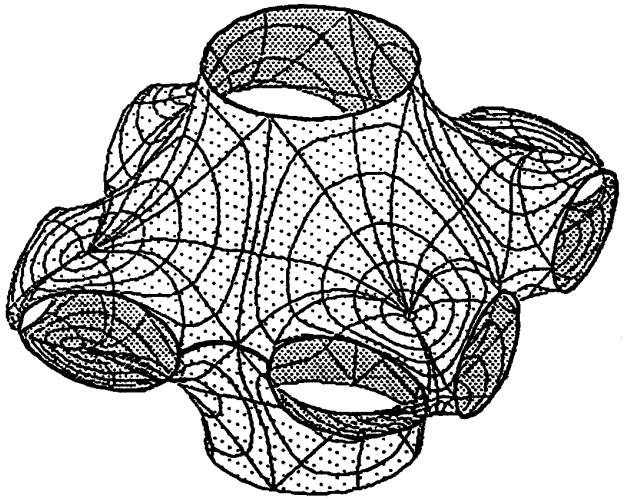

ε correct

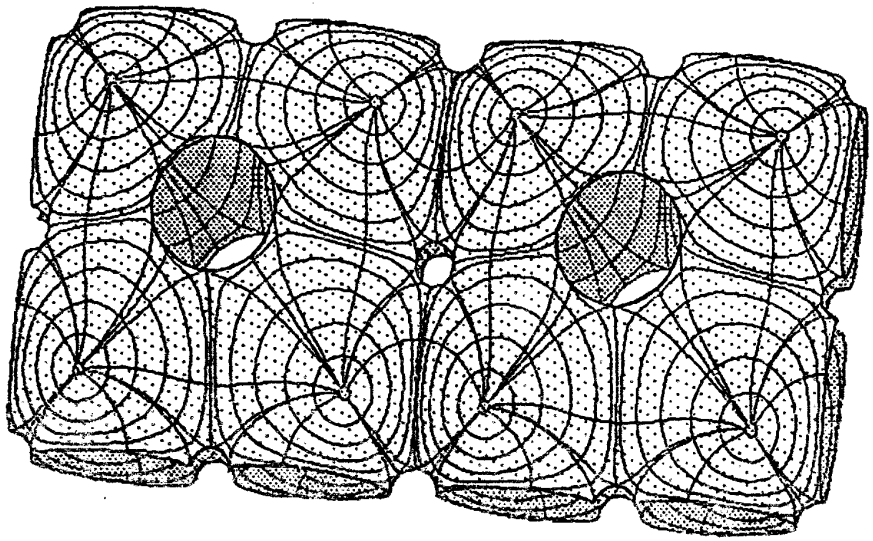

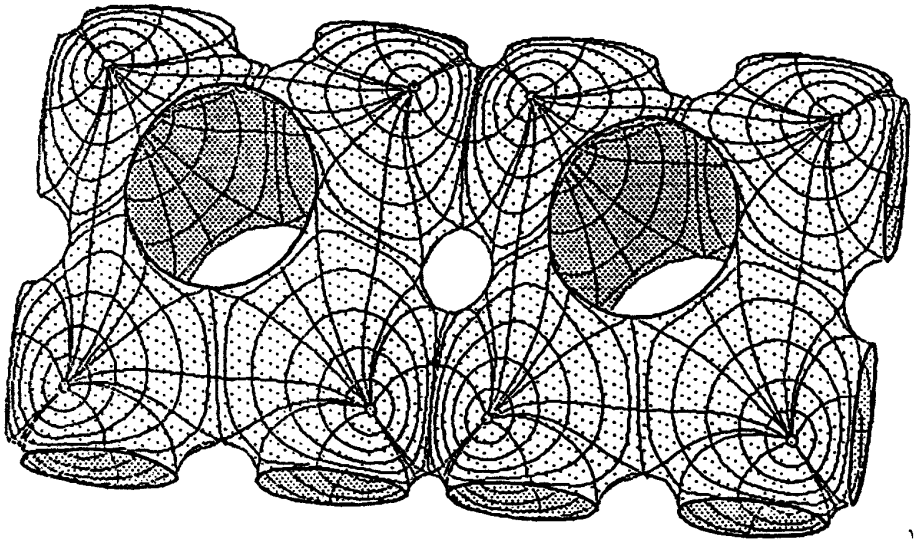

that these two symmetry lines lie in the same horizontal plane then the tunnel has the correct length (see figure). Also, this conjugate piece is embedded because of 4.1.5 and the reflections extend the piece to an embedded triply periodic minimal surface.

5. Higher Genus Weierstrass Representations

We aim for a description as in section 3:

(i) The compact Riemann surface is given by an equation between two functions.

Examples: $p'^2 = p(1 - p^2)$ or $\gamma^2 = \frac{2}{\frac{1}{p} - p}$.

(ii) Each function is a local coordinate away from it branch points; together they provide local coordinates everywhere. *Example:* p and γ have no common branch points; at the common multiple point (pole) of p and p' the quotient p/p' is a coordinate.

(iii) Gauss map and (height-)differential are given in terms of these defining functions.

Example: $g = p$, $dh = \frac{1}{p'} \cdot dp$.

As guiding background I first explain that such a description is always possible in the case of embedded triply periodic minimal surfaces. (We will see then that more cases are covered.)

5.1.1 Definition. To get the underlying compact Riemann surface M^2 we first identify points on the minimal surface which differ by an orientation preserving translational symmetry; then we use the natural complex structure from section 1.3.

5.1.2 Definition. The Gauss map g and the holomorphic differential from the height function

$$dh = dF_3 - i \cdot dF_3 \cdot D^{90^\circ}$$

are well defined on M^2 (the height function is not). This gives us two geometrically defined functions

$$g \ , \quad \mu := \frac{dh}{\frac{1}{g}\, dg} \ .$$

5.1.3 Claim. At multiple points of g the multiplicities of g and μ differ by 1. Therefore: together they provide local coordinates everywhere on M^2.

Proof: (i) If g has at p a *k-fold* zero or pole, then dg/g has a simple pole and dh has a k-fold zero — since otherwise the metric (1.4.2) would either be degenerate at p or p would be a puncture. Therefore μ has a *(k + 1)-fold* zero at p.
(ii) If g has at p an *l-fold* value $\neq 0, \infty$ then dg/g has a zero of order *(l - 1)* and dh has neither a zero nor a pole. Therefore μ has an *(l - 1)-fold* pole at p.

I find it natural to divide out *all* the (orientation preserving) translational symmetries of the minimal surfaces. Therefore

I include the

5.1.4 Claim. The pair (g,μ) seperates points on M^2 .

Proof: Since g and μ provide local coordinates everywhere, they locally seperate points. Define a compact Riemann surface N^2 by identifying those sets of points which are not seperated by (g,μ) . Then the function field of N^2 is generated by g and μ and an algebraic equation $A(g,\mu) = 0$ can be found. Of course $A(g,\mu) = 0$ also holds on M^2 . Consider two points p, q on the minimal surface with $(g,\mu)(p) = (g,\mu)(q)$; it is enough to stay away from the branch points, zero and poles of g . We use $A(\mu,g) = 0$ to have near p and q

$$\mu = \varphi(g) \quad \text{(same } \varphi \text{ near } p \text{ and } q \text{)} .$$

Now metric and second fundamental form of the minimal surface near p and near q are the same and also the Gauss map. This gives a translational symmetry, hence $p = q$ on M^2 .

Remark. The above arguments are also applicable to finite total curvature examples with embedded ends. It is always true that at finite points the multiplicities of g and μ are relatively prime, but one can have immersed ends where this is not the case.

Now that we know that the desired description of a minimal

surface exists in general we want to find it in special cases. One point, however, is different: we *do not have* the minimal surface at the beginning, but we want to find a minimal surface with certain properties — genus, symmetries, behaviour near punctures. It is only from these properties that we want to derive the Weierstrass data; then we need to prove that these data define a minimal surface with the desired properties.

5.2 Weierstrass representation of Schwarz P-surface [Sz].

If we look at the picture and divide out the translations, then we clearly get a sphere with 3 handles. More specifically this Riemann surface is tessalated by eight 90°-hexagons . This is still a 3-parameter family of Riemann surfaces. (In the hyperbolic picture a 90°-hexagon has three edgelength parameters.) Since we expect — up to scaling — only a 2-parameter family we look for more symmetries. If we put the midpoint of the conjugate Plateau contour at the origin, then (- id) is a symmetry of its (unique) Plateau solution. Such - id symmetries are symmetries for all members of the associate family (1.3.5), in particular for Schwarz P-surface.
Now indeed: hyperbolic 90°-hexagons with midpoint-symmetry have *two* edgelength parameters, i.e., we know the family of possible Riemann surfaces in the hyperbolic picture.
As in the torus case we hope to be able to find an equation between g and μ if we write all the special values of these geometric functions into a picture of the Riemann surface.

In view of the symmetries it is enough to write these special values into one of the eight hexagons. We sketch the hexagon so that it resembles the piece on the P-surface.

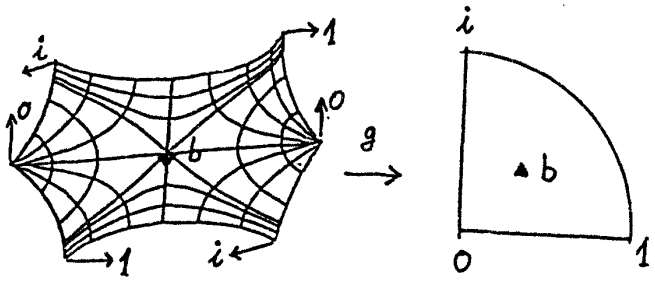

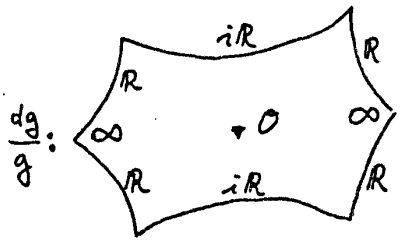

Distinguished values of the Gauss map in hexagon domain and image on S^2 . There is only *one* branch point in each hexagon by (4.1.8).

0-∞-pattern of $\frac{dg}{g}$.

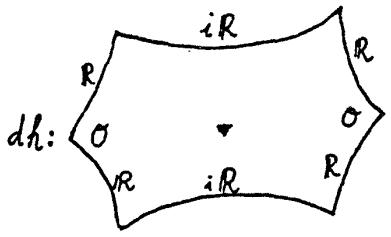

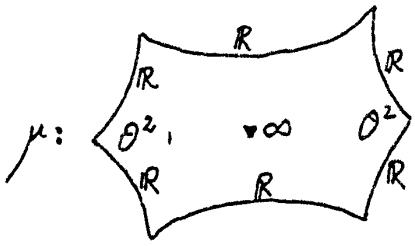

Zeros of dh (since there are no punctures dh has no poles) and special values of μ . Note that μ is real on all the symmetry lines since

$$\mu \cdot \left(\frac{dg}{g}(\dot{\sigma}) \right)^2 = \frac{dg}{g}(\dot{\sigma}) \cdot dh(\dot{\sigma}) \in R \ .$$

Let b be one branch value of g ; the symmetries imply that $\{ \pm b, \pm \bar{b} \}^{\pm 1}$ are all the branch values. The following two functions therefore have the same zeros and poles:

$$\mu^{-2} \quad \text{and} \quad g^{-4} \cdot \prod_{i=1}^{\infty} \left(g - b_i \right)$$

$$= \left(g^2 + g^{-2} - b^2 - b^{-2} \right) \cdot \left(g^2 + g^{-2} - (\bar{b})^2 - (\bar{b})^{-2} \right) .$$

Observe that these two functions are positive near 0 on the symmetry lines and then conclude (abbreviation $B := b^2 + b^{-2}$):

5.2.1 Weierstrass data for Schwarz P-surface:

$$\mu^{-2} = (\text{ pos. const.}) \cdot \left(g^2 + g^{-2} - B \right) \cdot \left(g^2 + g^{-2} - \bar{B} \right)$$

g : Gauss map

$dh := \mu \cdot \frac{dg}{g}$ (height-) differential.

5.2.2. Finally, if only these equations are given, how can one see that they describe Schwarz P-surface ?
Except for $\mu = 0, \infty$ we have for $g \in S^2$ precisely two values $\pm \mu$. The Riemann surface (given by the equation) is therefore described as a branched double covering of the sphere, i.e., g is of degree 2 , μ is of degree 8 on this Riemann surface. We fix the (irrelevant) pos. constant in the equation to be $|B|^{-2}$; then we can start the analytic continuation (for μ as

a multivalued function of g) at a point where $g^2 = i$ with $\mu = 1$. As long as we stay with g on R, iR, S^1 the right hand side of the equation remains positive and we obtain values $\mu \in R$.

Reflection in these lines is therefore (!) an isometry for the metric (1.4.2)

$$ds = \left(|g| + \frac{1}{|g|} \right) \cdot |\mu| \cdot \left| \frac{dg}{g} \right|$$

and since indeed

$$\frac{dg}{g}(\dot{\sigma}) \cdot dh(\dot{\sigma}) = \mu \cdot \left(\frac{dg}{g}(\dot{\sigma}) \right)^2 \in R$$

these reflections are symmetries for the minimal surface defined by the above data (5.2.1). Moreover, as g approches 0 or ∞, $\mu(g)$ has a double zero (and $\frac{dg}{g}$ a simple pole), therefore these points are at finite distance for the metric. Each of the eight simple factors $(g - b_i)$ in the equation gives (at b_i) $\mu = \infty$, and these are simple poles of μ because degree$(\mu) = 8$. On the Riemann surface, therefore, $(g - b_i)$ has a double zero, so that also these points are regular points at finite distance for the metric. We now also know that μ changes sign if we go (with g) once around one of the branch points b_i . The eight triangles on S^2 (between R, iR, S^1), doubly covered around their branch points b_i , therefore represent the eight $90°$-hexagons on the Riemann surface. Each edge of a hexagon is — on the minimal surfaces — a planar convex arc

whose tangent rotates through 90° . It lies in a plane parallel to a coordinate plane and it starts and ends on (orthogonal) symmetry planes. (In particular, four such congruent arcs close up.) The conjugate piece of one hexagon therefore solves the Plateau problem for the contour used in section 4 to define the P-surface. Finally, this Plateau solution is unique.

This example is typical for all those cases where at *all* branch points of g holds: multiplicity of g at branch point = degree(g) . This is very special. We therefore treat two more cases.

5.3 Weierstrass representation of A. Schoen's H'-T surface which meets all the faces of a hexagonal prisma in convex curves [Ka2].

We first count the handles which come from identifying opposite faces of the prisma by translation:

$$\text{genus} = 4 , \quad \text{degree}(g) = 3 .$$

The simply connected pieces on the surface which are cut out by symmetry lines are 90°-pentagons (i.e., *one* hyperbolic parameter, in agreement with the expectation of a 1-parameter family of examples). We reflect such a pentagon in that vertical symmetry line which has no inflection point and get again a 90°-hexagon (twelve of which cover the Riemann surface). We sketch one such hexagon to resemble the shape on the minimal

surface and note the special values of g and μ :

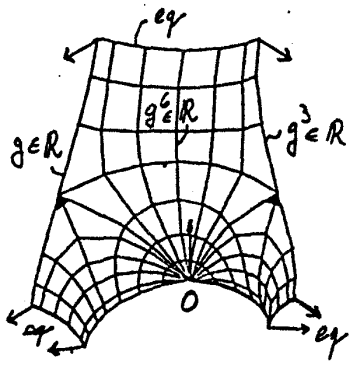

Special values of g , no other branch points than (4.1.8).

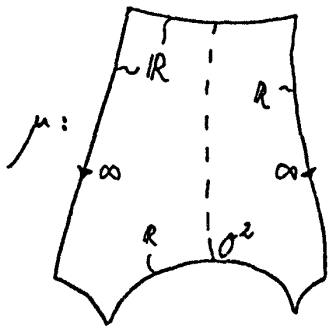

Special values of μ , μ is real on all symmetry lines and has degree 12 .

We look for an equation in the form

$$\text{rational}_1(g) = \text{rational}_2(\mu)$$

and we list, what we already know,

$$\text{degree}(\text{rational}_1) = 12 = \text{degree}(\mu)$$

$$\text{degree}(\text{rational}_2) = 3 = \text{degree}(g) \ .$$

If $g = 0, \infty$ (always simple), then $\mu = 0^2$.
At the branch points of g we have $\mu = \infty$, branch values $b_i \in \{ b\cdot\xi, \frac{1}{b}\cdot\xi \mid \xi^6 = 1 \}$. On all symmetry lines both sides of the wanted equation must be real.
All the branch values b_i of g occur again as simple values of g . We call the value of μ at these twelve points r .

From this we guess (with $B := b^6 + b^{-6}$) :

5.3.1. $$g^6 + g^{-6} - B = \frac{r - \mu}{\mu^3} .$$

This equation contains two instead of one parameter. Indeed, if we differentiate, we see that not all the known properties of the branch points of g and μ are satisfied for arbitrary B, r :

5.3.2. $$6 \left(g^6 - g^{-6} \right) . \frac{dg}{g} = \left(\frac{2}{\mu^2} - \frac{3r}{\mu^3} \right) . \frac{d\mu}{\mu} .$$

We know that $\mu = \infty$ causes all the desired simple branch points of g . But at $\mu = \frac{3}{2} r$ we would also have $dg = 0$ from this equation, *unless* $g^{12} = 1$ there. We know that all vertices of the pentagons must be branch points of μ , this includes *all* points where $g^6 = + 1$. But on the horizontal symmetry line in the middle of the cristallographic cell there are points with $g^6 = - 1$ which are not vertices. We have to assume $\mu = \frac{3}{2} r$ at these points to avoid unwanted branch points of g from the equation. Therefore

$$- 2 - B = \frac{r - \mu}{\mu^3} \Big|_{\mu = \frac{3}{2} r} = - \frac{4}{27} r^{-2} .$$

5.3.3. $$g^6 + g^{-6} + 2 - \frac{4}{27} r^{-2} = \frac{r - \mu}{\mu^3}$$

g : Gauss map, $dh = \mu \cdot \frac{dg}{g}$: differential.

The proof that these data indeed define the desired surface is very similar to the case of the P-surface. In cheking $\mu \in R$ on the symmetry lines we have to use the additional information: If $g^6 = -1$ at a nonvertex then $\mu = \frac{3}{2} r$.

5.4 The use of other functions on the Riemann surface.

The previous example illustrates that the degree of μ easily gets rather large. It is useful to look for other simple functions on the Riemann surface. An optimal example for such a situation is the pair γ , p on the torus: We have two dual tessalations of the torus, each by four rectangles, namely: the branch points of p are the vertices, the branch points of γ the midpoints for one tessalation, and the roles of p and γ switched for the other tessalation.
In the case of Schwarz P-surface such a simple function can be defined by mapping a hexagonal piece to a halfsphere (e.g. the upper halfplane) and extend by analytic reflection. It is easy to see that such a function is compatible with the translational identifications of the P-surface, i.e., it is defined on the Riemann surface. This leads to a simpler description of the P-surface and also allows to derive a Weierstrass representation

of (4.2.3). We call this function Z . We keep the additional 45°-symmetry of (4.2.3). Then (with a 3-boundary-point-normalization as in 3.1) we write its special values into a hexagon:

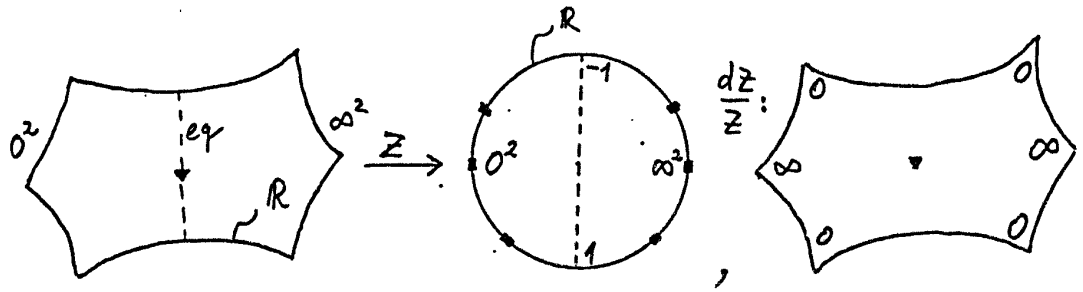

Special values of the function Z on the hexagon of a P-surface, degree(Z) = 4 .

This information combined with the earlier data on g and dh for the P-surface gives:

5.4.1. $$g^2 + g^{-2} = c \cdot (Z^{-1} - Z)$$

$$dh = (g^2 - g^{-2})^{-1} \cdot \frac{dZ}{Z} .$$

It is easier then with the previous data to check that these data define the P-surface.

5.4.2 Claim. The Weierstrass representation for the P-surface with vertical tunnels (4.2.3) is:

$$g^2 + g^{-2} = c \cdot \left(\frac{1 + a^4}{1 - a^2} \cdot (Z^{-1} - Z) + \frac{a}{2} \cdot (Z^{-2} - Z^2) \right)$$

$$dh = (g^2 - g^{-2})^{-1} \cdot \frac{dZ}{Z} ,$$

here the parameter a has to be adjusted so that the vertical tunnels have the correct length. In the limit $a \longrightarrow 0$ we obtain the P-surface.

For better comparison with section 4 we sketch the octogon pieces in the shape of the conjugate contours and write the special values of our functions into these pictures.

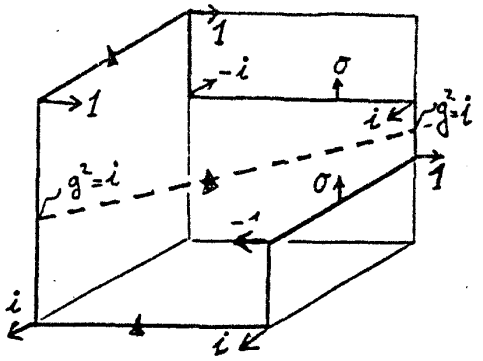

Special values of g on the conjugate octogon and position of branch points.
degree(g) = 4 .

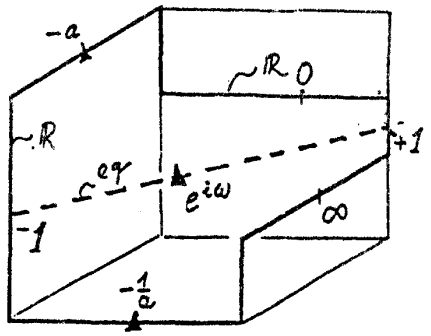

Z maps the octogon to the upper halfplane, the symmetry line to the equator.
degree(Z) = 4 .

With the 3 boundary point normalization we put Z = 0, ∞ at the points where g = 0 and Z = ± 1 at the intersection with the symmetry line.

$-a$, $-\frac{1}{a}$, $e^{i\omega}$ are the names for the values of Z at the branch points of g .

Branch points of Z are at all the vertices of the octogon,

i.e., at the points where $g^4 = 1$; there are no other branch points of Z and no other points with $g^4 = 1$.
All this information is compatible with the ansatz:

$$5.4.3. \quad 2\left(g^2 - \frac{1}{g^2}\right)\frac{dg}{g} = \text{const.}\cdot\left(Z + \frac{1}{Z} - 2\cos\omega\right)\cdot\left(Z + \frac{1}{Z} + a + \frac{1}{a}\right)\frac{dZ}{Z} .$$

(The left hand side needs the factor $g^4 - 1$ and cannot have other zeros for $g \neq 0, \infty$ because this would lead to more branch points for Z . The right hand side needs simple zeros at $-a, -\frac{1}{a}, e^{i\omega}, e^{-i\omega}$ and no others for $Z \neq 0, \infty$ because this would lead to additional branch points for g . The powers of g and Z on both sides have been adjusted for the behaviour at $0, \infty$.)
The right side of (5.4.3)

$$\left(Z^2 + Z^{-2} + (Z + Z^{-1})\cdot(-2\cos\omega + a + \frac{1}{a}) + 2 - 2\cos\omega\cdot(a + \frac{1}{a})\right)\cdot\frac{dZ}{Z}$$

is not the differential of a rational function unless we choose

$$\cos\omega\cdot(a + \frac{1}{a}) = 1 .$$

We integrate the equation (5.4.3) and use $\lambda^2 = 1$ if $g^2 = \pm i$ to get

$$g^2 + g^{-2} = \text{const.} \cdot \left(\frac{1}{2}(Z^2 - Z^{-2}) + (Z - Z^{-1}) \cdot \frac{a^4 + 1}{a(a^2 + 1)} \right) .$$

Putting $c = - \frac{\text{const.}}{a}$ we get the claimed equation.
Finally dh has no poles and has to keep the points where $g = 0, \infty$ at finite distance by having simple zeros there. The given dh has these properties. Moreover $ds = \left(|g| + \frac{1}{|g|} \right) \cdot |dh|$ has the desired reflections and for these symmetry lines:

$$\frac{dg}{g}(\dot{\sigma}) \cdot dh(\dot{\sigma}) \in R .$$

5.5 Finite total curvature immersions and embeddings of higher genus.

5.5.1. The first such example with one puncture is the genus 2 example by Chen-Gackstatter [CG], an Enneper surface with two horizontal handles above each other. — The vertical symmetry lines tessalate this surface into four 90°-hexagons; two more straight lines through the middle saddle are diagonals of the hexagons, giving a 1-parameter family of Riemann surfaces. The natural functions are the Gauss map $g = r \cdot \tilde{\gamma}$ and the $\tilde{\gamma}$ and the map Z which is defined by sending one

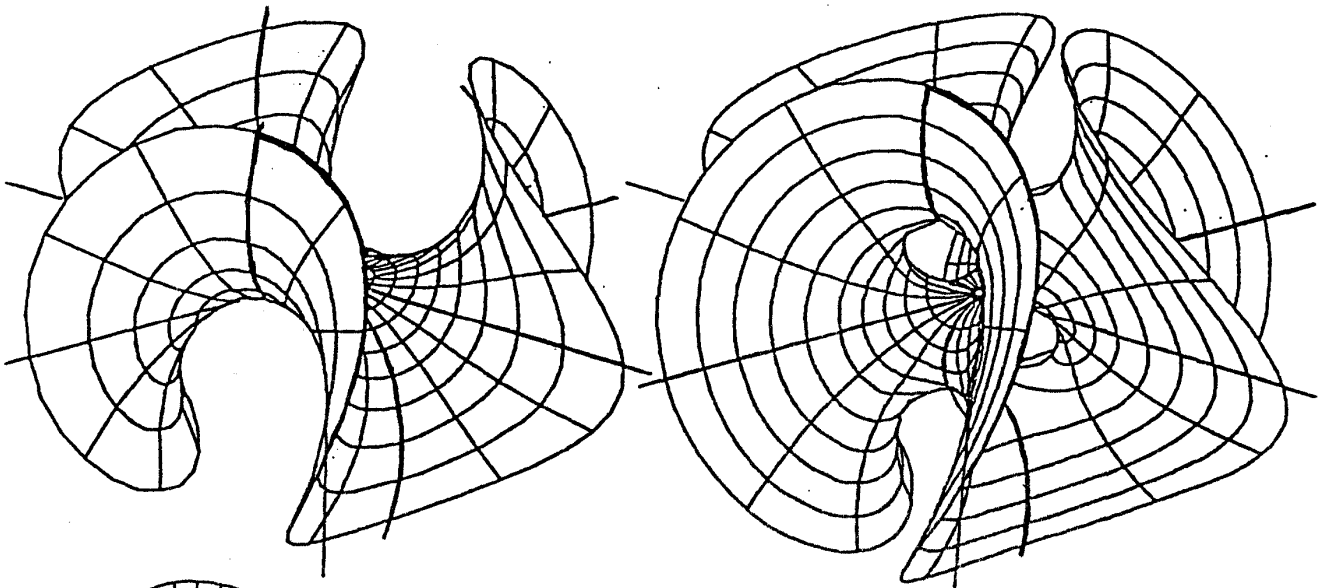

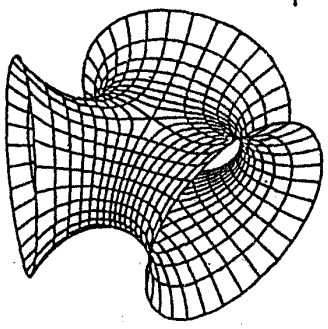

Higher order Enneper surface and Y-handle suggest a genus 2 minimal surface with the same end and the same symmetry lines through the middle saddle (5.5.2).

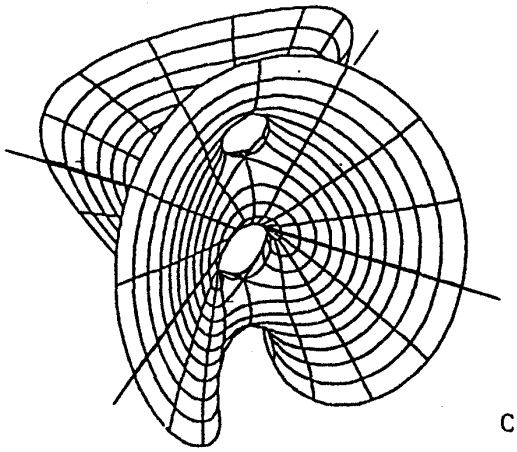

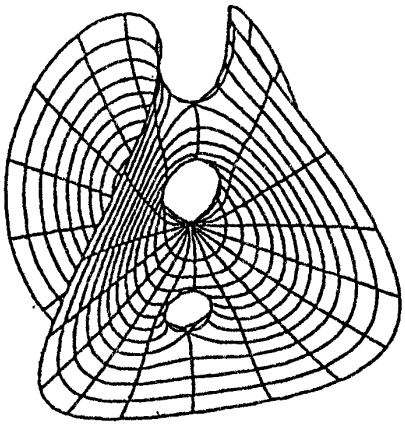

Chen-Gackstatter genus 2 minimal surface with the simplest Enneper end (5.5.1).

such hexagon to the upper halfplane. There are two horizontal periods to kill. As in the genus 1 case each can be separately made to zero by choosing r^2 as the quotient of two integrals. One of these real quotients depends on the conformal parameter such that it is bounded away from $0, \infty$, the other approaches zero and ∞. Therefore both periods can be killed. — This idea gets technically unmanagable for larger genus.

5.5.2. Another idea to increase the genus is by increasing the *dihedral symmetry* [HM1]. The toroidal Chen-Gackstatter – and the Costa – surface are cut by $k = 2$ vertical symmetry planes into 90°-quadrilaterals (with one symmetry-diagonal from the straight lines). Assume that we have a similar surface piece in a $\frac{\pi}{k}$-wedge for $k > 2$, then reflection in the vertical faces of the wedge produces a surface with dihedral symmetry D_k. It is tessalated by $2k$ quadrilaterals which have all angles equal to $\frac{\pi}{k}$ (and which have one diagonal symmetry from k straight lines through the middle saddle). The Riemann surface is therefore uniquely determined and it is the same for both cases! It has two particularly simple functions on it, one function Z of degree k is defined by mapping one such quadrilateral to the unit disc, the other function W of degree 2 mapping one of the four 2k-gons (90° angles) of the *dual tessalation* to the unit disc. After appropriate rotations this gives the equation of the Riemann surface as

5.5.3. $$W^k \cdot Z^2 + W^k + Z^2 = 1$$

or $$W^k = \frac{1 - Z^2}{1 + Z^2}, \quad Z^2 = \frac{1 - W^k}{1 + W^k} .$$

This Riemann surface will be minimally immersed with one Enneper end, and will be embedded with three ends.

5.5.4 Data with one Enneper end (picture: k = 3).

The function W has simple zeros and poles at the vertices of the quadrilaterals which are going to be the three saddles and the Enneper puncture; all are points of order (k - 1) . This gives (compare section 2)

$$g = r \cdot W^{k-1} \quad !$$

Now dh needs zeros of order (k - 1) at three of the four vertices to keep these at finite distance, poles can only be allowed at the end. Now $\frac{dZ}{Z}$ has zeros of the desired order (k - 1) at all vertices of the quadrilaterals and unwanted simple poles at their midpoints. Let us assume, the Enneper puncture is at W = 0, Z = 1 . Then

$$dh = \frac{iZ}{(Z - 1)^2} \cdot \frac{dZ}{Z} = i \cdot \frac{1}{Z + \frac{1}{Z} - 2} \cdot \frac{dZ}{Z}$$

is a differential with the correct zeros and poles (all others

are proportional). The expected symmetry lines are mapped by W to meridians; Z maps the planar ones to equator arcs and the straight arcs to R. Reflections in the expected symmetry lines therefore indeed preserve the metric (1.4.2).

Also $\frac{dg}{g}(\dot{\sigma}) \cdot dh(\dot{\sigma}) \in \begin{cases} R \\ iR \end{cases}$ as expected.

The Weierstrass data (5.2.4) on the Riemann surface (5.2.3) therefore define a minimal surface which has the desired puncture and symmetries. All periods are horizontal and equal. They have to be killed by choosing r as in (3.5).

5.5.5. Data for embedded minimal surfaces with two catenoid and one planar end, Hoffman-Meeks' examples of genus ≥ 1 [HM1]. As in the last example, the only zeros and poles of the Gauss map are at the vertices of the quadrilaterals — simple poles at the two catenoid punctures, a pole of order $(k - 1)$ at the middle saddle and therefore a zero of order $(k + 1)$ at the planar end.

The function W is 0 at the vertices where $Z^2 = 1$ and $W = \infty$ where $Z^2 = -1$. This determines the Gauss map

$$g = r \cdot W \cdot \frac{Z + 1}{Z - 1}$$

(the middle saddle being at $Z = 1$, $W = 0$).

Now dh needs simple poles at the catenoid ends, and zeros of order $(k - 1)$ at the middle saddle and at the planar end (2.24).

Recall: $\frac{dZ}{Z}$ has simple poles at the simple zeros and poles of Z, and zeros of *order* $(k - 1)$ at the vertices of the quadrilaterals. The following definition therefore meets the requirements for dh :

$$dh = \frac{i}{Z + \frac{1}{Z}} \cdot \frac{dZ}{Z} \quad .$$

Again the symmetries are immediate; they show that the punctures have no periods and that the horizontal periods are equal in size. We have to kill one of them by choosing r similar to section 3.5.

Remarks. (i) The known 4-ended examples of Callahan-Hoffman-Meeks [CHM2] can be imagined by putting two of the 3-ended examples on top of each other. The description can be obtained along the lines of this lecture. There are two periods to be killed; this cannot be done as in 5.1.1 and is rather unpleasant. (ii) Another interesting family of embedded examples by Callahan-Hoffman-Meeks [CHM1] combines the features of Riemann's example (3.4) with the above 3- or 4-ended ones. They have one translational (or even skrew motion) period, infinitely many planar ends (as in 3.4); but the minimal surface grows out of the planar ends not as in (3.4) but as in (3.5) or (5.2.5). (iii) We have concentrated on minimal surfaces which are either embedded or not too wildly immersed (so that one can still describe their main features quite precisely). Gackstatter and

Kuhnert [GK] took another point of view: they proved that *every* compact Riemann surface can be minimally immersed if one allows a small number of punctures and around these a behaviour as for an Enneper surface of sufficiently high order.

Bibliography

For background and reference I used

[Me] Meeks III, W.H.: A Survey of the Geometric Results in the classical theory of Minimal Surfaces. Bol. Soc. Brasil Mat. 12(1981), 29-86.

[Ni1] Nitsche, J.C.C.: Vorlesungen über Minimalflächen. Grundlehren Band 199, Springer 1975.

[Os] Osserman, R.: A Survey of Minimal Surfaces. Dover Publication 2nd ed., New York 1986.

Nitsche gives many page numbers in his references. He discusses the famous examples from the following four papers in detail.

[En] Enneper, A.: Analytisch-geometrische Untersuchungen. Z. Math. u. Phys. 9(1864), 96-125.

[Ri] Riemann, B.: Gesammelte Mathematische Werke. 2. Aufl., B. G. Teubner, 1892.

[Sk] Scherk, H.F.: Bemerkungen über die kleinste Fläche innerhalb gegebener Grenzen. J. r. angew. Math. 13(1835), 185-208.

[Sz] Schwarz, H.A.: Gesammelte Mathematische Abhandlungen.

2 Bände, Springer, 1890.

[Br] Bryant, R.L.: A duality theorem for Willmore surfaces. J. Dif. Geom. 20(1984), 23-53.

[CG] Chen, C.C., Gackstatter, F.: Elliptische und hyperelliptische Funktionen und vollständige Minimalflächen vom Enneperschen Typ. Math. Annalen 259(1982), 359-369.

[CMH1] Callahan, M., Hoffman, D., Meeks III, W.H.: Embedded minimal surfaces with an infinite number of ends. To appear in Inv. Math.

[CMH2] Callahan, M., Hoffman, D., Meeks III, W.H.: Embedded minimal surfaces with four ends. In preparation.

[Co] Costa, C.: Example of a complete minimal immersion in R^3 of genus 1 and three embedded ends. Bull. Soc. Bras. Mat. 15(1984), 47-54.

[FK] Fischer, W., Koch, E.: On 3-periodic minimal surfaces with non-cubic symmetry. Z. f. Kristallographie 183(1988), 129-152.

[GK] Gackstatter, F., Kunert, R.: Konstruktion vollständiger Minimalflächen von endlicher Gesamtkrümmung. Arch. Ration. Mech. Anal. 65(1977), 289-297.

[HM1] Hoffman, D., Meeks III, W.H.: Complete embedded minimal surfaces of finite total curvature. Bull. A.M.S. 1985, 134-136.

[HM2] Hoffman, D., Meeks III, W.H.: Properly embedded minimal surfaces of finite topology. Bulletin(New Series) A.M.S. 17(1987), 296-300.

[HM3] Hoffman, D., Meeks III, W.H.: A variational approach to the existence of complete embedded minimal surfaces. Duke J. Math. 57(1988), 877-894.

[HM4] Hoffman, D., Meeks III, W.H.: The strong halfspace theorem for minimal surfaces. Preprint.

[JS] Jenkins, H., Serrin, J.: Variational Problems of Minimal Surface Type II. Arch. Rat. Mech. Analysis 21(1966), 321-342.

[Ka1] Karcher, H.: Embedded minimal surfaces derived from Scherk's examples. Manuscripta Math. 62(1988), 83-114.

[Ka2] Karcher, H.: The triply periodic minimal surfaces of Alan Schoen and their constant mean curvature companions. Manuscripta Math. 64(1989), 291-357.

[Kr] Krust, R.: The conjugate of a minimal graph over a convex domain is a graph. Personal communication.

[LaR] Langevin, R., Rosenberg, H.: A maximum principle at infinity for minimal surfaces and applications. Duke J. Math. 57(1988), 819-828.

[LoR] Lopez, F.J., Ros, A.: On embedded complete minimal surfaces of genus zero. Preprint Granada 1989.

[MR] Meeks III, W.H., Rosenberg, H.: The global theory of doubly periodic minimal surfaces. To appear inInv. Math.